DEVELOPMENT OF PREDICTIVE FINITE ELEMENT MODELS FOR COMPLETE CONTACT FRETTING FATIGUE

A thesis submitted to the University of Manchester

for the degree of

Doctor of Philosophy (PhD)

in the Faculty of Engineering and Physical Sciences

2015

MOHAMAD HAIDIR MASLAN

School of Mechanical, Aerospace and Civil Engineering

Table of Content

List of Figures

List of Tables

Abstract

Nucleation and propagation of cracks under fretting conditions has been a subject of study for many years. An extensive experimental investigation to study these cracks was undertaken by Royal Aerospace Establishment (RAE Farnborough). Of particular interest to RAE was an Aluminium alloy (L65) developed for aerospace applications.

Many researchers have studied fretting damage and fatigue cracks. Some have examined damage development due to wear, whilst others have analysed cracks under linear elastic fracture mechanics (LEFM) domain. To date, no attempt has been made to develop an integrated numerical model which incorporates all aspects of fretting fatigue i.e. nucleation, initial (or early) crack growth, and long crack propagation. The development of such a model is the principal aim of this work. It is expected that the integrated approach will provide the basis for a standard fretting fatigue analysis of other materials, components, and structures using the finite element method (FEM).

This study uses the earlier experimental results with RAE as the reference for comparison. The approach followed is to implement the various stages of fretting in a commercial finite element code, ABAQUS. Unlike previously used simple FE models, both specimen (Aluminium alloy) and the fretting pad (steel) are modelled to simulate the real contact conditions including slip.

Various predictive models for crack nucleation (based on damage) and propagation (based on fracture mechanics) are developed, tested, and implemented in ABAQUS. Results clearly show that these models together provide a good estimation tool for predicting total life in complete contact fretting fatigue. It is envisaged that the integrated model will be easily utilised for other materials, components, and structures subjected to fretting fatigue conditions with minimum experimental testing required.

Declaration

No portion of the work referred to in the thesis has been submitted in support of an application for another degree or qualification of this or any other university or other institute of learning.

Mohamad Haidir Maslan

January 2016

Copyright Statement

i. The author of this thesis (including any appendices and/or schedules to this thesis) owns certain copyright or related rights in it (the "Copyright") and s/he has given The University of Manchester certain rights to use such Copyright, including for administrative purposes.

ii. Copies of this thesis, either in full or in extracts and whether in hard or electronic copy, may be made only in accordance with the Copyright, Designs and Patents Act 1988 (as amended) and regulations issued under it or, where appropriate, in accordance with licensing agreements which the University has from time to time. This page must form part of any such copies made.

iii. The ownership of certain Copyright, patents, designs, trademarks and other intellectual property (the "Intellectual Property") and any reproductions of copyright works in the thesis, for example graphs and tables ("Reproductions"), which may be described in this thesis, may not be owned by the author and may be owned by third parties. Such Intellectual Property and Reproductions cannot and must not be made available for use without the prior written permission of the owner(s) of the relevant Intellectual Property and/or Reproductions.

iv. Further information on the conditions under which disclosure, publication and commercialisation of this thesis, the Copyright and any Intellectual Property and/or Reproductions described in it may take place is available in the University IP Policy (see http://documents.manchester.ac.uk/DocuInfo.aspx?DocID=487), in any relevant Thesis restriction declarations deposited in the University Library, The University Library's regulations (see http://www.manchester.ac.uk/library/aboutus/regulations) and in The University's policy on Presentation of Theses

Acknowledgements

First and foremost, I would like to express my sincerest gratitude to my supervisor, Dr Mohammad Sheikh who has giving me guidance, support and inspiration throughout my PhD programme. Without his patient, kind and assistance, the completion of this thesis would not have been possible.

Many special thanks go to The Ministry of Education Malaysia and Universiti Teknikal Malaysia Melaka (UTeM) as the sponsor of my tuition fees and provided the financial support during my research years in Manchester.

I would like to thank to all technical staffs in The University of Manchester that may have given direct and indirect support in completing various stages of this research. Not forget to mention supportive colleagues especially those in Floor D and F of Pariser Building that always keen to help each other in completing our courses

I could not have thanks enough for the moral support and unconditional love given by my parents, Maslan Isa and Kaujah Yahok. Thanks for all the financial backings that they have given me.

Finally, I wish to thank my lovely wife, Noraini Kurdi. Her understanding towards the challenges faced by me, her patience and supports were very much needed and tremendously appreciated. Thank you to all my kids, Nazurah Hana, Muhammad Taqiuddin, and Muadz Daniel for always cheering me up during all this period.

Thank you to everyone who at some point has contributed any means of support during the course of my PhD. I am forever in your debt.

Nomenclature

Acronyms

ASTM	American Society for Testing and Materials
ΔMTS	Maximum Tangential Stress Range
EPFM	Elastic-Plastic Fracture Mechanics
FEM	Finite Element Method
FS	Fatemi-Socie
LEFM	Linear Elastic Fracture Mechanics
MERR	Maximum Energy Release Rate
MTS	Maximum Tangential Stress
NTSB	National Transportation Safety Board
SWT	Smith-Watson-Topper

Roman Symbols

a	semi contact width
B	Specimen thickness
b	fatigue strength exponent
c	fatigue durability exponent
D	damage fraction
R	Cylinder radius
2D	two dimensional
P	Normal Load (N)
E	Young Modulus (MPa)
E*	combined modulus (MPa)
$F_{friction}$	Friction load (N)

H	Hardness
J	Strain energy release rate or work input rate (J/m^2)
K_I, K_{II}, K_{III}	Mode I, II, and III stress intensity factors ($MPa\sqrt{m}$)
K_{IC}	Plane strain fracture toughness ($MPa\sqrt{m}$)
N	Normal load (N)
N_f	Life (cycle to failure)
P	contact pressure (MPa)
$p(x)$	contact pressure (MPa)
p_o	maximum normal pressure (MPa)
r_p	Plastic zone size (μm)
S	Sliding distance (μm)
W	rate of wear (m^3/m)
W_s	Work required to create new surfaces

Greek Symbols

v	Poisson Ratio
μ	coefficient of friction
ε_a	strain amplitude
ε_{ea}	elastic strain amplitude
ε_{pa}	plastic strain amplitude
$\varepsilon_f^{'}$	fatigue ductility coefficient
γ	shear strain
σ_a	normal stress amplitude (MPa)
$\sigma_f^{'}$	fatigue strength coefficient (MPa)
$\sigma_{xx}, \sigma_{yy}, \tau_{xy}$	2-D stress components in Cartesian Coordinates (MPa)

σ_{rr}, $\sigma_{\theta\theta}$, $\tau_{r\theta}$	2-D stress components in Polar Coordinates (MPa)
σ_y or σ_{ys}	Yield Stress (MPa)
σ_{max}	maximum stress (MPa)
τ	shear stress (MPa)
θ	direction in front crack tip

CHAPTER 1. INTRODUCTION

1.1 Introduction

Fatigue failure was detected as early as 1837. Despite many attempts that have been made to understand and to avoid accidents due to fatigue failure, these failures still continue to occur. In the aircraft industry for example, fatigue failure was the cause of catastrophic accident of the first commercial aircraft de Havilland Comet in 1953[1]. Three aircrafts broke up during mid-flight within one year after the commercial aircraft was launched. Investigations indicated that the main cause of these catastrophic failures was by metal fatigue in the airframes. Windows with sharp corners followed by rivet holes around increased the stress concentration, as shown in Figure 1.1. Lack of knowledge about fatigue at the time contributed to this rather inferior design. These accidents, however, led the company and the competitors to invest more on research on metal fatigue resulting in better and safe design of aircrafts.

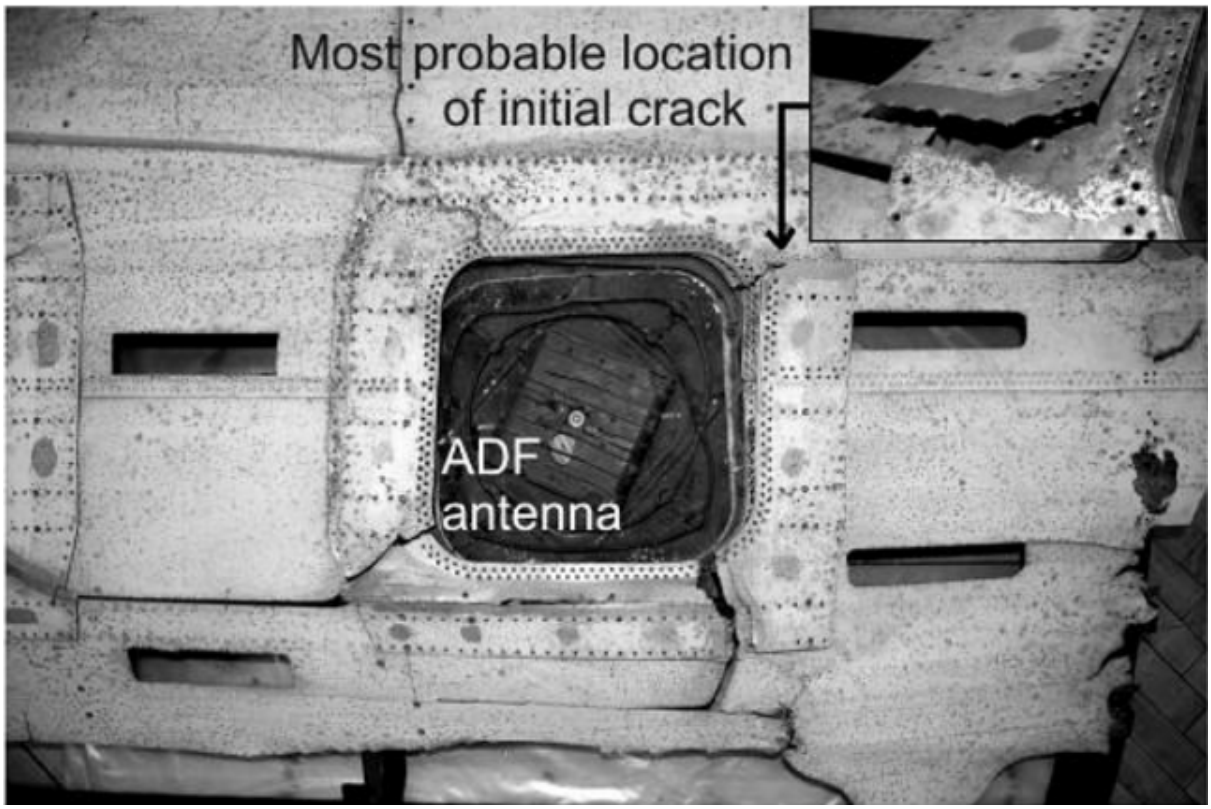

Figure 1.1: Fuselage fragment of Comet [2].

Despite improvements, another fatigue failure involving a rivet joint occurred 35 years later in 1988. A Boeing 737-200 owned by Aloha Airlines, experienced an explosive decompression due to mechanical structural failure during flight. Approximately 5.5 m of the cabin skin and structure of the cabin entrance door above the passenger floor had separated from the aircraft (Figure 1.2).

Figure 1.2: Aloha Airline flight 243 accident [3].

Failure was found to have initiated along a fuselage skin longitudinal lap joint that had been cold bonded and also contained three rows of additional countersunk rivets. Fuselage hoop loads were intended to be transferred through the joint rather than through the rivets. However, some areas of the lap joints did not bond at all, the hoop load transfer though the joint was borne by the three rows of countersunk rivets. The countersinking extended through the entire thickness of the sheet which resulted in a knife edge being created at the bottom of the hole, as shown in Figure 1.3. Stress concentrated at the knife edge and promoted fatigue crack nucleation. For this reason, fatigue cracking began in the outer layer of the skin at a lap joint along the upper and highly stressed row of rivet holes.

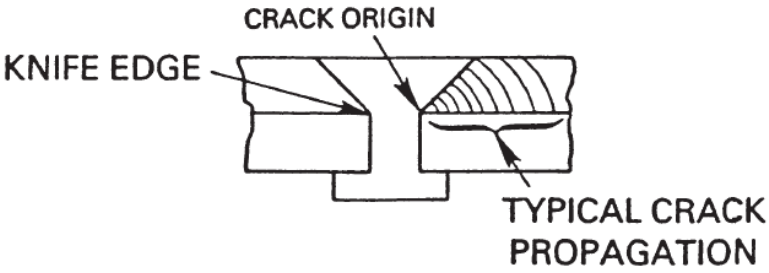

Figure 1.3: Schematic view of a countersunk rivet and the associated fatigue crack observed in Aloha Airlines 737 accident [3]

More recently, in April 2011, a Boeing 737 operating for Southwest Airlines [3] experienced a rapid decompression during flight. The aircraft sustained substantial damage; post-accident inspection revealed that a section of fuselage skin had fractured and flapped open on the upper left side above the wing, Figure 1.4. The entire section of skin remained attached along the lower edge and was deformed outward, as shown in Figure 1.5. The fracture along the upper edge was through the lower rivet row of the lap joint. There was no visible damage to the surrounding frames, stringers, and stringer clips. At National Transportation Safety Board (NTSB) materials laboratory, microscopic examination of the fracture surfaces of the ruptured skin revealed fatigue cracks emanating from at least 42 out of the 58 rivet holes. Non-destructive eddy current inspections were conducted around the intact rivets on the removed skin section forward of the rupture revealed indications of cracks at nine rivet holes in the lower rivet row of the lap joint.

Figure 1.4: Photograph of Southwest airliner with a hole in the upper left fuselage [4]

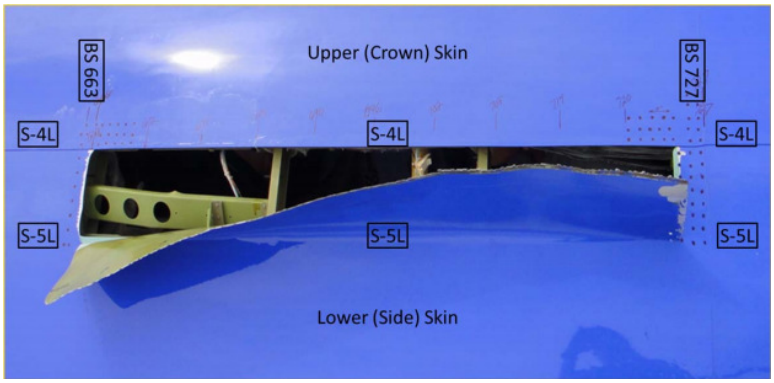

Figure 1.5: Close-up view of the hole in the fuselage side skin [4]

According to NTSB technical report [4], at the inner surface of the lap joint, the rivet holes in the upper and lower skins were found to be slightly offset relative to each other, and many of the rivet holes on the lower skin were not circular but slightly oval. The fracture (fatigue cracks) intersected the majority of the lower-row rivet holes. The corresponding area located at the underside of the expanded portion of the rivets also showed fretting damage consistent with the underside of the expanded portion of the shank rubbing against the plate.

With this simple example, it can be concluded that continuous in-depth study of each accident is necessary. Although accidents may be unavoidable, design improvements can hopefully reduce the chance for such accidents to occur.

1.2 Fretting Fatigue

Fretting is a rubbing process between two surfaces due to oscillatory micro-slip which occurs between them. It occurs in machine components subjected to a clamping pressure and vibratory excitation or an oscillatory tangential force. Fretting damage can be classified into fretting fatigue and fretting wear.

Fretting wear is the result of repeated fretting between two surfaces over a period of time which will remove material from one or both surfaces in contact. In fretting wear, damage is measured by the volumetric material loss.

Fretting fatigue, on the other hand, is defined in terms of the reduction in fatigue strength or fatigue life due to small amplitude movement between contacting surfaces as one of the members is subjected to a cyclic stress.

Fretting fatigue is common in many mechanical systems and engineering structures (for example: aircrafts, spacecrafts, automobile, electrical equipment, manufacturing equipment, human body implants, etc.) which are subjected to variable cyclic loading on the components in contact. There are many practical applications that are subjected to fretting fatigue, such as bolted and riveted connections, bearing shafts, blade-disk attachment in gas and steam turbines and aero-engine splined couplings.

Figure 1.6 shows two examples of fretting fatigue in aircraft machinery components.

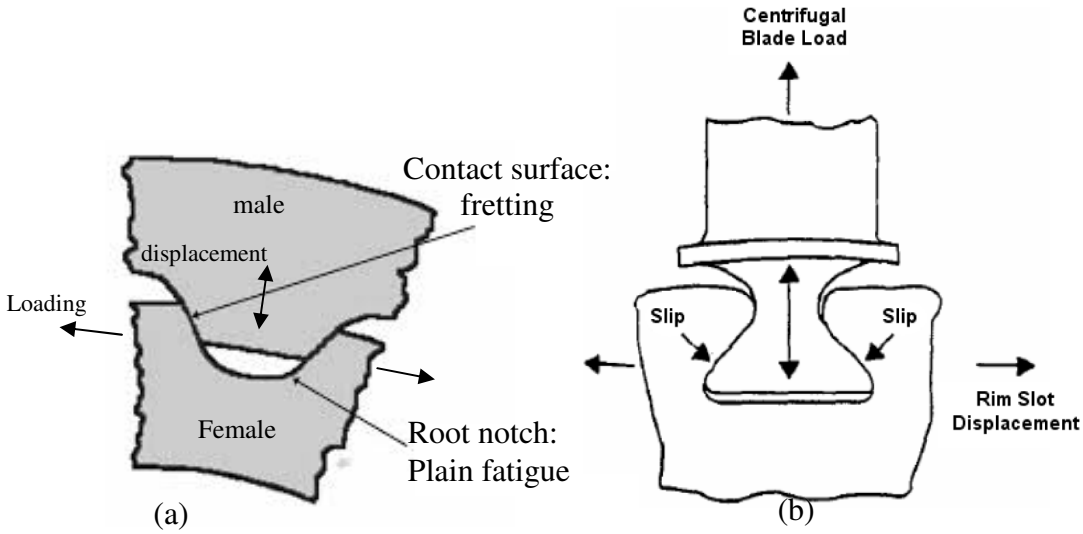

Figure 1.6: fretting fatigue on (a) spline coupling (b) dovetail joint.

1.3 Previous Research

Most of previous fretting fatigue studies have been carried out for aerospace applications where weight and strength are main concerns. The most extensively studied materials are aluminium and titanium alloys as they are used for aerospace structures and engine parts. In the experimental work, these materials are studied in either a bridge or a single pad configuration in complete or incomplete fretting contact. Experimental studies are also carried out on actual components such as rivet joints, dovetail joints and spline couplings.

Besides experimental work, fretting fatigue is also studied using computer simulations. Finite element methods are used to investigate in detail stress, slip, and several other parameters which affect fatigue life. FEM is also used to model crack initiation and propagation in fretting fatigue using critical plane analysis and fracture mechanics. Wear

surface profiles affected by adhesive wear and plastic ratcheting can also be modelled with FEM.

Despite the extensive experimental and modelling work which has been carried out previously on fretting fatigue, it has concentrated mainly on incomplete contact and complete contact has largely been ignored. Although the two types of contact have many similarities, there are several characteristics of complete contact with sharp edges which can cause different tribological effects. Hence, this study intends to include tribological parameters such as wear to improve the current state of complete contact fretting fatigue modelling.

1.4 Overall Aim and Objectives

The ultimate aim of this research is to develop a modelling methodology for predicting fretting fatigue life which includes the tribological aspects of fretting.

The specific objectives are:

- To model fretting crack initiation which includes evolution of surface profile and surface degradation due to wear.
- To model fatigue crack growth of a short crack until fracture by considering multiaxial effects.
- To integrate all the models to produce a total fretting life model in fretting fatigue.

1.5 Structure of report

Following the introduction **(Chapter 1)**, this report is divided into the following chapters:

Chapter 2 Parameters in Fretting Fatigue

This chapter presents a fundamental understanding of the parameters associated with fretting fatigue. It includes contact mechanics, tribology, fatigue, and fretting fatigue.

Chapter 3 Literature Review

This chapter presents a literature review on previous relevant works, discussing state of the art in the field according to scope of this thesis. It consists of contact and failure mechanics

in fretting fatigue including damage mechanics, metal fatigue, as well as fracture mechanics.

Chapter 4 Model Development for Fretting Fatigue Life Prediction

This chapter elaborates in adequate detail the method and procedure to perform each essential step required in this research in order to obtain an accurate and valid life prediction model for fretting fatigue.

Chapter 5 Review of Previous Experimental Work

This chapter describes the experimental work which is the main reference to be used for finite element modelling validation. Details of experimental setup, measuring technique are presented as well as the results from the experiments.

Chapter 6 Crack Initiation in Complete Contact Fretting Fatigue

This chapter presents crack initiation prediction modelling using the critical-plane fatigue approach with Smith-Watson-Topper (SWT) and Fatemi-Socie (FS) relations. This chapter starts by discussing a linear elastic model, followed by elastic plastic model and also includes wear effect on the analysis. Finally, a discussion on averaging analysis to overcome the heterogeneous stress field on the problem is presented. Experimental and finite element predictions are compared in order to validate the developed approach.

Chapter 7 Crack Propagation in Complete Contact Fretting Fatigue

This chapter represents crack growth in fretting fatigue using fracture mechanics approaches. This chapter also combines the predicted fretting fatigue crack initiation and propagation lifetimes to predict total fretting fatigue lifetimes.

Chapter 8 Summary of Results, Conclusions and Future Work

This chapter concludes the current state of the investigation, gives a summary of key results and provides details of the planned future work.

CHAPTER 2. PARAMETERS IN FRETTING FATIGUE

2.1 Introduction

This chapter reviews the parameters which are important in studying fretting fatigue. Firstly, a brief review of contact mechanics, tribology and fatigue is presented. This is fundamental to the understanding of fretting fatigue. Then, fretting fatigue mechanisms are introduced, followed by experimental work on fretting fatigue.

2.2 Contact Mechanics

Contact mechanics considers the analysis of deformation and stress as in contacting bodies. The birth of contact mechanics is associated with the paper by Hertz in 1881 [5]. Since then many researchers have made significant contributions to the field of contact mechanics. Generally contacts can be classified depending on the geometry of the contacting bodies [6].

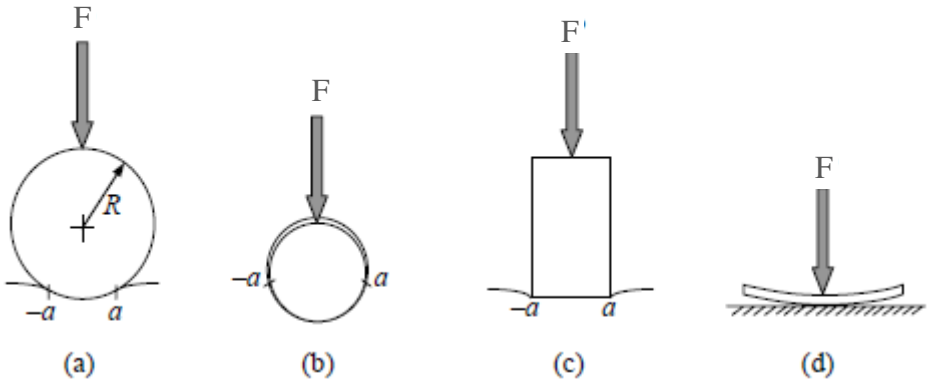

Figure 2.1: Various types of contact (a) Incomplete and non-conformal (b) Incomplete and conformal (c) Complete (d) Receding [6].

The first type of contact is known as incomplete contact and is shown in Figure 2.1(a) and Figure 2.1(b). In this type of contact, contact between two contacting bodies is made along a line which grows to form a narrow strip as the load is increased. Therefore, in incomplete contact, the extent of contact is dependent on the applied load and is not fixed by the geometry of the contacting bodies. Also, in incomplete contacts, the contact pressure falls continuously to zero towards the edges of the contact. Examples of incomplete contact are seen in gears, railway wheels and roller bearings.

Incomplete contacts can be further divided into conformal or non-conformal contacts. If the contact half-width a is very small compared to the radius of the cylinder R, Figure 2.1(a), the contact is considered as non-conformal. In this case, the cylinder may be approximated as a half-plane during the calculation of deformation and stresses. In contrast, for the case of conformal contact, shown in Figure 2.1(b), the contact half-width is not negligible in comparison with the radius of the cylinder and the hole. Therefore, neither of the bodies can be approximated as a half-plane.

The second type of contact is known as complete contact. Figure 2.1(c) shows a complete contact where a flat-ended punch is pressed into an elastic plane. In this case, the size of the contact is independent of the contact load. The two contacting bodies do not have a common tangent at the edges of the contact. In complete contacts, the corresponding contact pressure is singular at the edges of the contacts. Complete contacts arise in many practical fretting problems such as in some spline joints and in bolted flange connections.

The third type of contact that is very rare in practice is known as receding contact. Figure 2.1(d) shows a thin elastic plate placed on an elastic plane. The edges of this plate will lift if a normal load is applied to the plate causing the contact patch to recede.

Incomplete contact between normally loaded bodies was developed by Hertz [5] and it became the basis for analysis in contact mechanics. In Hertz analysis, solutions were given for both two dimensional (2D) contact between a pair of elastic half spaces, and the 3D case of contacting spheres. 2D case of the contact, depicted in Figure 2.2, is discussed here.

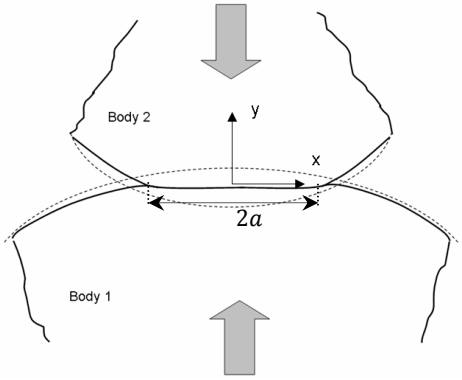

Figure 2.2: Schematic of 2D Hertzian contact.

Elastic deformation within the bodies results in a contact with finite width of $2a$, given by

$$a^2 = \frac{4FR^*}{\pi E^*} \tag{2.1a}$$

where F is the normal load, R^* is the combined radius of curvature and E^* is the combined modulus, given by:

$$E^* = \frac{1}{\left(\frac{1-v_1^2}{E_1} - \frac{1-v_2^2}{E_2}\right)} \tag{2.1b}$$

$$R^* = \frac{1}{\left(\frac{1}{R_1} + \frac{1}{R_2}\right)} \tag{2.1c}$$

where E_i, R_i, and v_i are Young's modulus, radius of curvature and Poisson's ratio for contact body i respectively.

The contact pressure distribution is governed by the following equation,

$$p(x) = \frac{2F}{\pi E^*}\sqrt{a^2 - x^2} \tag{2.2}$$

where *x* is the horizontal distance from the centre of contact.

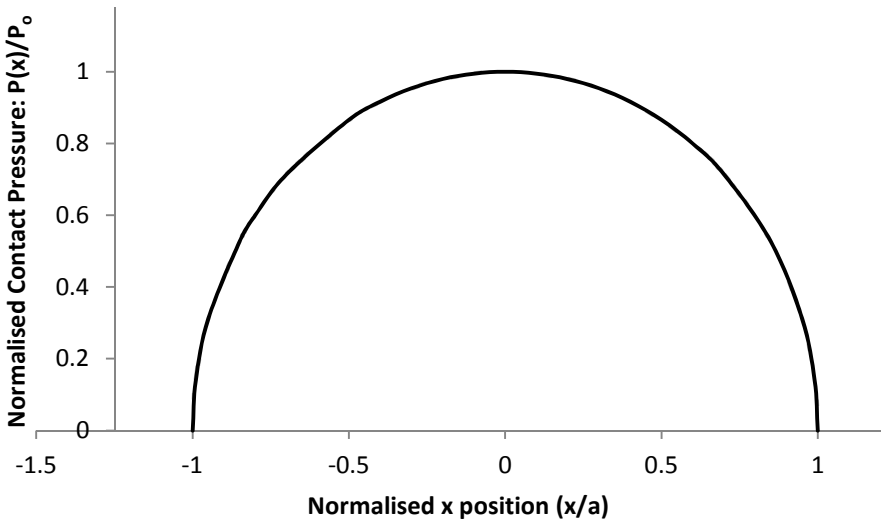

Figure 2.3: Pressure distribution based on Hertz equation.

The maximum normal pressure, p_o, shown in Figure 2.3, occurs on the centreline, falling continuously to zero at the edge of the contact.

$$p_o = \sqrt{\frac{FE^*}{\pi R}} \tag{2.3}$$

The Hertzian theory is subject to the following assumptions:

- The surfaces are continuous and non-conforming
- The strains are small
- Each solid can be considered as an elastic half space
- The surfaces are frictionless

The cylinder on flat configuration creates an incomplete contact. Hertz' original theory has been extended to cover the complete contact in punch on flat configuration (Figure 2.4).

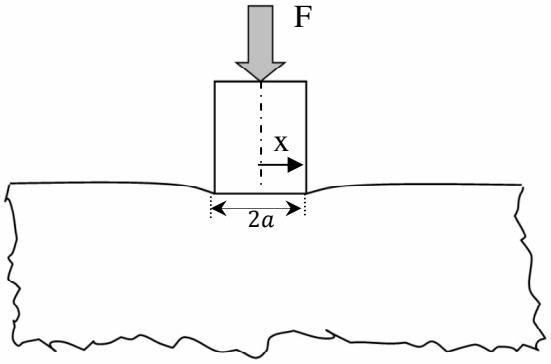

Figure 2.4: Punch on flat contact configuration.

The solution for a rigid punch indenting a plane elastic half-space shows that these discontinuities give rise to an asymptotic pressure distribution [7].

$$p(x) = \frac{F}{\pi\sqrt{a^2 - x^2}} \tag{2.4}$$

The pressure peaks, shown in Figure 2.5, indicate a theoretical pressure singularity at the contact edges ($x = \pm a$). In reality, the inclination of the punch, the relative modulus between the punch and half-space, the coefficient of friction at the contact, and plasticity would affect the singularity at the contact edges. Analytical techniques are generally limited as singularities cannot be described by a simple quadratic expression.

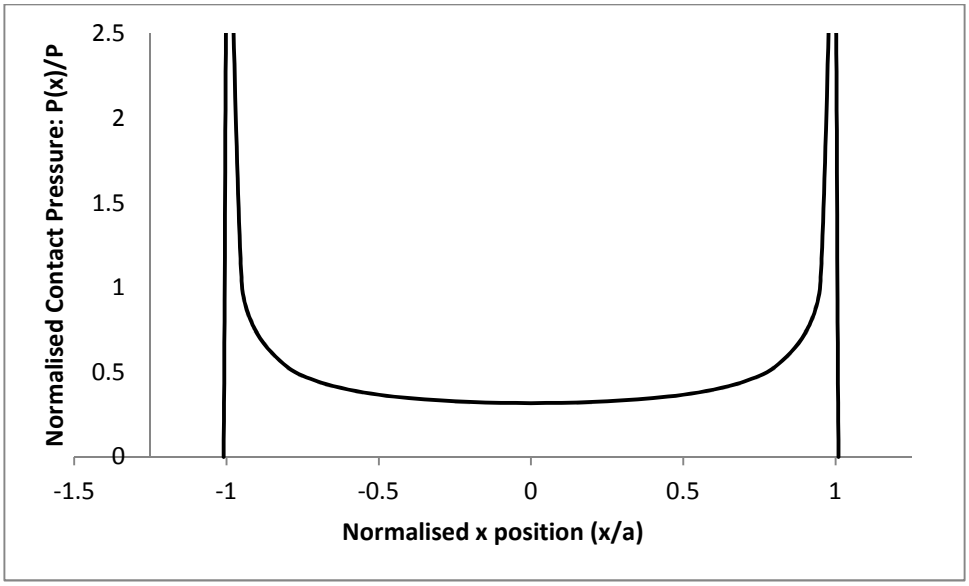

Figure 2.5:Pressure distribution for a rigid, frictionless punch on a flat elastic half-space.

2.3 Tribology

Tribology is the study of interaction between contacting bodies and can be subdivided into three broad areas: friction, wear and lubrication. A brief overview of friction and wear, based on the work of Bhushan [8], is given below.

2.3.1 Friction

Friction is the resistance created at the contact interface due to a relative tangential displacement between the two contacting bodies. There are three main causes of friction: Adhesion, Ploughing and Asperity deformation.

The total friction can be typically approximated with sufficient accuracy by the sum of these components.

Adhesion

Adhesion relates to the galling tendency of some materials. Junctions formed at asperity contacts due to normal load are deformed and later fractured by relative motion.

Ploughing

Ploughing occurs either when one body is much harder than the other or when hard wear particles such as oxides are present. As the hard asperity/particle is traversed across the softer surface, the softer material is forced to plastically deform out of the path of the hard ‘plough’. This friction component is principally a function of the hard asperity

geometry. However, as wear progresses, the geometry is altered by the build up of the material on the plough. This partially explains why friction coefficient can change as wear progresses.

Asperity deformation

Asperity deformation generally forms the most significant portion of total friction in metallic contacts. This component arises from the deformations in asperities as they slide across each other such that compatibility is maintained.

Friction is a complex phenomenon. A material's response is altered by the material structure (in terms of its crystal structure e.g. dislocations, crystal size and orientation), temperature, and loading history. It is therefore apparent that friction coefficient will not only be a function of original material condition (material combination, heat treatment, surface roughness etc.) but will also be dependent on a number of environmental variables, and their histories such as sliding velocity, distance slid, normal load and temperature.

A model which can predict the behaviour of friction under a wide range of different conditions is not yet available. Currently, approximations of friction still use the Coulomb friction model which was established more than 200 years ago. Coulomb law assumes that the friction (shear) load, $F_{friction}$, across the contact is proportional to the normal load, N.

$$F_{friction} = \mu \ N \tag{2.5}$$

Where μ is the coefficient of friction.

2.3.2 Wear

The deformation mechanisms associated with friction, as mentioned above, result in damage sustained by material close to the contact interface. Eventually this results in particle detachment which is cumulatively observed as wear. The mechanisms cited above with regard to friction generation are also found to be the characteristic wear mechanisms. Bhushan & Gupta [8] categorised wear into several categories:

Adhesive Wear

Adhesive wear processes occur as a result of interfacial adhesive junctions which form when solid materials are in contact on atomic scale. The load applied to the contacting asperities is so high that they deform and adhere to each other forming micro-

joints. The motion of the rubbing ruptures the micro-joints. Thus some of the material is transferred from one surface to another.

Abrasive Wear

Abrasive wear may be described as damage to a surface by harder material. In abrasive wear process, asperities of the harder surface press into the softer surface with plastic flow of the softer surface occurring around the asperities from the harder surface. When a tangential motion is imposed, the harder surface removes the softer materials by combined effects of microploughing, microcutting, and microcracking.

Fatigue Wear

Fatigue wear occurs due to periodic variation of stress in contact. An element of metal at the surface of a rotating shaft, for example, is subjected to reversal of bending stresses, The race of a rolling contact bearing will experience continual application and release of hertzian stress. Since the shear stress is maximum at some distance below the surface in contact, the failure initiates at the subsurface.

Corrosive Wear

In corrosive wear, the dynamic interaction between environment and mating material surface plays a significant role. In the process, the contacting surfaces react with environment and reaction products are formed on the surface. Attrition on the reaction products occur as a result of crack formation and abrasion in the contact interactions of the materials. This process results in increased reactivity of the asperities because of the changes in their mechanical properties.

Fretting Wear

Fretting wear occurs when components are subjected to a very small relative vibratory movement at high frequency. Fretting wear is typically a combination of adhesion, abrasion, fatigue, and corrosion wear.

Archard wear equation [9] is a simple model commonly used to describe surface wear. The relation is based on the principle that the rate of wear (W) for a given material is proportional to the contact pressure (P) and the sliding distance (S), and inversely proportional to the hardness (H):

$$W = K\frac{PS}{H} \tag{2.5}$$

2.4 Fatigue

American Society for Testing and Materials (ASTM) defines fatigue as "The process of progressive localised permanent structural change occurring in a material subjected to conditions that produce fluctuating stresses and strains at some point or points and that may culminate in cracks or complete fracture after a sufficient number of fluctuations" [10].

Components of machines, vehicles and structures frequently subjected to repeated loads are exposed to fatigue failure. Research on fatigue of metallic materials has been carried out by both manufacturers and researchers from around the world for more than 150 years.

Fatigue damage can be considered in three stages; Crack Initiation, Crack Propagation, and Final Fracture.

2.4.1 Crack initiation

It is well known that fatigue cracks initiate from invisible microcracks in slip bands. Microscopic investigations have shown that nucleation of microcracks generally occurs very early in fatigue life [11]. However, microcracks remain invisible for a considerable part of the total fatigue life. Once cracks become visible, the remaining fatigue life of a laboratory specimen is usually a small percentage of the total life.

Plain Fatigue

An accepted theory that is used to explain the crack initiation stage is the Persistent Slip Band theory developed by Venkataraman et al. [12]. According to this theory, repeated cyclic straining of the materials lead to different amount of net slip on different glide planes. The irreversibility of shear displacements along the slip bands then results in

the roughening of the surface of the material. The roughening is manifested as microscopic hills and valleys at sites where slip bands emerge at the free surface, as shown in Figure 2.6. The valleys thus generated act as micronotches and the effect of stress concentration at the root of the valleys promotes additional slip and fatigue crack nucleation.

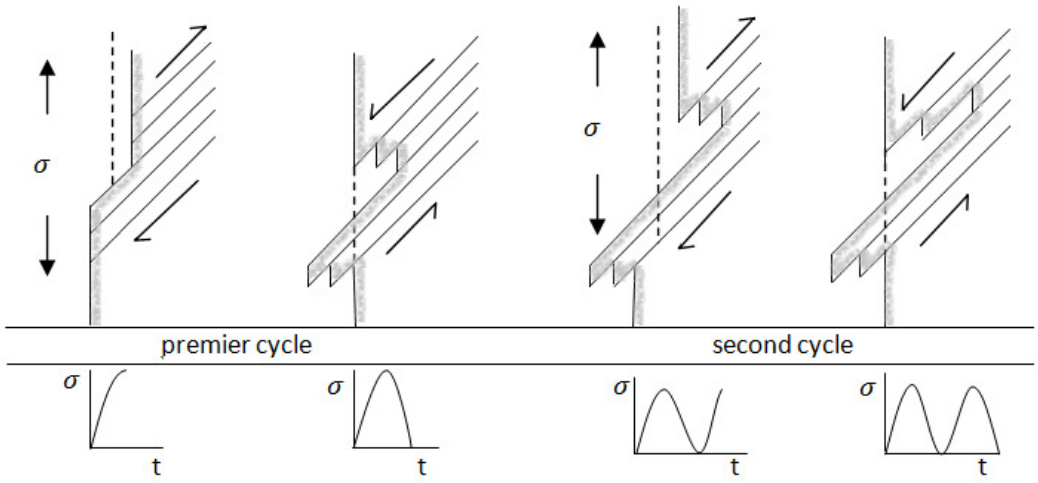

Figure 2.6: Illustration of the irreversibility of slip: formation of a microscopic hills and valleys on the surface of a material loaded in fatigue.

Critical plane analysis

Critical planes in crack nucleation analysis refer to the location and planes where material is subjected to the most extensive range of stress or strain. Recently, strain based approach has been widely used as it considers the plastic deformation that may occur in localized regions.

Figure 2.7 shows a schematic of strain amplitude versus life curves used in strain based approach [13]. The actual strain amplitude (ε_a) is given by the curve labelled total. The curves labelled as elastic and plastic refer to elastic strain amplitude (ε_{ea}) and plastic strain amplitude (ε_{pa}) such that:

$$\varepsilon_a = \varepsilon_{ea} + \varepsilon_{pa} \tag{2.7}$$

where the elastic strain amplitude is related to the stress amplitude by $\varepsilon_{ea} = \sigma_a/E$. By referring to the plot, elastic strain and plastic strain can be determined by equations,

Parameters in fretting fatigue

$$\varepsilon_{ea} = \frac{\sigma_a}{E} = \frac{\sigma_f^{'}}{E}\left(2N_f\right)^b \tag{2.8}$$

and

$$\varepsilon_{pa} = \varepsilon_f^{'}\left(2N_f\right)^c \tag{2.9}$$

Combining these equations gives the expression relating the total strain amplitude ε_a and life N_f as:

$$\varepsilon_a = \frac{\sigma_f^{'}}{E}\left(2N_f\right)^b + \varepsilon_f^{'}\left(2N_f\right)^c \tag{2.10}$$

The quantities $\sigma_f^{'}$, b, $\varepsilon_f^{'}$ and c are considered to be material properties. This equation is commonly referred to as the Coffin-Manson criterion in critical plane analysis.

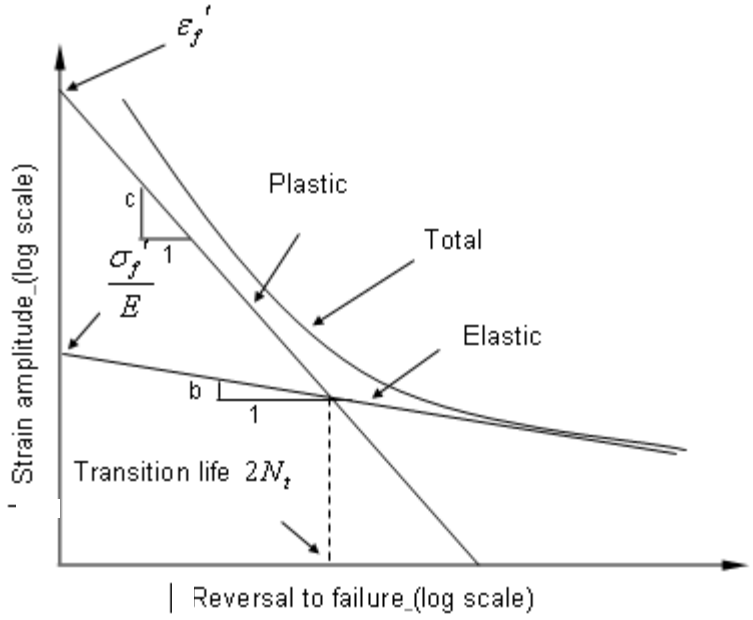

Figure 2.7: Schematic diagram of Strain Life curve [13].

Another model which is widely used to correlate crack nucleation observations is based on Smith-Watson-Topper or *SWT* criterion. Smith, Watson and Topper [14] introduced a function with the intention of including the effect of mean stress.This approach assumes that the life for any given mean stress depends on the product of $\sigma_{max}\varepsilon_a$. The Smith-Watson-Topper (SWT) parameter is given below:

Parameters in fretting fatigue

$$SWT = \sigma_{max}\varepsilon_a = \frac{\sigma'^2_f}{E}(2N_i)^{2b} + \sigma'_f\varepsilon'_f(2N_i)^{b+c} \quad (2.11)$$

Fatemi and Socie [15] suggested the use of SWT parameter for cases where cracks grow on high tensile strain planes but proposed a variant of this model for cracks that grow on high shear strain planes. In this case, the maximum shear strain amplitude and the maximum normal stress on the plane are considered. This leads to the definition of the Fatemi-Socie (FS) parameter.

$$FS = \gamma_a\left(1 + k\frac{\sigma_{max}}{\sigma_y}\right) = \frac{\tau'_f}{2G}\left(2N_f\right)^b + \gamma'_f\left(2N_f\right)^c \quad (2.12)$$

Where γ_a is shear strain amplitude and τ'_f is the fatigue shear coefficient.

In determining crack nucleation life, Fatemi and Socie [15] proposed the use of one of the two criteria based on the given situation. For tensile dominant cracking failure modes, SWT parameter will give a better prediction while for shear dominant cracking failure modes, FS theory is more relevant.

2.4.2 Linear Elastic Fracture Mechanics(LEFM)

Once a crack has initiated and has a length of the order of several grain sizes then, depending on the process zone, the problem should be analysed by Linear Elastic Fracture Mechanics (LEFM) or Elastic Plastic Fracture Mechanics (EPFM).

In discussing crack behaviour, it is necessary to understand the mode of loading. There are generally three modes of loading which involve different crack surface displacements, as shown in Figure 2.8. The three modes are:

Mode I: Opening or tensile mode (the crack faces are pulled apart)

Mode II: Sliding or in-plane shear mode (the crack surfaces slide over each other)

Mode III: Tearing or anti-plane shear mode (the crack surfaces move parallel to the leading edge of the crack and relative to each other)

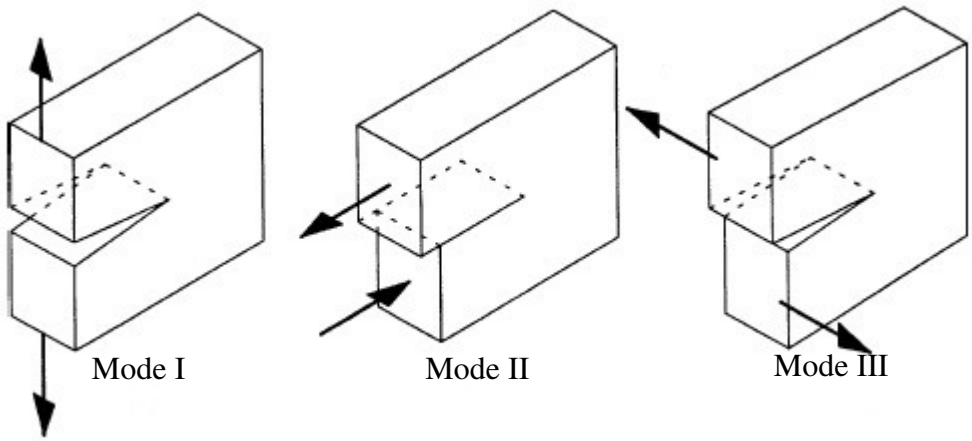

Figure 2.8: Crack loading modes: Mode I, opening; mode II, sliding; mode III, tearing.

LEFM is applicable only when materials obey Hooke's law. Although, since 1960, fracture mechanics theory has been developed to account for various types of nonlinear material behaviour, all are extensions of LEFM.

Based on isotropic linear elastic theories, when the elastic cracked body is subjected to external forces, the stress field in the vicinity of a crack tip, shown in Figure 2.9, is given by equation 2.13 and equation 2.14 :

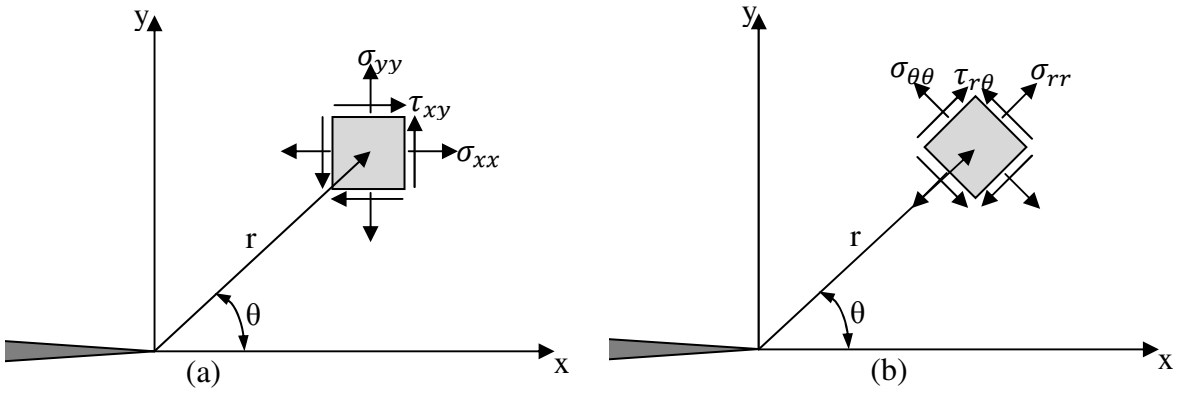

Figure 2.9: Definition of the coordinate axes and the stress field ahead of a crack tip in (a) cartesian coordinates, (b) polar coordinates.

In Cartesian coordinates:

$$\sigma_{xx} = \frac{K_I}{\sqrt{2\pi r}} cos\frac{\theta}{2}\left[1 - sin\frac{\theta}{2} sin\frac{3\theta}{2}\right] - \frac{K_{II}}{\sqrt{2\pi r}} sin\frac{\theta}{2}\left[2 + \cos\frac{\theta}{2} cos\frac{3\theta}{2}\right] \qquad (2.13a)$$

$$\sigma_{yy} = \frac{K_I}{\sqrt{2\pi r}} cos\frac{\theta}{2}\left[1 + sin\frac{\theta}{2} sin\frac{3\theta}{2}\right] + \frac{K_{II}}{\sqrt{2\pi r}}\left[\sin\frac{\theta}{2}\cos\frac{\theta}{2}cos\frac{3\theta}{2}\right] \quad (2.13b)$$

$$\tau_{xy} = \frac{K_I}{\sqrt{2\pi r}}\left[\cos\frac{\theta}{2}\sin\frac{\theta}{2}cos\frac{3\theta}{2}\right] + \frac{K_{II}}{\sqrt{2\pi r}} cos\frac{\theta}{2}\left[1 - sin\frac{\theta}{2} sin\frac{3\theta}{2}\right] \quad (2.13c)$$

or in polar coordinates,

$$\sigma_{rr} = \frac{K_I}{\sqrt{2\pi r}}\left[\frac{5}{4}\cos\frac{\theta}{2} - \frac{1}{4}cos\frac{3\theta}{2}\right] - \frac{K_{II}}{\sqrt{2\pi r}}\left[\frac{5}{4}\sin\frac{\theta}{2} - \frac{3}{4}\sin\frac{3\theta}{2}\right] \quad (2.14a)$$

$$\sigma_{\theta\theta} = \frac{K_I}{\sqrt{2\pi r}}\left[\frac{3}{4}\cos\frac{\theta}{2} + \frac{1}{4}cos\frac{3\theta}{2}\right] - \frac{K_{II}}{\sqrt{2\pi r}}\left[\frac{3}{4}\sin\frac{\theta}{2} + \frac{3}{4}\sin\frac{3\theta}{2}\right] \quad (2.14b)$$

$$\tau_{r\theta} = \frac{K_I}{\sqrt{2\pi r}}\left[\frac{1}{4}\sin\frac{\theta}{2} + \frac{1}{4}\sin\frac{3\theta}{2}\right] + \frac{K_{II}}{\sqrt{2\pi r}}\left[\frac{1}{4}\cos\frac{\theta}{2} + \frac{3}{4}cos\frac{3\theta}{2}\right] \quad (2.14c)$$

The stress intensity factors (K_I or K_{II}), introduced in equation 2.13 and equation 2.14, define the magnitude of the local stresses around the crack tip. These factors depend on loading, crack size and geometry. It can be expressed in a general form as:

$$K = \sigma\sqrt{\pi a}\, f\left(\frac{a}{W}\right) \quad (2.15)$$

where:

σ = remote stress applied to the component,

a = crack length,

$f\left(\frac{a}{W}\right)$ = correction factor that depends on specimen and crack geometry.

In materials science, fracture toughness K_{Ic} is a property which describes the ability of a material containing a crack to resist fracture. The subscript I denotes mode I loading (crack opening) under a normal tensile stress perpendicular to the crack.

Fracture toughness (K_{Ic}) is a quantitative way of expressing the resistance of a material to brittle (or fast) fracture when a crack is present. It is independent of the size and geometry of the cracked body under certain conditions. The materials with higher values of fracture toughness are more likely to undergo ductile fracture, whereas materials with low value fracture toughness usually undergo brittle fracture. The largest crack that a structure can sustain under specific residual strength requirements can be predicted through this critical value of the stress intensity factor (K_{Ic}) where crack propagation becomes unstable.

LEFM can also be explained with energy criterion. Griffith [16] was the first to propose the energy criterion for fracture. Griffith formulated this criterion for unstable extension of a crack in a brittle solid by applying the first law of thermodynamics. According to first law of thermodynamics, when a system goes from a non-equilibrium state to equilibrium, there is a net decrease in energy. In other words, an existing crack can grow only if such a process causes the total energy to decrease or remain constant.

Griffith's energy balance for an increase in the crack surface area *dA*, under equilibrium conditions, can be expressed in the following way:

$$\frac{dE}{dA} = \frac{d\Pi}{dA} + \frac{dW_s}{dA} = 0 \tag{2.16}$$

Where:

E = total energy,

Π = potential energy supplied by the internal strain energy and external forces,

W_s = work required to create new surfaces.

For a through-thickness crack in an infinitely wide plate subjected to a remote tensile stress, Grifith used the stress analysis of Inglis [17] to show that :

$$\Pi = -\frac{\pi\sigma^2 a^2 B}{E'} \tag{2.17}$$

Where

$E' = \frac{E}{1-\nu^2}$ for plane strain,

and $E' = E$ for plane stress,

and the work required to create new surfaces as:

$$W_s = 4aB\gamma_s \tag{2.18}$$

Where γ_s is the surface energy of the material.

Irwin [18] extended the Griffith model by introducing energy release rate, G, which is a measure of the energy available for crack extension:

$$G = -\frac{d\Pi}{dA} = \frac{\pi\sigma^2 a}{E'} \tag{2.19}$$

and can be related to K by:

$$G = \frac{K_I^2 + K_2^2}{E'} \tag{2.20}$$

According to Irwin, crack extension occurs when G reaches a critical value, G_C, which is a measure of fracture toughness and can be considered as a material property.

From equations 2.13 and 2.14, the stress would theoretically increase to infinity when approaching the crack tip (r → 0). In ductile materials, this is not the case because of plasticity which is activated as soon as the local stress exceeds the yield stress (σ_{ys}) of the material. Irwin identified this phenomenon and estimated the size of the plastic zone at the crack tip for monotonic loading in mode I and under plane stress as:

$$r_y = \frac{1}{2\pi}\left(\frac{K_I}{\sigma_{ys}}\right)^2 \tag{2.21}$$

Considering the stress redistribution due to the presence of the plastic zone (Figure 2.10):

$$r_p = 2r_y = \frac{1}{\pi}\left(\frac{\Delta K}{2\sigma_{ys}}\right)^2 \tag{2.22}$$

The basis of LEFM remains valid if this region of plasticity remains small in relation to the overall dimensions of the crack and the cracked body.

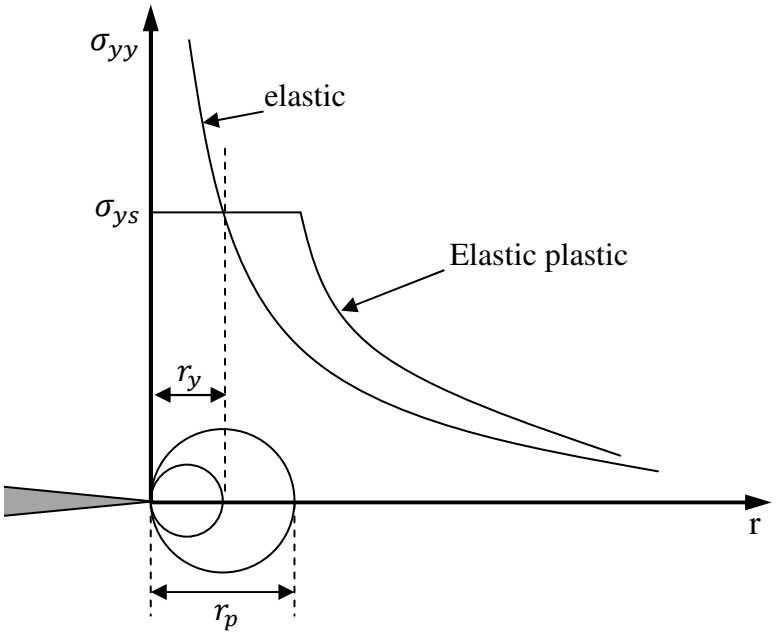

Figure 2.10: Plastic zone size estimation based on Irwin postulate.

2.4.3 Elastic Plastic Fracture Mechanics (EPFM)

In many materials, it is impossible to characterize the fracture behaviour with LEFM and another approach namely Elastic Plastic Fracture Mechanics (EPFM) is employed. EPFM applies to materials that exhibit time-independent, nonlinear material behaviour i.e. plastic deformation.

The *J*-Integral is employed as a fracture characterizing parameter for materials having elastoplastic deformation with non-linear material behaviour. Rice[19] applied deformation plasticity to the analysis of a crack in a non-linear material. He showed that the non-linear energy release rate (*J)* could be written as a path independent line integral. Rice also showed that *J* uniquely characterizes crack tip stresses and strains in a non-linear material. For an elastic material, the *J*-integral can be viewed as both an energy parameter (strain energy release rate, *G*) and a stress intensity parameter (*K*) in the following fashion:

$$J = G = \frac{K_I^2 + K_2^2}{E'} \tag{2.23}$$

Rice presented J-integral for the analysis of cracks by considering an arbitrary counter clockwise path (Γ) around the tip of a crack, as in

Figure 2.11. The J integral is given by:

$$J = \int_{\Gamma} \left(W dy - T \frac{\delta u_i}{\delta y} dS \right) d\Gamma \tag{2.24}$$

Where

Γ is contour surrounding the crack tip,

W is the strain energy density,

T is the traction vector with respect to the outward normal (n) along Γ,

u_i is the displacement vector,

ds is an elemental arc length along Γ.

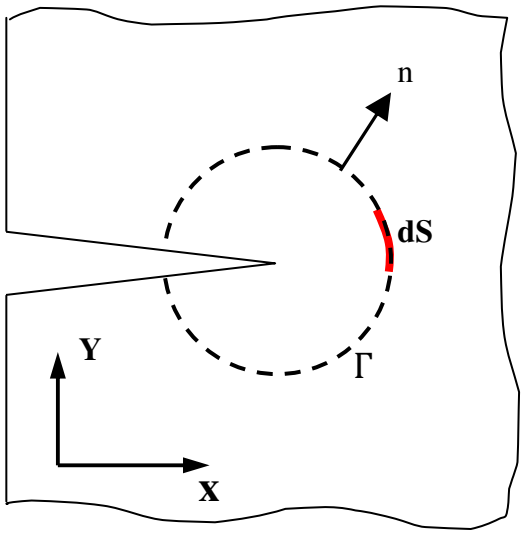

Figure 2.11:Arbitrary contour around the tip of a crack.

2.4.4 Fatigue Crack Growth

Fatigue crack growth models are empirical models which are generally developed by performing one or a series of experiments and fitting the resulting data to a function of crack growth rate (da/dN) versus the stress intensity factor range ΔK, as shown in Figure 2.12.

Fatigue crack propagation behavior for metals can be divided into three regions (Figure 2.11). The behavior in region 1 exhibits a fatigue-threshold cyclic stress intensity factor range, ΔK_{th}. Crack is assumed not to propagate under cyclic stress fluctuations below ΔK_{th}. In this stage of crack growth, there is large influence of microstructure, mean stress, and environment on the fatigue crack growth [20].

The second region is widely studied for fatigue crack propagation. In this stage, fatigue crack propagates in a stable manner. In this stage, fatigue crack propagation is expressed by Paris equation:

$$\frac{da}{dN} = C(\Delta K)^m \tag{2.25}$$

where constants C and m are obtained from experimental fatigue crack growth data. Crack growth rate in this area is influenced by microstructure, and by a certain combination of environment, mean stress, and frequency. There is typically a unique combination of *C* and *m* for each combination of environment, temperature, and the stress ratio.

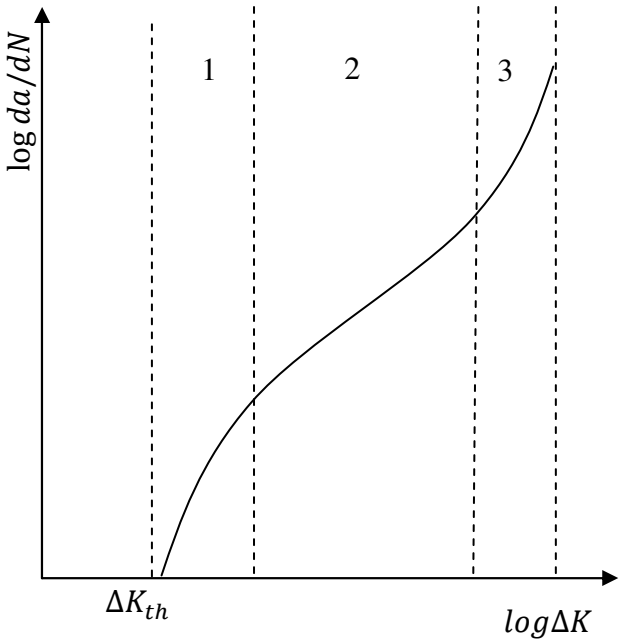

Figure 2.12: Fatigue Crack Growth Plot.

In Region 3, unstable fatigue crack growth and then failure occurs. The fatigue crack growth per cycle in this region is higher than that predicted for region 2. In this stage, there is a large influence of microstructure, mean stress, and thickness but little influence of environmental cleavage and dimples.

2.5 Fretting Fatigue

Fretting fatigue can occur when two structural components are in contact together under normal load and at least one of them in undergoing cyclic load. In the contact area, although both surfaces in contact may appear to be stationary, cyclic deformation from cyclic loading will give a small reciprocating displacement. Fretting occurs in many nominally static mechanical arrangements undergoing vibrations or cyclic stresses. The microslip causes damage to the surfaces and eventual failure due to combination of fretting fatigue or fretting wear.

Fretting was first observed in the grips of a plain fatigue test by Eden and Rose in 1911 [21]. The presence of fretting is often unexpected and causes reduction in life in comparison to plain fatigue, emphasising the importance of recognising and avoiding the phenomenon for practical design cases. The understanding of fretting is complicated by the presence of friction at the contact interface. Directly or indirectly the damage in fretting

fatigue is caused by several factors/variables. It has been reported that up to 50 factors might influence the magnitude and rate of the fretting process [22]. Some of the most important variables/factors that influence fretting fatigue phenomena are material microstructure, work hardening, surface hardness, corrosion susceptibility, temperature, humidity, contact force, tangential force, other external loads, load ratio, surface roughness, size, adhesive wear, lubricants etc.

The field of fretting fatigue life prediction still presents significant challenges. The number of factors involved and the lack of understanding of their interaction adds complexity as compared to plain fatigue. In addition, a unified fretting fatigue life prediction methodology is required which is equally applicable to complete and incomplete contacts.

Fretting fatigue cannot be predicted from plain fatigue data. A significant limitation is that all the proposed methodologies do not account for the experimentally observed effect of slip amplitude on fretting fatigue life. Neglecting wear, the stress-state under the limiting partial slip condition is predicted to be equal to that of the full sliding condition. A life prediction obtained by using stress and strain-based parameters in the gross sliding regime can therefore be regarded as a conservative estimate. An additional shortcoming of such approaches is that the real materials usually contain inherent flaws and total life methods are not able to predict self-arrest of flaws or nucleated cracks that are sometimes experimentally observed. Crack arrest occurs due to the high stress gradients induced by the fretting contact which means that the stress field rapidly decays with distance from the contact.

2.6 Fretting Fatigue Experimental Test and Modelling

A unified fundamental theory for predicting fretting fatigue has not as yet been established and therefore experimental testing is essential to improve understanding. Although, fretting tests have been carried out for many decades but the procedure has only been standardised in March 2011 with the establishment of ASTM E2789-10 [23].

In general, most of experimental research on fretting fatigue has concentrated on aerospace applications. Hence, the materials that are most widely used in experimental fretting fatigue tests are aluminium alloys Al 2014[24], Al 2024[25], Al 7075[26] and Titanium alloy Ti-6Al-4V[27]. All of them have some common features such as aiming to

control fretting fatigue variables such as the slip regime, applied axial stress, tangential and contact loads and so on.

This section will outline the main experimental fretting setups, type of fretting contacts, and other fretting fatigue tests based on real applications.

2.6.1 Fretting Pad Configuration

Based on ASTM standard for fretting fatigue testing, there are two configurations based on how fretting pad is attached to the specimen; Bridge and single clamp.

Bridge configuration

Bridge configuration involves a fatigue specimen in contact with two bridges, with each bridge comprising of two feet, typically shown in Figure 2.13. A normal force is applied to the bridges to enforce contact. Most test apparatus apply an in-plane bulk fatigue load (or displacement) to the specimen.

The relative slip is generated by the difference in strain of the fatigue specimen in relation to the specimen pads. The bridge type geometry has the advantage that it is easy to fabricate and assemble. However, it also has several disadvantages. One of the disadvantages is the contact pressure distribution when the friction forces generated along the bridge feet produce a significant tilting moment on the contact pads. Another disadvantage for bridge type geometry is the appropriate finish of the four contacting pads. Their cleanliness is difficult to achieve, and there may exist adhesion between one pair of feet and the specimen, whilst the other pair undergoes total relative displacement.

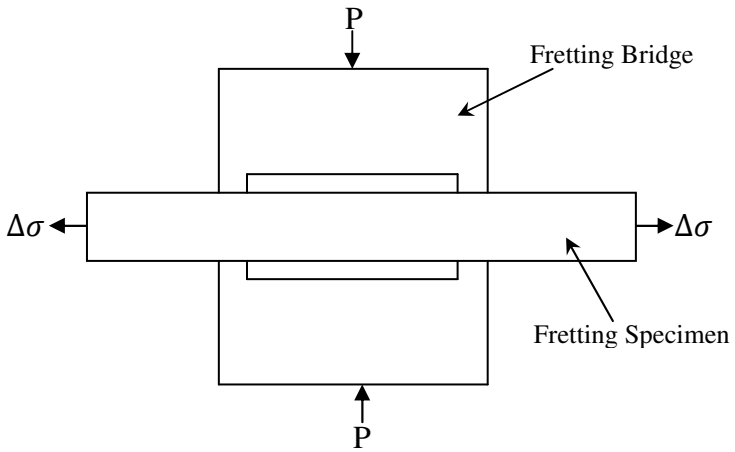

Figure 2.13: Schematic of a typical bridge-type experimental setup.

Single Clamp Configuration

Single clamp configuration is another type of fretting pad configuration that is also commonly used [28, 29]. This type of fretting pad has only one pad per side, as shown in Figure 2.13.

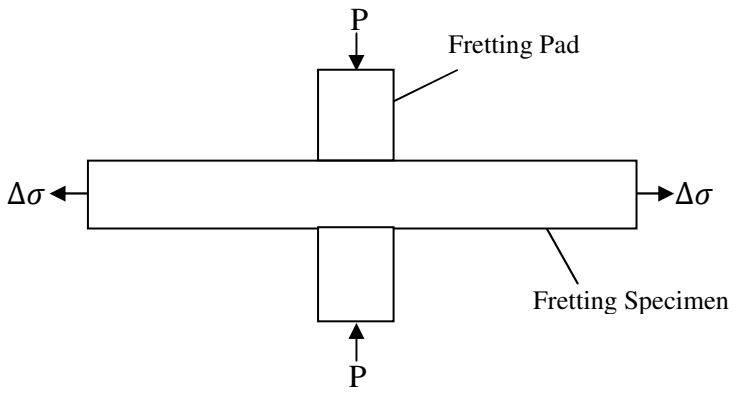

Figure 2.14: Schematic of a typical single fretting pad experimental setup.

It has the advantage of avoiding some of the problems mentioned above for the bridge-type test rig. This arrangement has gained popularity due to pad alignment being less critical in comparison with bridge setups.

2.6.2 Fretting Contact Types

There are two types of contact used in fretting fatigue tests; complete [30, 31], and incomplete contact [32, 33].

In complete contact, a flat contact surface is used for fretting pad. This geometry has an advantage in that it is easy to produce but contact alignment is more critical. Theoretically, based on (Eq. 2.4), complete contact produces contact pressure with singularities at the pad edge, where the stress is theoretically infinite. Hence, plastic deformation is expected to occur near the pad edge of the specimen.

On the other hand, in incomplete contacts, cylindrical and spherical pads are used. Compared to complete contact, pad alignment is less critical for incomplete contact because of the roundness. Another advantage of incomplete contact is the pressure distribution, given Hertz theory (Eq. 2.2), which makes it easier to be compared with the analytical solutions.

Complete contact was more popular in earlier works on fretting fatigue, but in the last two decades incomplete (or cylindrical) contact has become more popular. This trend has also affected the development of fretting fatigue life prediction models which is now focussed on incomplete contact.

2.6.3 Other configurations

A major limitation of simplified test geometries is their inability to readily reproduce complex fretting conditions experienced by a real component. Representative testing attempts to overcome this have been made by testing a laboratory specimen that is designed to reproduce the key variables of the in-service component. Some of the popular fretting fatigue tests on real components are riveted lap joints, bolted lap joints, dovetail joints, spline couplings, bearing shafts, steel wires connections, shrink-fitted joints, and artificial hip joints.

Ruiz [34] devised a biaxial test rig to simulate the dovetail-root connection of the fan blades in a gas turbine aeroengine, as shown in Figure 2.15. The contacts were idealised with a two-dimensional rounded punch-on-flat geometry. The rig was capable of high and low frequency loading that leads to fretting from centrifugal loading or in-flight fluctuations.

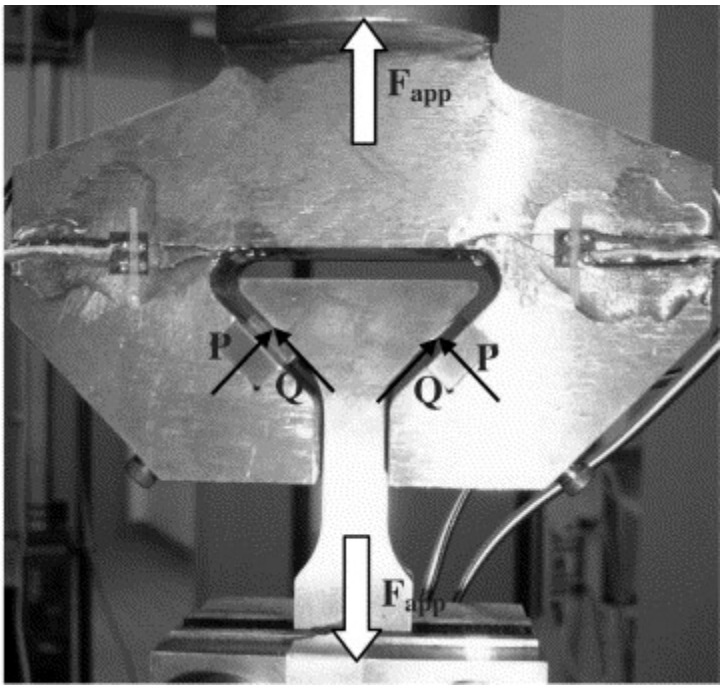

Figure 2.15: Dovetail fretting fatigue experimental configuration [34].

Wavish [35] designed and implemented a multiaxial representative specimen (MRS) for spline couplings, as shown in Figure 2.16. The test set up consists of a fretting specimen in contact with a pair of fretting bridges whereby a profile is machined onto the bridge feet to imitate the spline tooth form. This setup is capable of simulating the combined major and minor cycle loading of the spline coupling.

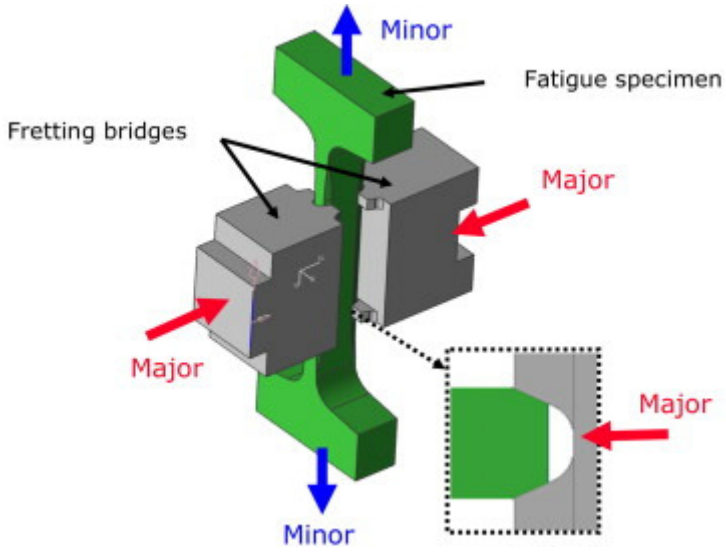

Figure 2.16: Schematic of multiaxial representative specimen for spline coupling [30].

CHAPTER 3. LITERATURE REVIEW

3.1 Introduction

Fretting fatigue life prediction still presents significant challenges. The number of factors involved and the lack of understanding of their interaction adds complexity to the problem. Nevertheless, a unified fretting fatigue life prediction methodology which is applicable to any geometry and conditions is required.

The ultimate aim of research on fretting is to be able to predict fretting fatigue life under complex and realistic engineering coupling or contact conditions. Fretting fatigue fracture mechanism can be divided into four stages; initiation, short crack growth, stable long crack growth and final fracture (Figure 3.1). This chapter gives a detailed explanation of every stage of the process and also describes the method of analysis that has been used for each stage.

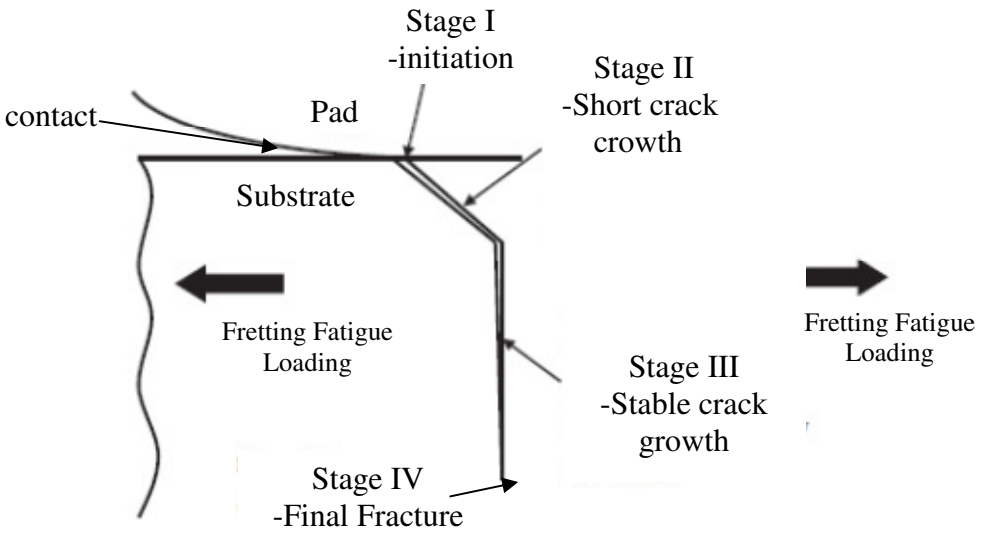

Figure 3.1: Schematic representation of the different stages of fretting fatigue crack initiation, propagation, and final failure [36].

3.2 Crack Initiation

In general, fretting fatigue failure is analysed in conjunction with fretting wear and fretting fatigue. To describe crack initiation process in fretting fatigue, the following

sections discuss the evolution of damage which is affected by both fretting wear and fretting fatigue.

3.2.1 Friction evolution

During the early stage of fretting fatigue process, most fretting contacts experience an increase in the coefficient of friction [24, 31, 37-40].

This increase in the friction coefficient occurs in very early stages and constitutes only less than 5% of fretting life. Hills [38] has reported that this increase occurs within the first 20 cycles. However, the coefficient of friction remains constant after this early increase. A commonly accepted reason is that a thin oxide layer or surface film is wiped or abraded away to form intermetallic joints by adhesion and abrasive wear [31, 39, 41].

In the analysis, the coefficient of friction increment is usually ignored and only the constant coefficient of friction value is used as this increment occurs only after a few cycles of fretting life.

In an intensive study on frictional force during fretting fatigue [42], it has been found that other fretting parameters also have an influence on the frictional force. An increase in bulk stress, relative slip, and hardness of pad material cause an increase in the coefficient of friction, while an increase in contact load, frequency and temperature decreases the coefficient of friction.

3.2.2 Wear

Wear in fretting Fatigue occurs either by adhesive wear, abrasive wear or delamination wear. Adhesive wear occurs when in contact asperities forming the junctions break due to fretting movement, as shown schematically in Figure 3.2 [27, 43]. Furthermore, plastic deformation and strain hardening may strengthen the junctions of the original contact. The junctions then break in locations different from the original contact joints, as shown in the figure. Metal transfers from one surface to another, usually to the harder surface [44, 45].

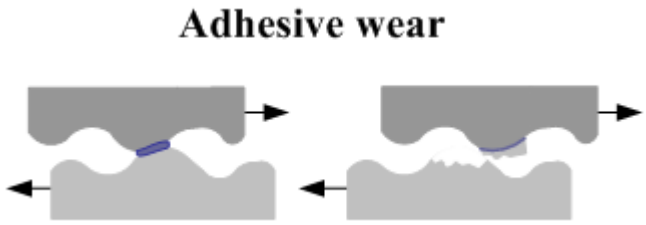

Figure 3.2: Schematic of Adhesive Wear.

As the process continues, free surfaces and internal discontinuities that are exposed to the adsorption of gaseous oxygen are dissociated and oxidised [43, 44]. Pieces of transferred metal would oxidize and may break off to form partially oxidized third body particles to produce abrasive wear (Figure 3.3) [44].

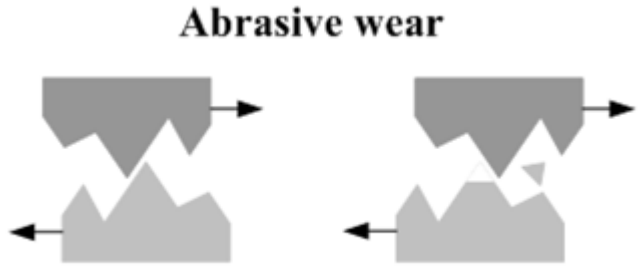

Figure 3.3: Schematic of Abrasive Wear.

Adhesive and abrasive wear are part of a continuous and simultaneous process and the transformation depends on oxidation rate. Wear rate can either increase or decrease in the process depending on the situation. Brygment [46] has found that both adhesion and abrasion contribute to the fretting fatigue process by producing wear debris and fretting microcracks, as shown in Figure 3.4.

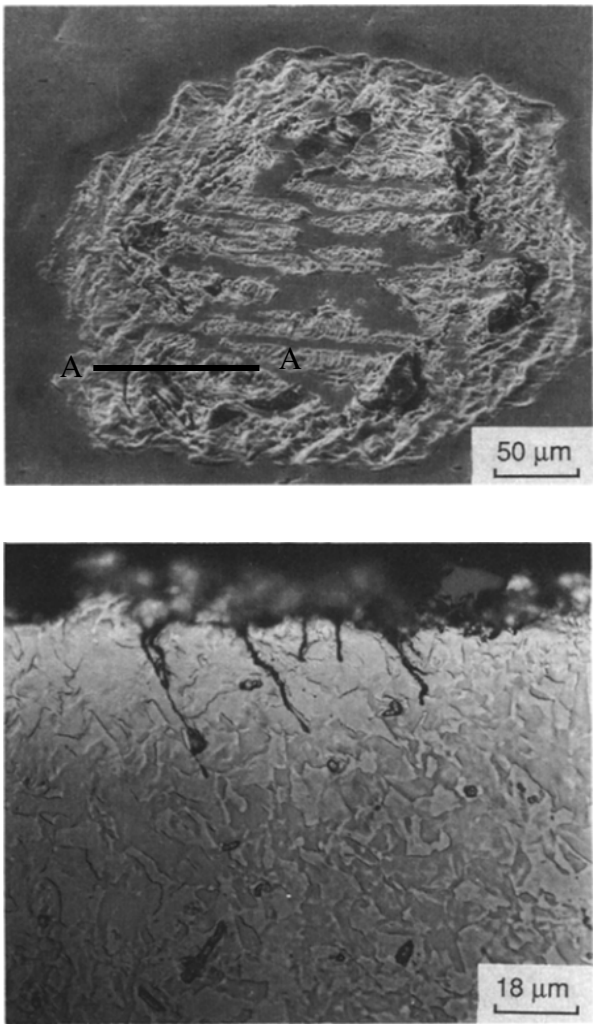

(a)

(b)

Figure 3.4: Fretting wear (a) scar and (b) etched cross sectional view at line AA [46].

Wear also occurs due to particle wear as it is observed that debris particles are often thin plate-like sheets [47, 48]. The theory of delamination is often used to explain this. Everitt et al. [49], in their research on debris, found that wear produces compacted and oxidised debris layer with high hardness and low stiffness compared to the bulk material. The thickness is proportional to the loading, wear and number of cycles. This suggests that material near the surface is cold worked less than the subsurface layer. A pile-up of dislocations occurs at a finite distance from the surface (Figure 3.5). Voids form and then coalesce to form crack. Cracks are also formed as the material's stiffness decreases [48, 50].

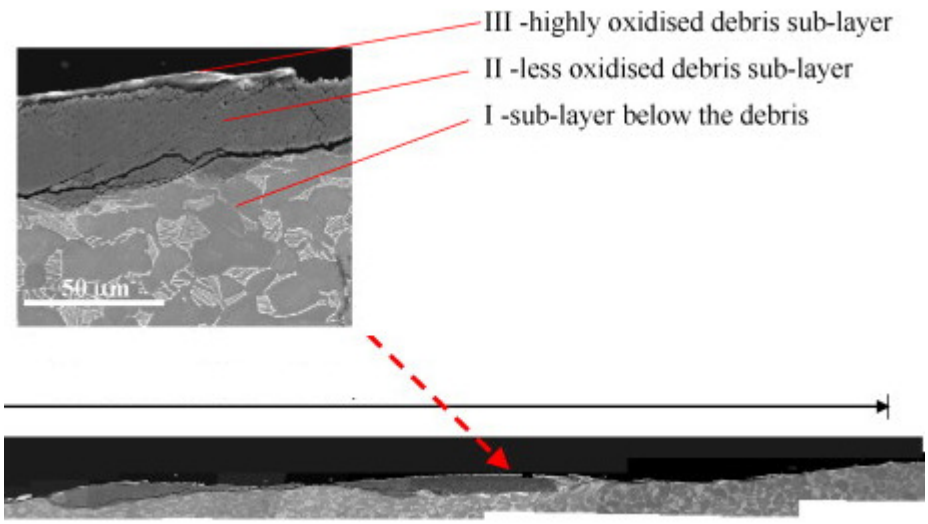

Figure 3.5: SEM images of a cross-section of the flat specimen [49].

The application of wear modelling to fretting has received increasing attention. This has been justified by the observation that normal load pattern and slip appears to be linked to fatigue life through wear behaviour. The earliest application of wear to the fretting phenomenon was by Johansson [51] who used a numerical implementation whereby the geometry was updated after a small wear increment. This was achieved by applying the Archard equation [9] in a local context, based on shear traction and slip distributions across the contact interface.

Goryacheva et al. [52] presented an analytical formulation which was applied to the cylinder on flat geometry under partial slip conditions. The study found wear in the slip regions owing to the relative movement.

McColl et al [39] also used an approach based on the Archard wear model [9] in incomplete contact, but implemented it within a finite element framework. The method was compared with experimental tests in the gross sliding regime and found a reasonable agreement with experimental wear scars (Figure 3.6).

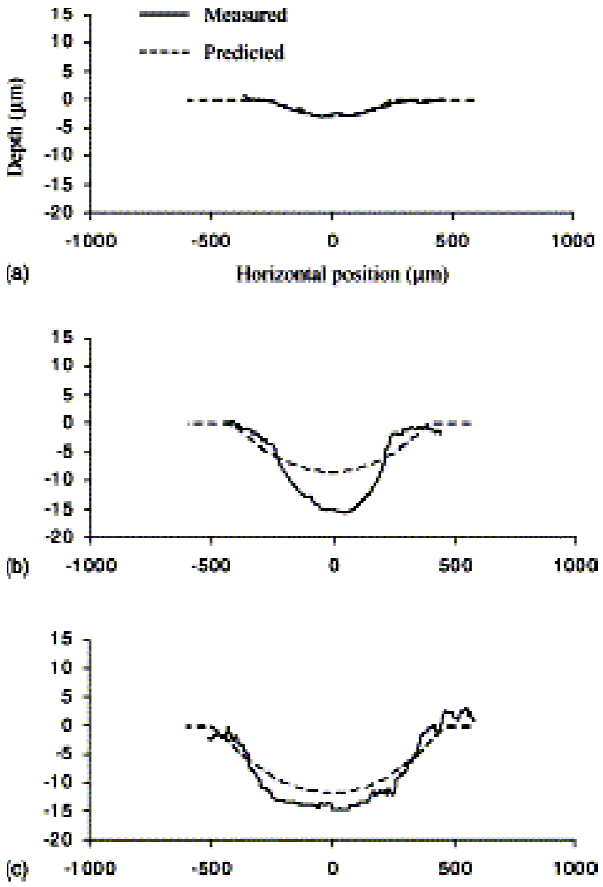

Figure 3.6: Comparison of Archard Equation based fretting wear predictions and experimental wear scars for three increasing normal loads [39].

The method was then used to compare the wear behaviour under partial slip and gross sliding conditions in incomplete contact by Ding et al [53]. It was shown that the predicted wear behaviour of the two regimes is very different; partial slip was predicted to result in the characteristics predicted by Goryacheva et al [52], whereas gross sliding was predicted to cause a significant reduction in peak contact pressure and a widening of the contact patch. Ding et al [54] also studied the predicted effect of wear on subsurface stress distributions. The partial slip simulations predicted a large increase in the shear stresses at the stick-slip interface. This suggested a possible mechanism by which the cracking observed in the stick-slip boundary could be explained.

A further development by Madge et al. [55] incorporated a number of key phenomena that are significant in fretting fatigue, namely crack nucleation combined with crack propagation in the presence of wear. Mixed-mode fracture mechanics techniques along with the short crack propagation behaviour for short crack growth were accounted for. It was concluded that the reduction in stresses caused by gross sliding could cause self

arrest of a nucleated crack, highlighting the potential benefit of wear for the increase of component life.

Although modelling approach based on the Archard wear model [9] is a great achievement in fretting fatigue, Archard model still has several limitations as this approach neglects some important factors of the fretting process such as change of microstructure, wear debris, the appearance of local plastic deformation and oxidation. Further research on this phenomenon is therefore needed. It is also found that wear contact modelling is more focussed on incomplete contact and hence the effect of singularities in complete contact has not been included.

3.2.3 Plastic Deformation

Other than wear, contact surface is also exposed to plastic deformation in the contact region due high stress in adhesive contact. Nowell et al. [56] reported the occurrence of slip bands which thicken at the edge of frictional contact due to plastic deformation. Kapoor [57] then presented the concept of ratchetting in sliding wear. It was suggested that the accumulation of plasticity by ratchetting led to ductility exhaustion and thus induced cracks parallel to the surface leading to delamination wear. Fouvry et al. [58] studied the elastic-plastic wear behaviour and suggested that the high wear regime in fretting is due to the occurrence of global surface shear plasticity, while the low wear regime is governed by local asperity plasticity. This effect has been attributed to high tensile stresses at this location to produce crack.

Peng et al. [59] have described fretting damage due to plastic deformation with the aid of diagram shown in Figure 3.7. This is explained as follows:

a. Firstly, the damage zone is of annular shape, the wear zone presents some ploughing grooves and few oxidative debris particles scatter at the loading end of the scars. No cracks can be detected on the cross-section. In this stage, the wear mechanism of fretting damage zone is the combination of abrasive wear and oxidative wear.

b. Secondly, with the increase of the number of cycles, the damage is aggravated with enlarging damage zone, deepening of ploughing grooves, detachment of particles and debris accumulation. Also, no surface crack and fatigue crack initiate at this stage.

However, the wear mechanism in the fretting damage zone is changed to abrasive wear, oxidative wear and delamination.

c. Thirdly, damage is further aggravated as a function of the number of cycles and the detached area is greatly enlarged. Surface inclined cracks are formed both on the contact surface and the cross-section. But no fatigue crack with higher propagation rate can be found. The wear mechanism in the fretting damage zone is never changed during this stage.

d. Lastly, the fatigue crack nucleates at the subsurface. It is controlled by the contact stress and propagates along a direction near 60° to the contact surface and links up to the surface inclined crack on the other side. When the crack depth exceeds that of the maximal contact stress, crack propagation turns to a higher level due to the coupling of contact stress and plain bending fatigue stress. Finally, the crack turns to a direction perpendicular to the contact surface, which is controlled only by the plain bending fatigue stress. Once the crack propagation enters into Stage III, the rupture of the sample occurs soon.

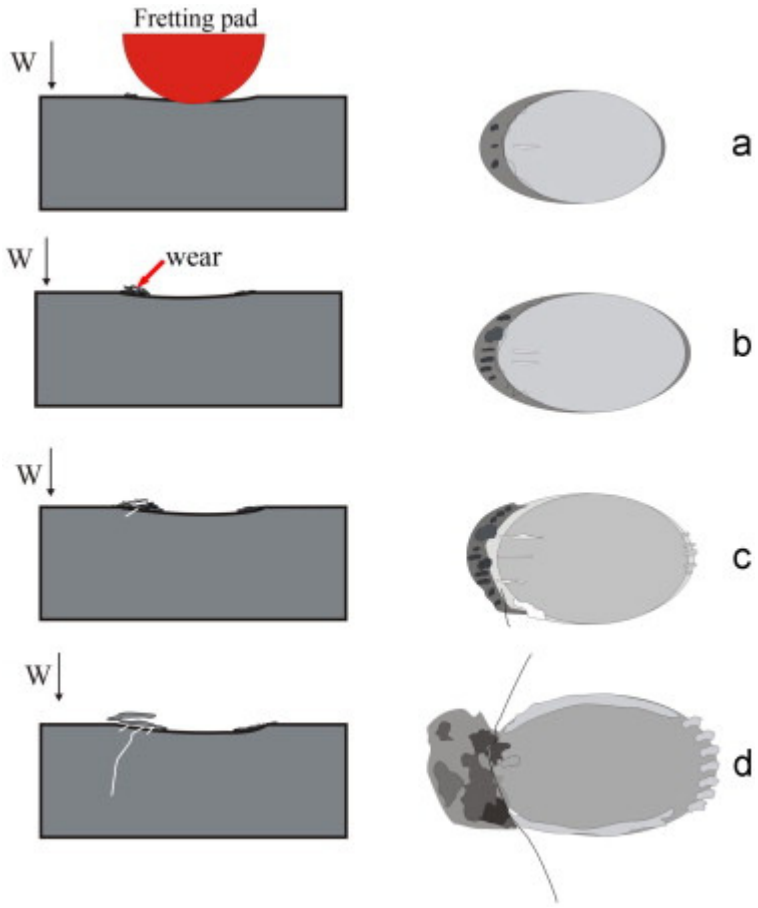

Figure 3.7: Physical model of damage development in bending fretting fatigue.

Ambrico and Begley [60] have used finite element models to study plasticity in fretting for the partial slip case under severe normal loading conditions. Several plasticity models are studied in their analysis; elastic/perfectly-plastic, isotropic strain hardening and kinematic strain hardening. Several authors have continued this research [61-65]. Their work has good agreement with experiments on simulating ratcheting, subsurface plasticity, and wear scar at the edge that leads to crack nucleation in fretting contact.

Most works on plastic deformation during wear process are concerned with fretting wear. Applying this work to fretting fatigue problem could enhance fretting fatigue analysis.

3.2.4 Other factors which affect crack initiation

Cracks can nucleate during fretting fatigue by several possible mechanisms. The most commonly proposed is high localised cyclic stress affected by the contact configuration [66, 67]. The other factors are adhesively contacting asperities, stress concentration of asperities from abrasion, delamination, pits, and rupture of surface films with subsequent exposure to the environment that reduce fracture energy [50].

It has been suggested by Hoeppner [68] that fretting decreases fatigue life by creating an initial "flaw" or crack at a very early stage of fatigue. Tests were conducted during which the fretting pads were removed at different periods during the life of specimens. The tests showed that fatigue life reduction occurred even after a specific amount of fretting damage.

3.2.5 Fretting Fatigue Crack Initiation Prediction

Fatemi-Socie (FS) and Smith-Watson-Topper (SWT) have developed popular models in fretting fatigue life prediction methodology. Lykins et al [66, 67] evaluated the performance of various lifing parameters for a titanium alloy, Ti-6Al-4V, in cylinder-on-flat geometry. They conducted a finite element analysis to obtain the stress and strain distributions and found fretting fatigue failure to be in good agreement with SWT and FS criteria. A plot of the SWT parameter against the number of cycles to initiation is shown in Figure 3.8 for plain fatigue and fretting fatigue tests. A reasonable correlation was obtained, although some experimental scatter was observed for fretting fatigue results.

They found that the predicted angles using the SWT parameter were not in agreement with experimental observations but the maximum shear stress range parameter showed a better correlation. It was suggested that initiation in Ti-6Al-4V is governed by the maximum shear stress range on a critical plane.

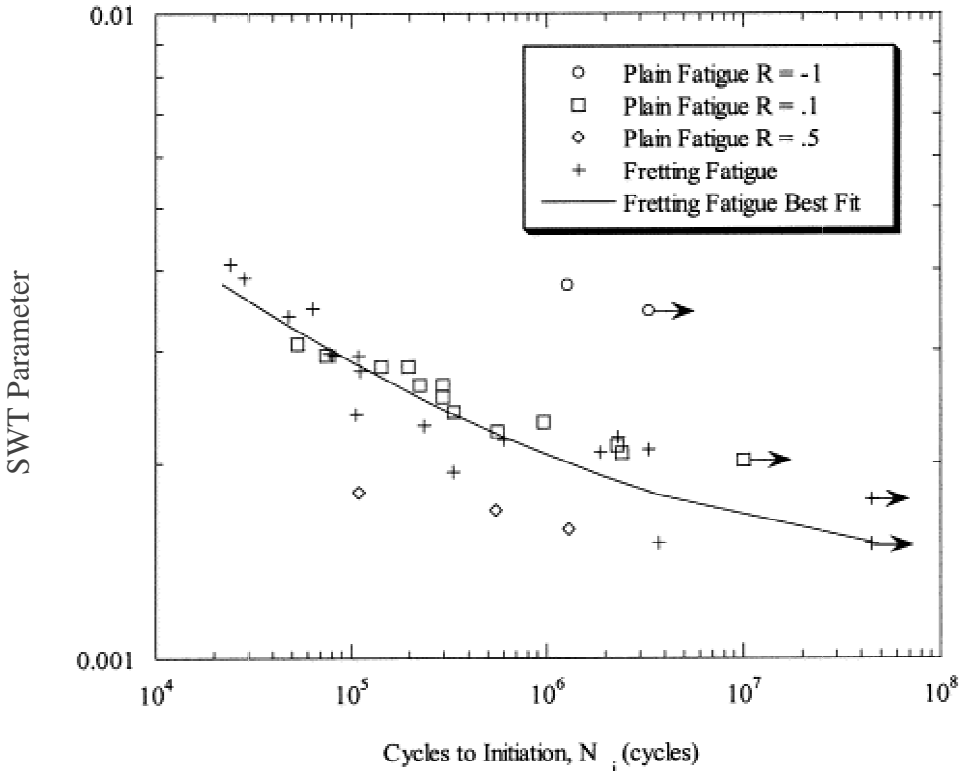

Figure 3.8: The SWT parameter against number of cycles to initiation [66].

Araujo and Nowell [69] have used SWT and FS approaches to estimate fretting fatigue initiation life in nearly complete contact and found that these methods are not adequate for rapidly varying contact stress. Averaging methods are then developed to allow the extension of the critical plane approach in cases of rapidly varying contact stress fields. It is found that a critical averaging dimension with the size of grain size of the material appears to give realistic estimates of fatigue life and predicts the observed size effect reported in the experimental work.

Talemi [26] in his prediction on incomplete contact fretting fatigue using energy based approach also used averaging methods. The averaging dimension (radius of semi-circle) was determined as the distance at which the stress is independent of mesh refinement. These results suggest that the averaging parameter may not be a true material constant and depends on geometrical and loading factors.

Madge et al [70] included the effect of material removal due to wear using Archard method [71] in incomplete contact. Their analysis show that wear over lifetime produces a major evolution of SWT and hence affect the predicted fatigue life and failure position. SWT parameter is calculated in conjunction with Miner's rule to determine the fretting fatigue damage fraction, D.

$$D = \sum_{i}^{N} \frac{n_i}{N_{fi}} \tag{3.1}$$

Where n_i is the number of cycles experienced at condition i, N_{fi} is the number of cycles for crack initiation at constant condition i. N is the number of different types of conditions experienced. Crack initiation is assumed to have occurred when D reaches a value of 1. However, this method still has a weakness as it neglects the effects of near-surface features and wear debris, which is significant in severe wear [49].

3.3 Early Crack Propagation

3.3.1 Propagation

In fretting fatigue crack propagation, almost all previous research works have used fracture mechanics approach to calculate crack growth lifetime. The propagation stage in a fretting fatigue problem is substantially different from that of plain fatigue during the phase in which the crack length is less than the characteristic dimension of the contact zone [6]. In such a situation, it is essential to account for the effect of the contact stress field on the crack and contact-crack interaction. It is important, therefore, to estimate realistic values of the stress intensity factors (SIFs).

Rooke and Jones [72] used Green's function to derive the stress intensity factor for an edge crack with a point force (normal or tangential) acting at the edge of the sheet. Rooke [73] then improved his previous work to calculate the stress intensity factor for an inclined crack.

FEM has been used widely to calculate SIFs at the crack tip in pre-cracked specimens as FEM can be used to model a realistic contact behaviour. Several authors have studied the propagation stage in two dimensional analysis. Kimura and Sato [74] used an approach which extended to inclined mixed-mode cracks. Sheikh et al. [75] used a finite element model of the classic fretting bridge and studied the SIFs for several crack lengths and different crack angles with respect to the contact surface. Mutoh et al. [76] produced a

finite element model that included the contact influence with the crack located at the end of the contact zone. They considered several crack propagation increments to simulate the crack growth path and applied the estimated values of the stress intensity factors to compute fretting fatigue life. Baietto et al. [77] used XFEM to get a deeper understanding of the cracking phenomena and obtained a mixed mode crack growth law which shows a good agreement with experimental results.

The stress field in the fretting process is also affected by the surface slip. Surface slip can be very beneficial as it significantly reduces stress levels [78]. Slip also absorbs energy and is a source of damping. Another factor that influences the stress field is the wear process. In wear region, the profile of surface as well as contact stress change due to material removal or wear. Madge et al. [70] in their work show that pressure redistribution due to wear reduces the risk of crack initiation as well as crack propagation.

Contact stress at the surface will produce a heterogeneous stress field across the thickness. By applying a cyclic bulk stress, cyclic heterogeneous stress fields are produced. The heterogeneous cyclic stress field affect crack growth. Retardation slows the crack growth rate and sometimes may stop propagation [79-81]. In this early stage, study found that propagation of crack in fretting fatigue follow a small crack growth where crack growth threshold (ΔK_{th}) is lower than ΔK_{th} for long crack [82].

One problem in crack growth analysis is to determine the length of the crack to be analysed for initiation or propagation. This crack initiation length is often fixed in advance on a rather heuristic basis; in [83, 84] for example, a fixed crack initiation length of 1 mm is proposed. A further improvement is to consider that the crack initiation length can vary depending on the contact stress gradient for the given problem. This is the approach proposed by Navarro et al. [85] and has been considered in this work. It is based on a variable initiation crack length concept introduced by Socie et al. [86] for notched specimens under uniaxial loading.

3.3.2 Crack Direction

During initial propagation, cracks usually grow inclined to the fretting surface. After they reach a certain length, cracks often change direction and proceed at 90 degrees to the surface [87, 88].

Several criteria have been developed in order to understand the crack propagation direction in multiaxial stress. Amongst these criteria, three have been incorporated in ABAQUS; Maximum Tangential Stress (MTS), Mode II stress intensity factor equal to 0 (K_{II}=0), and Maximum Energy Release Rate (MERR).

MTS criterion was proposed by Erdogan and Sih in 1963 [89]. In their findings, crack propagation is governed by tangential stress which develops opening deformation at the crack tip. Crack is assumed to propagate at an angle (θ) which makes the tangential stress($\sigma_{\theta\theta}$) field in front of the crack tip, Equation (2.14b) to be maximum. MTS has become the most commonly used criterion and based on this many other criteria have been developed.

$K_{II} = 0$ criterion by Cotterell and Rice [90], is based on local symmetry. The criterion states that the crack will propagate in the direction where $K_{II} = 0$ or when the shear stress ($\tau_{r\theta}$) in the direction is equal to zero. This criterion is basically similar to the MTS criterion. MTS expects the crack to propagate at the point where $\sigma_{\theta\theta}$ (Eq 2.14b) becomes maximum, or mathematically, when the derivative of equation 2.14b = 0,

$$\frac{d}{d\theta}(\sigma_{\theta\theta}) = 0 \tag{3.2}$$

and the outcome of the derivation is:

$$\frac{d}{d\theta}(\sigma_{\theta\theta}) = \frac{K_I}{\sqrt{2\pi r}}\left[\frac{1}{4}\sin\frac{\theta}{2} + \frac{1}{4}\sin\frac{3\theta}{2}\right] + \frac{K_{II}}{\sqrt{2\pi r}}\left[\frac{1}{4}\cos\frac{\theta}{2} + \frac{3}{4}cos\frac{3\theta}{2}\right] \tag{3.3}$$

This equation is exactly the same as for $\tau_{r\theta}$ given by Eq. (2.14c).

MERR was developed by Nuismer in 1973 [91]. Energy release rate was found to be maximum under conditions when the crack was fully opened and without any shear stress which results in friction energy loss. Hence, crack deflection angle by MERR will also produce same prediction as MTS and $K_{II} = 0$ criteria.

In fretting fatigue work, MTS, $K_{II} = 0$, and MERR criteria, all were used by Faanes [92] to predict crack direction. His analysis was based on stress intensity factors which were derived by using Green's functions by Rooke [73]. Talemi [26] also used MTS, $K_{II} = 0$, and MERR criteria but with the aid of finite element analysis and found that these

results deviated from the predefined path obtained from the experimental results. These differences occur as stress intensity factors derived by Rooke are based on the assumption that normal stress and shear traction at the fretting pad are uniform throughout the applied loading cycle, whereas finite element analysis by Talemi [26] used a more realistic stress distribution for contact, Fig. 3.9.

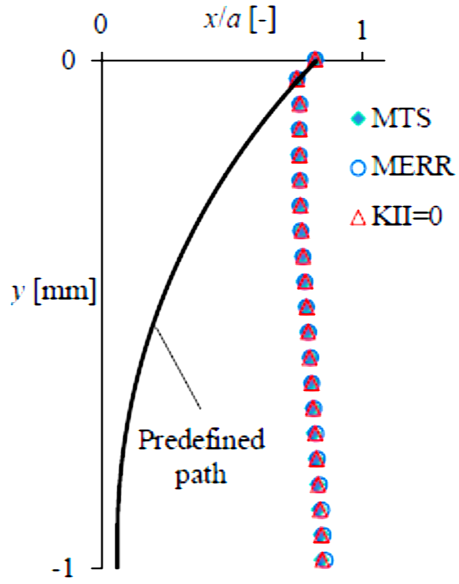

Figure 3.9: Comparison of crack propagation trajectories given by MTS, MERR, and $K_{II} = 0$ criteria with the predefined crack path based on experimental observation [26].

Giner [93] has proposed a minimum shear stress range criterion to predict crack propagation paths for fretting fatigue tests under complete contact conditions. As this criterion takes into account stress for a range of cycle, this criterion is capable of solving problems with non-proportional loading. Results based on this criterion are in good agreement with the experimental observations.

3.4 Crack Propagation and Final Failure

As the contact stress state changes with depth in the fretting specimen, a crack depth can be reached at which the contact stress state is insignificant in comparison to the bulk alternating stress**.** At this point, the effect of the fretting pads can be ignored and only the bulk alternating stress and the constant pad pressure need be considered. The propagation in this stage can therefore be analysed by using simple Paris Equation.

CHAPTER 4. REVIEW OF PREVIOUS EXPERIMENTAL WORK

4.1 Introduction

The basis for this finite element study is the experimental works of Fernando et al[24]. In this work, a general fretting fatigue test apparatus was used which consisted of flat fretting bridge pads over a specimen of rectangular cross section. A number of publications contain the information/data from this research [31, 75, 94-98] . This chapter will only briefly describe the experimental set up and present the key results from the experiments.

4.2 Experimental Setup and Specimen Geometry

The fretting fatigue test apparatus is shown in Figure 4.1. The normal load was applied through two symmetrically placed bridge pads, each with two flat feet, thereby providing a complete contact fretting action. The geometry of the specimen and the fretting pads is shown in Figure 4.2.

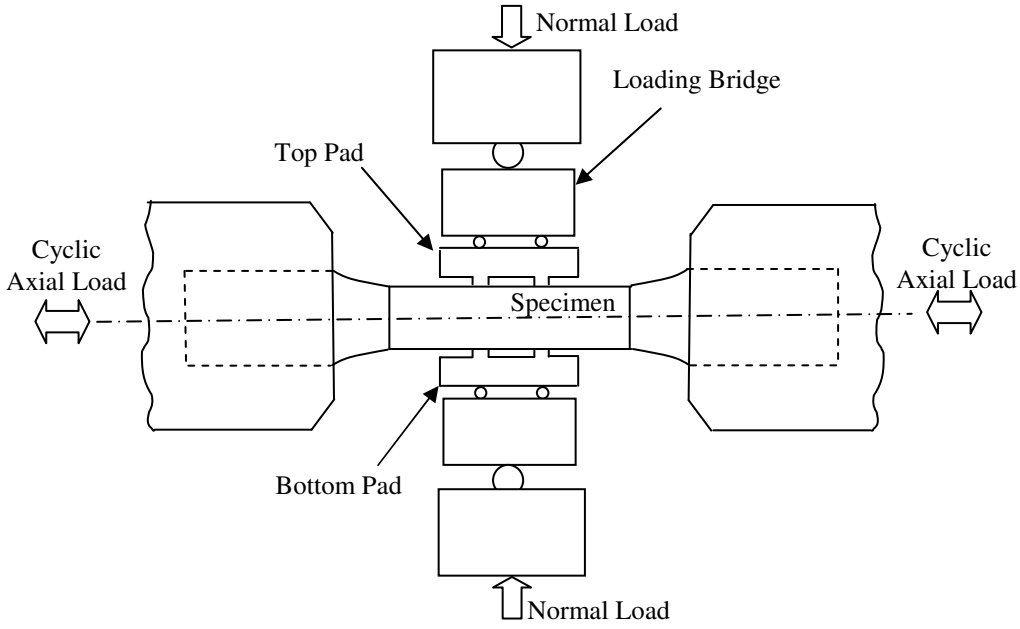

Figure 4.1: Fretting fatigue loading arrangement [24]

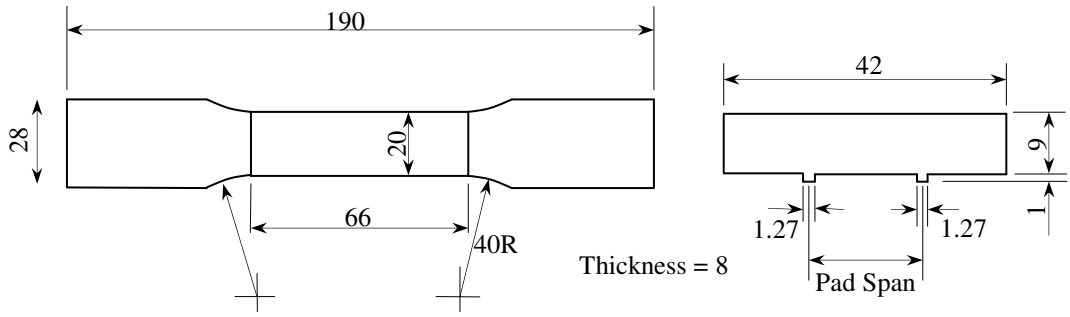

Figure 4.2: Specimen and fretting pads (all dimensions in mm) [24].

Axial load to the specimen was applied using a servo controller actuator. The normal load on the pads was applied using a proving ring. In all tests, fully reversed cyclic axial load was applied with a sinusoidal waveform of 15 Hz frequency.

The friction forces on the contact area were measured by strain gauging the pads. Each pad was kept in position, relative to the specimen, by using two symmetrically placed locating arms that were attached to the grips. The experiments used a Potential Drop technique for measuring the crack length in order to obtain crack growth data.

4.3 Material Properties

The material investigated was BS-L65, a fully artificially-aged 4 percent copper aluminium alloy (also known as Al 2014). It is a general purpose material widely used in aircraft structures, frames and external skins. The fretting pads were made of BS S98 steel (2.5% Nickel-Chrome-Moly steel), which is widely used as the main attachment and highly loaded fittings in aircrafts. Table 4.1 gives the elastic properties of these materials.

Table 4.1 Materials Properties[24].

Materials	Young Modulus, E	Poisson Ratio, ν	Yield Stress, σ_y
BS L65	74.0 GPa	0.33	420 MPa
BS S98	210 Gpa	0.29	1002 MPa

4.4 Experimental Parameters

Fernando et al. [24] used several parameters and studied their effects in fretting fatigue. Three different axial load amplitudes of 70 MPa, 100 MPa and 125 MPa with stress ratio, R= -1 were used together with various values of normal load covering the range of 20 MPa – 120 MPa. Three fretting spans were considered; 6.35 mm, 16.5 mm and 34.35 mm. Table 4.2 gives details of the parameters used for the experimental work.

Table 4.2 Experimental parameters[24].

Span (mm)	Maximum Axial Stress (MPa)	Equivalent Normal Stress (MPa)
34.35	70	80
		120
	125	80
		120
16.5	70	20
		80
		120
	100	20
		40
		60
		80
		100
		120
	125	20
		80
		120
6.35	125	60
		80

4.5 Experimental Results

In this section, some key results from the experimental works are presented and briefly discussed. The parameters of concern are the coefficient of friction, number of cycle for crack initiation, crack propagation, and fracture.

4.5.1 Coefficient of Friction

Friction force was found to be evolving in the early stage of the tests but became more or less constant for the rest of the tests. The variation of friction force amplitude with applied normal load for various values of axial load and fretting span = 16.5 mm, is shown in Figure 4.3. It can be seen that coefficient of friction (COF) is significantly affected by the normal load. A higher COF is observed at lower normal loads. The COF then falls gradually as the normal load is increased.

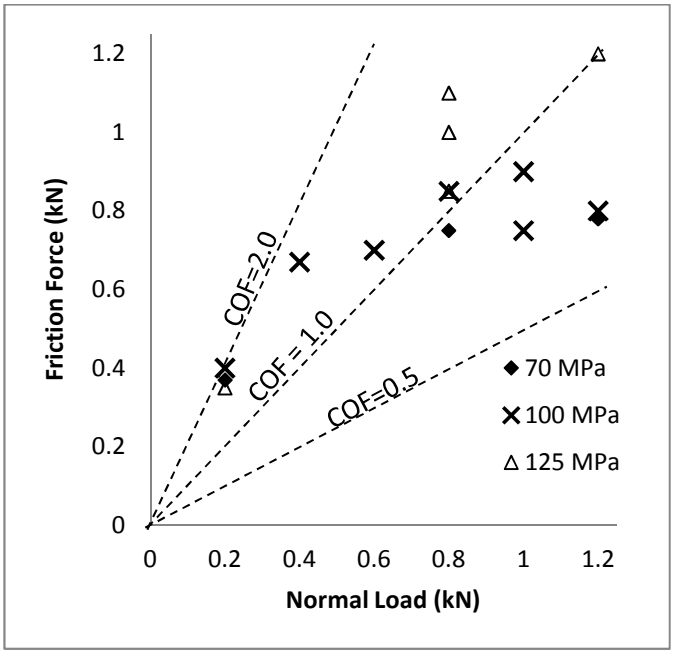

Figure 4.3: Friction force vs Normal load[24].

Fernando[31] explained this phenomena by investigating the influence of surface asperities and intersurface debris in the creation of friction force within fretting contact. The friction force was considered to be created by either direct interlocking of surface asperities, or by trapping oxide debris in between the surface asperities. In the early stage of the tests, the coefficient of friction was reported to be evolving as the fretting process polished the surface and began to create interlocking of the asperities. Friction then became constant as the interlocking process became saturated. At low normal loads, the value of friction force was insufficient to break the surface asperities and hence produced a higher

coefficient of friction. Coefficient of friction was reduced at higher normal loads as sufficient friction forces were generated to plastically deform and break some of the surface asperities to create oxide debris particles which in turn reduced the locking effect.

4.5.2 Fretting Fatigue Life

Fretting fatigue life results are presented in Figure 4.4. Due to extremely low sensitivity in measuring crack length below 0.1 mm with the technique used, detection and measurement of the crack was limited to approximately 80-100μm length. Result clearly show the effect of axial and normal load on fatigue life of fretting specimens. Both axial load and normal load make fatigue life decrease after crack initiation. The higher the axial load, the faster the specimen fail. Normal load, on the other hand, gives different patterns. At first, higher normal load makes life shorter, but then after a certain point, fatigue life increases. It seems that retardation occurs in fretting fatigue crack growth at higher normal stress.

4.5.3 Crack Propagation

Results of crack length measurements versus number of cycles normalised by fatigue life are presented in Figure 4.5. Crack initiation varies from 10% to 90 % but have different trends for each applied axial stress. For 70 MPa case, crack initiation is inclined to occur at high fatigue cycle ratio of 60 to 90%. In contrast, for 125 MPa case, crack initiation is inclined to occur at low fatigue cycle ratio of 10 to 40%. For 100 MPa case, crack initiation is scattered widely from 10 to 80%.

Focusing on the variation of crack length with fatigue cycle ratio, for specimens with axial stress values of 70 and 100 MPa, higher normal load gives longer fatigue cycle ratio for the crack to grow to a length below 2mm. However, for specimens with axial stress 125 MPa, all three normal loads produce the same trend. This trend clearly shows retardation in the crack growth process due to high normal load, as discussed in the previous section.

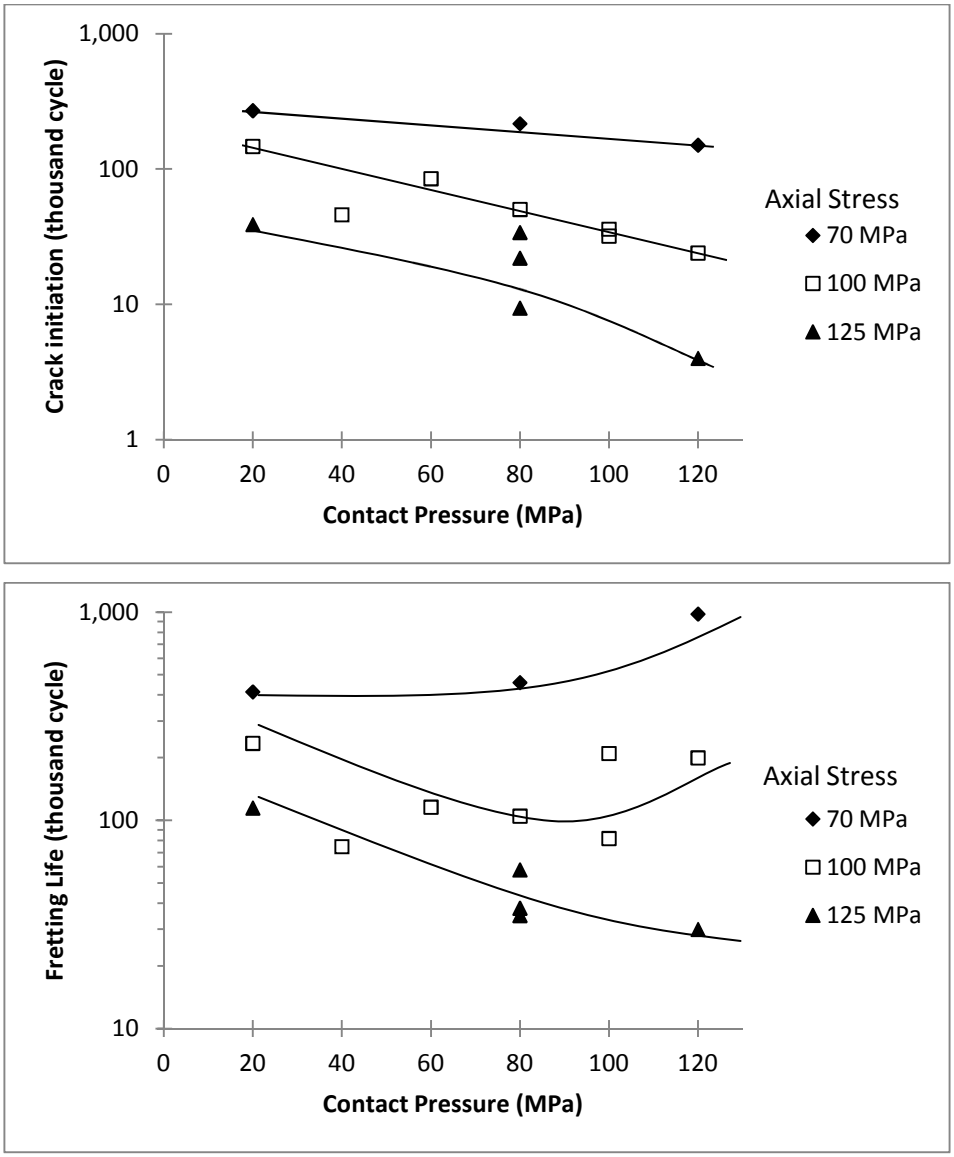

Figure 4.4: Number of cycles for fretting failure versus contact pressure[24].

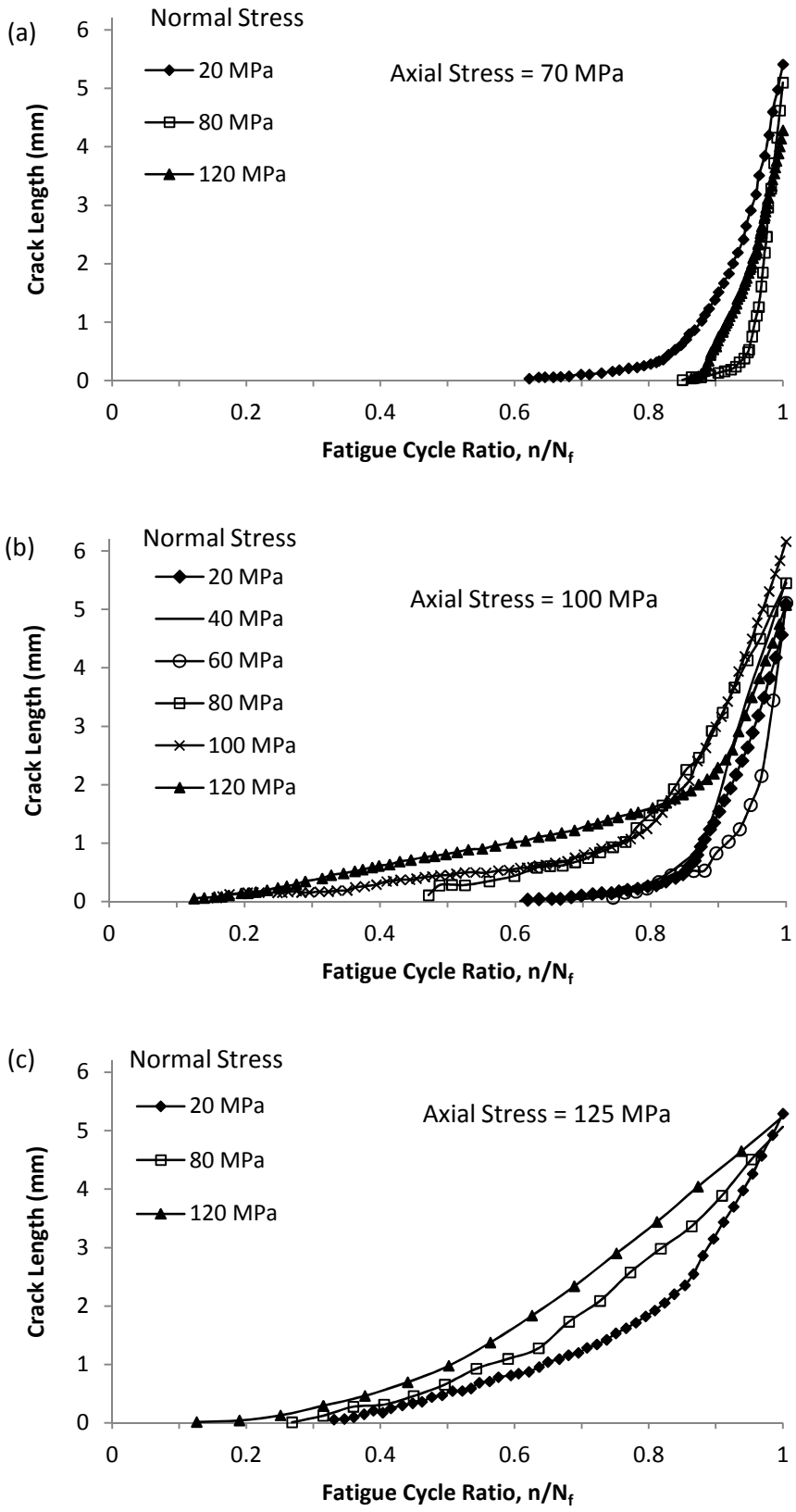

Figure 4.5: Crack length versus fatigue cycle ratio for axial load (a) 70MPa, (b) 100MPa, and (c) 125MPa[24].

Figure 4.6 shows fatigue versus crack length for different values of axial stress and normal load. In all three axial stress cases, specimen with 20 MPa normal load starts with a lower crack growth rate, but then steadily crack growth rates accelerate with crack size. In cases axial stress equal to 70 and 100 MPa, specimen with 120 MPa normal stress starts with a crack growth rate which is almost the same as with normal stress of 100 MPa. The growth rate then experiences retardation until the crack size approaches 2mm. Difference in crack growth rates for different normal loads narrows after 2mm crack length.

The crack propagation results for three different pad spans are compared in Figure 4.7. This plot has been obtained for the axial stress of 125 MPa and normal stress of 80 MPa. Pad spans of 34.35 mm and 16.5 mm give similar growth rates which are higher than the growth rate for pad span of 6.35 mm. Sheikh [75] found that the stress field for pad span 6.35 mm was being influenced by the adjacent pad.

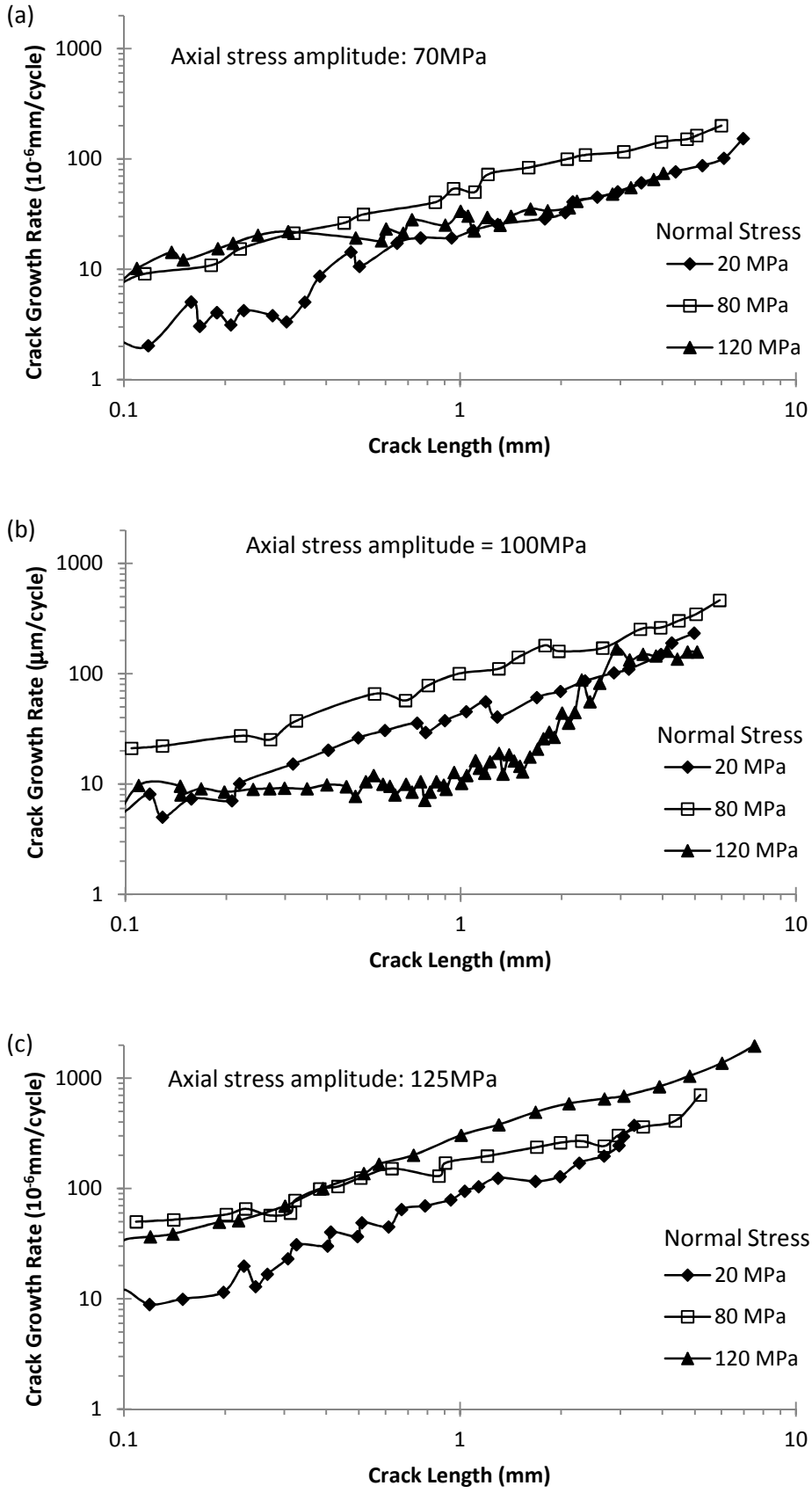

Figure 4.6: Crack Propagation rate versus crack length for normal stress of (a) 20MPa, (b) 80MPa, and (c) 120MPa[24].

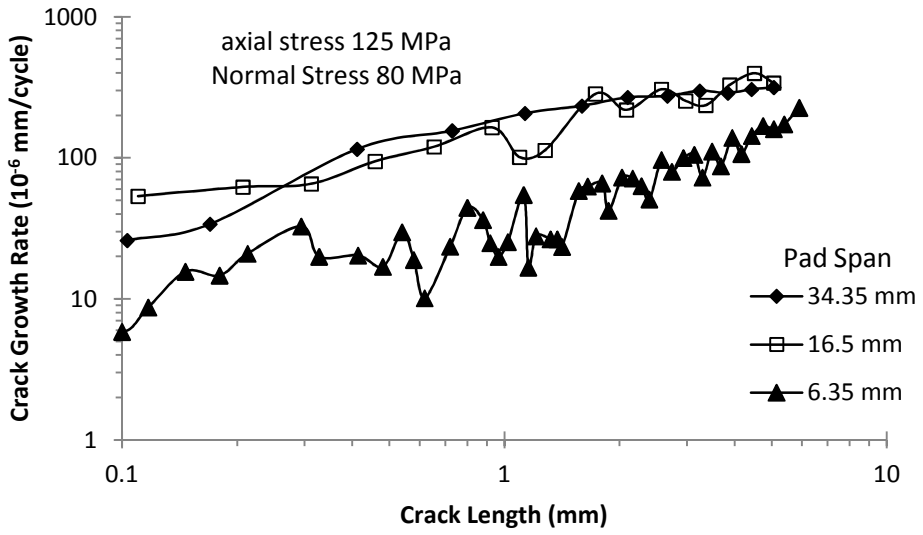

Figure 4.7: The influence of pad span on crack propagation rate versus crack length[24].

4.5.4 Crack Path

Observations from the fracture areas of the specimens revealed that multiple cracks had nucleated and grown at the contact location. However, in all tests, the main crack that caused the final failure was found to be located at or near the leading edge. The crack was found to initially propagate on an inclined path before the kink and then propagated normal to the axial direction. It was also found that crack path was less severe on the side faces as compared to the inner section. This was thought to be due to the influence of stress strain state. Therefore, the specimen was grinded 2-3 mm of the side in order to study the crack in the plane strain regime.

The crack path is illustrated in Figure 4.8 and results from the measurements given in Table 4.1. In almost all tests, the crack was found to nucleate at an angle of approximately 45 to 60 degrees to the normal axis, and this initial growth continued to a depth of up to 30 μm. The exact depth was difficult to measure as some surface was worn out due to fretting wear. The crack then turned to a path with less steep angle between 15 to 30 degrees to the normal axis. Finally the crack turned to a plane normal or very close to the normal axis.

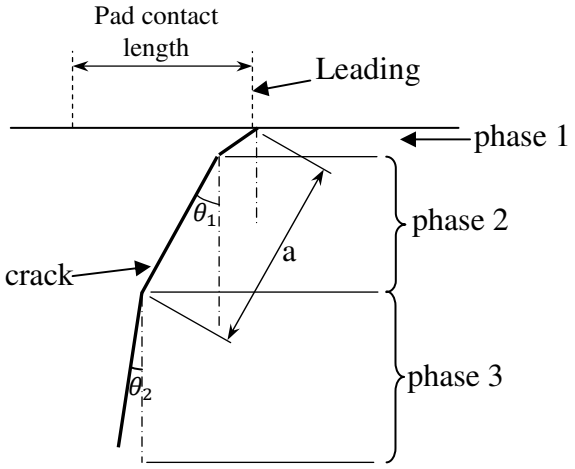

Figure 4.8: Fretting crack location and path[24].

Table 4.3 Crack path data[24].

Test no.	Axial Stress Amplitude (MPa)	Normal stress (MPa)	Friction stress (MPa)	a	θ_1	θ_2
1	70	20	36	0.52	21	0
2	70	80	74	0.93	18	4
3	70	120	77	0.21	27	4
4	100	20	39	0.46	25	2
5	100	80	84	0.46	22	3
6	100	120	79	0.34	25	3
7	125	20	34	0.40	28	0
8	125	80	98	0.75	19	0
9	125	120	118	0.43	22	5

4.6 Conclusions

This experimental work systematically investigated the effect of three parameters; normal load, axial load amplitude, and pad span, on fretting fatigue crack growth. With the experimental data for friction, number of cycle for crack initiation, crack propagation, and fracture, it is now possible to construct a comprehensive simulation model for fretting fatigue.

CHAPTER 5. MODEL DEVELOPMENT FOR FRETTING FATIGUE LIFE PREDICTION

This chapter describes the methodology behind the model development and analysis to predict life in complete contact fretting fatigue. This methodology utilises the Finite Element Method (FEM) for the development of the model. It is described here in detail with essential steps followed in this research in order to obtain accurate and valid results.

5.1 Research Framework

Modelling and analysis of life prediction in fretting fatigue have been carried out in various stages by different researchers [55, 99]. Most researchers divide fretting fatigue formulation into 3 stages; crack nucleation, stable crack growth, and final fracture.

A different approach is followed in this work for crack propagation in which small (short) and stable (long) cracks are considered separately. This approach thus gives due importance to small crack growth in the propagation stage. Hence, in this analysis, fretting fatigue failure simulation is divided into four stages; crack nucleation, short crack growth, stable (long) crack growth, and final fracture. The flowchart in Figure 5.1 shows the basic framework for the model to predict total life.

In depth studies have been carried out for each stage. A comparison with experimental results and the theory (discussed in literature review) has been made in order to understand better the correlation between the number of cycles to failure and the typical loading conditions in fretting.

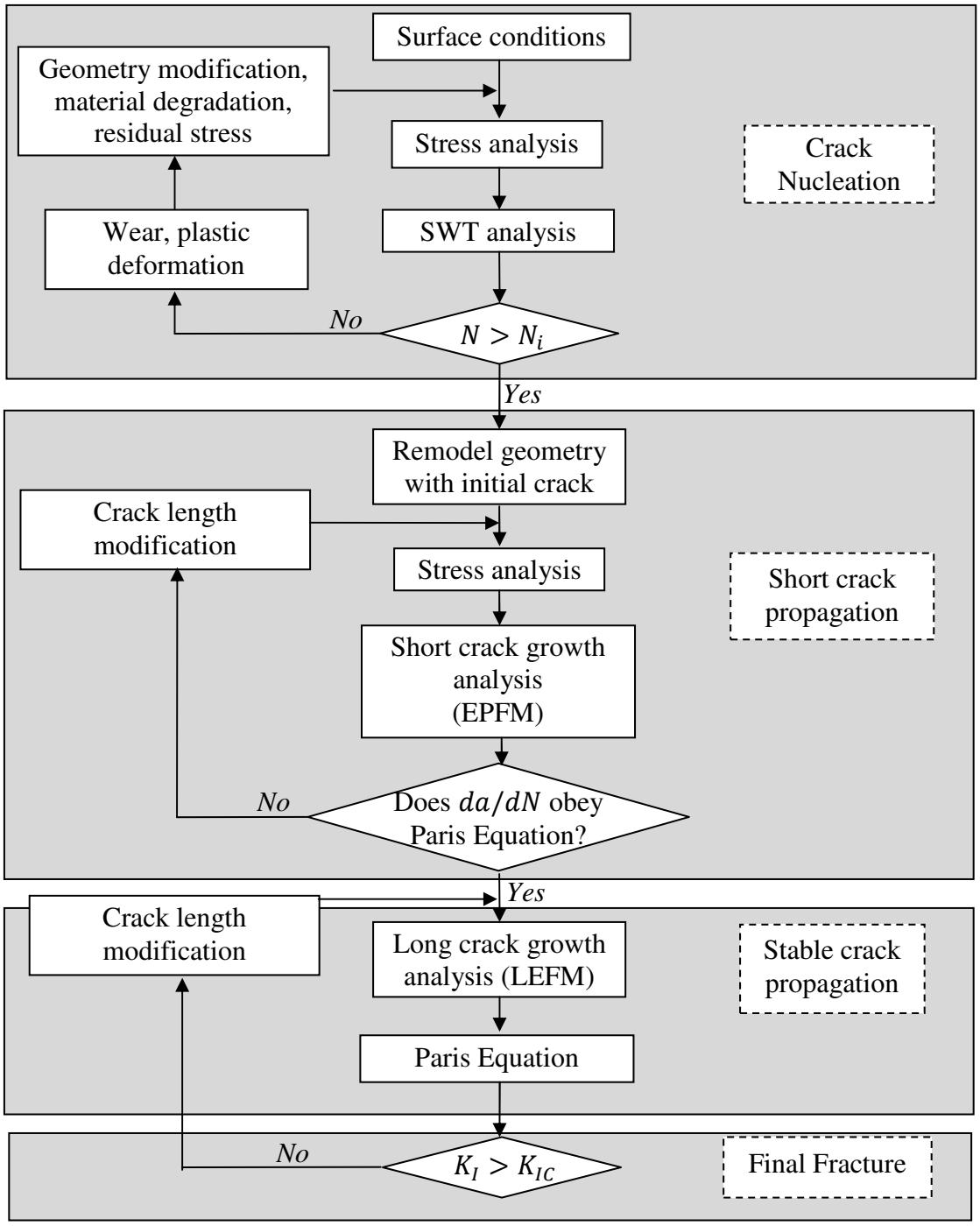

Figure 5.1: Framework for the model developed for total life prediction in fretting fatigue

[SWT: Smith Watson Topper, N_i: Number of cycles for crack nucleation, da/dN: crack propagation rate, K_I:Stress Intensity Factor ,K_{IC}:Fracture Toughness]

5.2 Crack Initiation

Wear and fatigue are the main factors in the formation of fretting fatigue cracks. Effects of wear and fatigue are dependent on several factors related to material, loading, and environment, as discussed in Chapters 2 and 3. Modelling and analysis of contact profile, wear, and crack growth [53, 70, 76, 98, 100, 101] have been included in crack initiation analysis.

5.2.1 Contact Friction Model Development

Coulomb friction model, as described in Chapter 2, is widely used in modelling contact friction. The commercial finite element software usually employs a relatively simple form of the Coulomb friction model. However, the discontinuous nature of friction implies that more sophisticated algorithms are required. In ABAQUS, two different contact algorithms are used. These are Lagrange multiplier method, and Penalty method.

The Lagrange multiplier enforces sticking following the Coulomb Friction Model. The computational cost is high and in some cases such as mixed stick-slip and penetration, this method prevents convergence when procedures such as Newton solution scheme are used. The Penalty method, on the other hand, allows a small ‘elastic slip’ to occur at surface points when the shear stress is less than the critical value for sliding. Elastic slip improves the convergence behaviour of the contact model.

In complete contact analysis, sharp edges give problems due to node penetration (Figure 5.2) although current version of Abaqus includes a special algorithm to avoid node penetration. In this analysis, the element size near contact edge is set to be very small ($10\mu m$) to minimise the node penetration effect. As the Lagrange multiplier method for friction modelling is found to be not convergent because of the penetration problem, the Penalty method is used in this work.

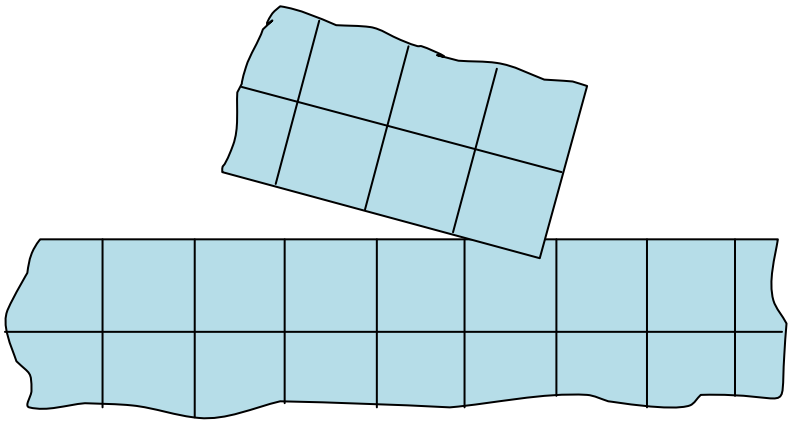

Figure 5.2: Node Penetration due to sharp edge

5.2.2 Wear Model Development

The wear simulation technique developed here closely follows the technique developed by McColl et al [39], and implemented by Ding [53] and Madge [55, 101]. Wear formulation using Archard equation [9] has been discussed in Section 2.32. Referring to Eq. (2.6), wear at a certain point on the contacting surfaces can be expressed as:

$$\frac{h}{S} = kP \tag{5.1}$$

where h is the wear depth (m), k is the dimensional wear coefficient and P is the contact pressure (MPa). The differential formulation of Eq. (5.1) is:

$$\frac{dh}{dS} = kP \tag{5.2}$$

Based on Eq. (5.2), a numerical approach has been developed to simulate fretting wear. The modified Archard equation is then applied as follows:

$$\Delta h(x,t) = k\, p(x,t)\, \delta(x,t) \tag{5.3}$$

where $\Delta h(x,t)$, $p(x,t)$ and $\delta(x,t)$ are the incremental wear depth, contact pressure, and relative slip at point x and time t, respectively.

Due to computational constraints it is not efficient to model each cycle explicitly. Hence, a cycle jumping technique, similar to that described by Ding[53], is employed which works on the assumption that wear is constant over a specified number of cycles.

By multiplying the incremental wear with a cycle jumping factor ΔN, N number of actual wear cycles are simulated in one finite element calculation step. Equation 5.3 thus becomes:

$$\Delta h(x,t) = \Delta N \; k \; p(x,t) \; \delta(x,t) \tag{5.4}$$

In order to ensure the validity of the assumption that the solution is approximately independent of the cycle jump size ΔN, the effect of varying the cycle jump factor ΔN on SWT parameter was investigated for each simulation. Figure 5.3 shows the comparison of the SWT parameter over a critical element using three different cycle jump factors. It shows a small difference in the early stage for lower values of equivalent cycles, but the difference is narrowed as the number of cycles increase. Although, all three cycle jumps are found to be in reasonable agreement, only 20 and 50 cycles are used in the analysis.

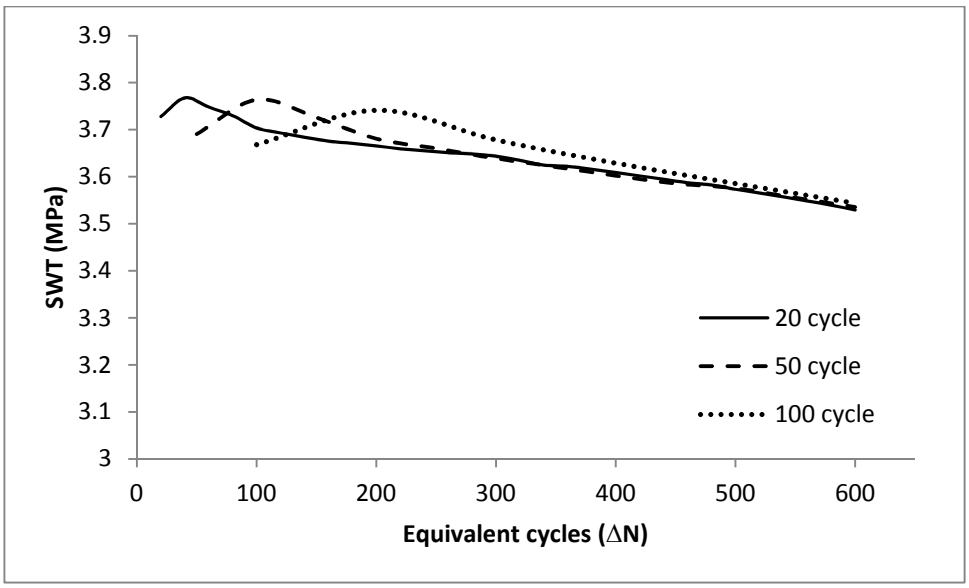

Figure 5.3: Effect of cycle jumping on SWT value for a specimen with axial stress = 100 MPa and Normal stress = 80 MPa

5.2.3 Critical Plane Damage Model

Smith Watson Topper (SWT) and Fatemi Socie (FS) methods are employed here. SWT is generally accepted as a reliable fatigue damage parameter in cases involving tensile cracking. FS, on the other hand, is often applied in cases where shear loading dominates failure. SWT and FS are used as fretting fatigue analysis involves the application of both parameters.

In order to calculate SWT and FS parameters, element centroidal stresses and strain ranges were calculated using a two-dimensional transformation for stress and strain on every 5^o intervals over a 180^o range:

$$\sigma_\theta = \frac{\sigma_{xx} + \sigma_{yy}}{2} + \frac{\sigma_{xx} - \sigma_{yy}}{2}\cos(2\theta) + \tau_{xy}\sin(2\theta) \tag{5.1a}$$

$$\varepsilon_\theta = \frac{\varepsilon_{xx} + \varepsilon_{yy}}{2} + \frac{\varepsilon_{xx} - \varepsilon_{yy}}{2}\cos(2\theta) + \frac{\gamma_{xy}}{2}\sin(2\theta) \tag{5.1b}$$

$$\gamma_\theta = -\frac{\varepsilon_{xx} - \varepsilon_{yy}}{2}\sin(2\theta) + \frac{\gamma_{xy}}{2}\cos(2\theta) \tag{5.1c}$$

Where σ_θ, ε_θ, and γ_θ are the normal stress, normal strain and shear strain on a Cartesian (x, y) plane at an angle θ.

As the contact surface profile and surface material properties continuously evolve due to plastic deformation and wear effects, the calculated nucleation life is also affected. Therefore, it is necessary to calculate cumulative SWT and FS parameters to represent the cyclic life. Miner's rule [102], is used in the cumulative damage model for failure in this analysis. According to Miner's rule, failure will occur when summation of number of applied cycles (n_i) over predicted number of cycles to failure (N_{fi}) for N blocks is equal to 1.

$$D = \sum_{i=1}^{N} \frac{n_i}{N_{fi}} = 1 \tag{5.6}$$

5.2.4 Averaging Method

Complete contact was found to produce stress singularities at the contact edge. This stress singularity is extremely localised and decreases very rapidly away from the contact edge. As the SWT parameter depends upon stress, this parameter is also singular for an element on the surface and rapidly decreases with depth, as shown in Figure 5.4.

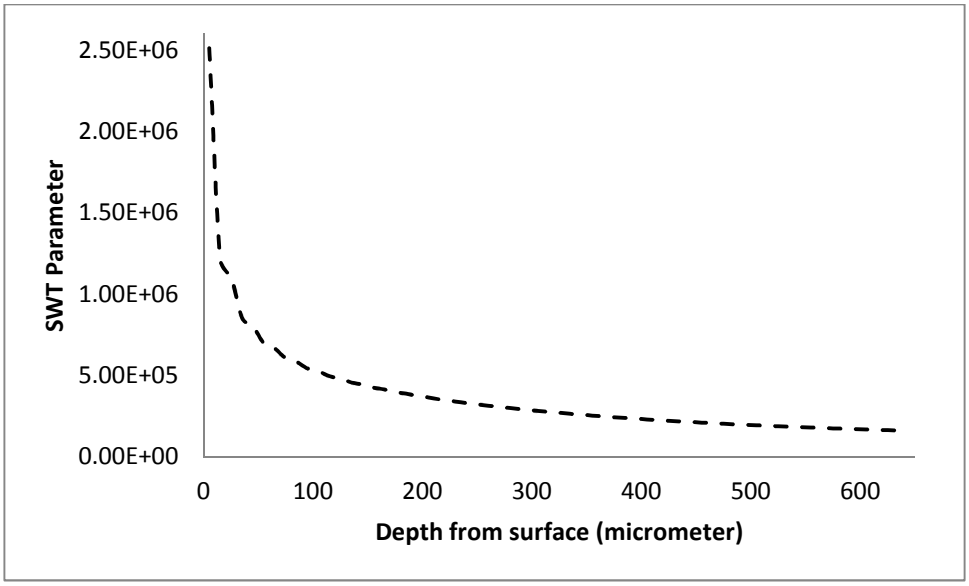

Figure 5.4: Variation of the SWT parameter with depth measured from the surface for a specimen with axial stress of 100MPa and Normal Stress of 80MPa.

In order to take the effect of singularities into account, an averaging technique is used in this analysis. This analysis uses averaging of SWT parameter, as proposed by Aroujo[84] over several elements on a certain area near the critical element to produce an average SWT parameter (SWT_{avg}).

Figure 5.5 gives a schematic representation of the averaging method used here. An assumption is made that the averaging area should be the square of the element that corresponds to crack nucleation and develops until the size measured in experimental work (0.1mm). The second assumption is that the crack nucleates at the critical element and produces a short crack in the direction of maximum shear stress. With these assumptions, the averaging area starts with the critical element at the corner, and a square area element to the crack direction. Several square areas with different average lengths of side (l_{avg}) are used to find the best averaging area size. The average stress and strain over all the elements in the chosen area are then obtained to determine the average SWT parameter (SWT_{avg}) and predict the number of cycles required to produce crack initiation.

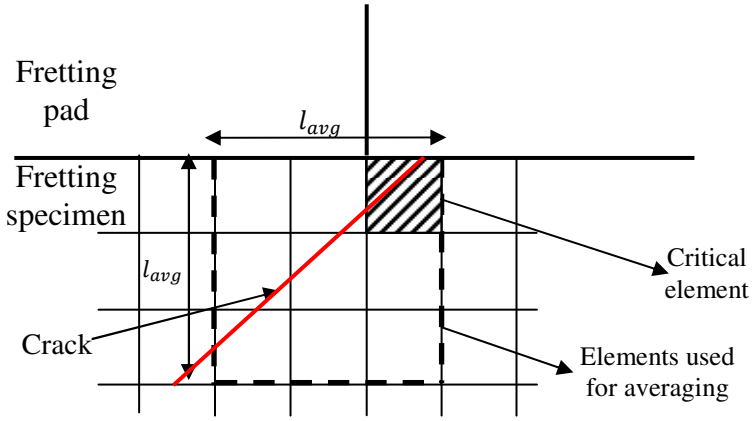

Figure 5.5: Schematic description of the averaging method used for obtaining an average value of the SWT parameter.

5.3 Early Crack Growth Modelling

Once the crack has nucleated, the analysis is then focussed on fracture mechanics analysis. As the contact stresses influence the early stage of crack growth, it can therefore be considered as multiaxial fatigue crack growth. However, the influence of multiaxial stress field progressively decreases as the crack grows. Consequently, under the multiaxial stress state created by fretting loads, it is possible for cracks to change direction. Hence, two important aspects to be considered in this phase are crack orientation and crack propagation.

5.3.1 Crack Orientation

Fatigue crack initiation has been found to be in the direction of maximum shear. Early crack will start to follow this direction (shear dominant) before changing to a mixed mode, and then gradually become perpendicular to the axial fatigue load.

As discussed in literature review, two methods that are widely used in predicting crack direction in early fretting fatigue crack propagation are based upon Maximum Tangential Stress (MTS) criterion and Maximum Tangential Stress Range (ΔMTS) criterion. Both criteria will be used and compared in this analysis.

In order to obtain the maximum value of MTS or ΔMTS, K_I and K_{II} values obtained from each simulation are used as input for Equation 2.14b to calculate the tangential stress ($\sigma_{\theta\theta}$). θ is varied for each degree and plotted to get the maximum tangential stress angle and maximum tangential stress range. An example of this procedure is shown in Fig. 5.6.

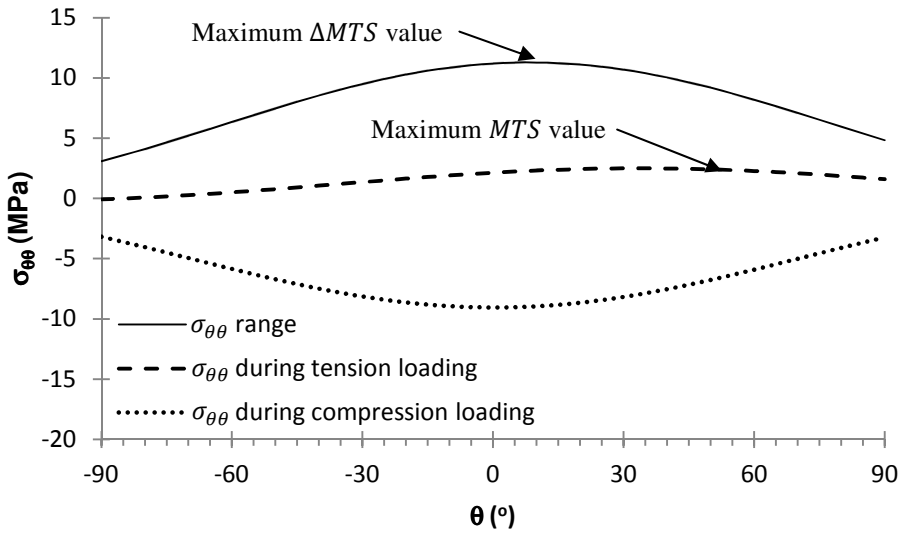

Figure 5.6: Example of $\sigma_{\theta\theta}$ value over 180° range

Crack direction is changed gradually for 0.05mm crack length increments until the crack direction become perpendicular to the axial fatigue load.

5.3.2 Crack Propagation

In Abaqus, crack propagation can be modelled by either using conventional Finite Element Method (FEM) or eXtend Finite Element Method (XFEM) approaches. In order to model stationary discontinuities, such as cracks with the conventional approach, it is required that the mesh conforms to the geometric discontinuities. Therefore, considerable mesh refinement is needed in the neighbourhood of the crack tip to capture the singular asymptotic fields adequately. Modelling a growing crack is even more cumbersome because the mesh must be updated continuously to match the geometry of the discontinuity as the crack progresses.

XFEM alleviates the shortcomings associated with meshing crack surfaces. It is an extension of the conventional FE method based on the concept of partition of unity[103], which allows local enrichment functions to be easily incorporated into a FE approximation[104]. The main advantages are that the mesh does not need to conform to the crack boundaries (crack faces) to account for the geometric discontinuity. Furthermore, mesh regeneration is not needed in crack propagation simulations. Therefore, only a single mesh, which is often easily generated, can be used for any crack length and orientation.

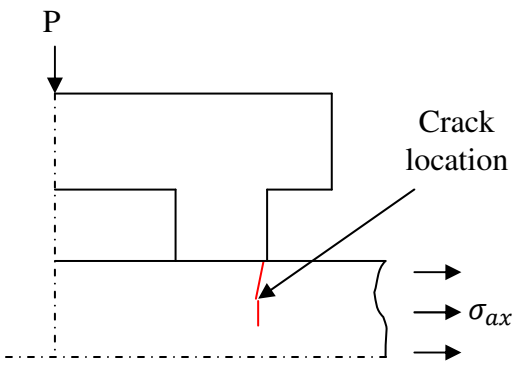

Figure 5.7: Location of crack initiation

The main fretting crack is nucleated at the leading edge (Figure 5.7) where the contact produce stress singularities on the specimen. These singularities make a large localised deformation on the surface near the edge. This phenomenon gives problem to XFEM method where large distortion occurs at locations where mesh is enriched by XFEM. Hence, conventional Finite Element Method (FEM) is the only option to analyse the crack propagation.

In the early stage of crack growth, the contact stresses influence the crack growth propagation, producing high stress gradients and resulting in multiaxial fatigue crack growth. In this stage, initially, crack growth rate (da/dN) is obtained by LEFM analysis and Paris equation. This model is then compared with EPFM model and discussed for the effects of multiaxial stress and high stress gradients at the edges of the fretting pad on crack growth rate.

5.4 Stable Crack Growth and Final Fracture Modelling

Stable crack growth is defined as the region where crack propagation obeys the well-known Paris law and follows the maximum K_I direction. This is the final stage after which the number of cycles for life prediction are obtained and compared to the experimental results. In this stage, as crack grows further, fretting pad effect is diminished and propagation is found to be solely influenced by fatigue loading.

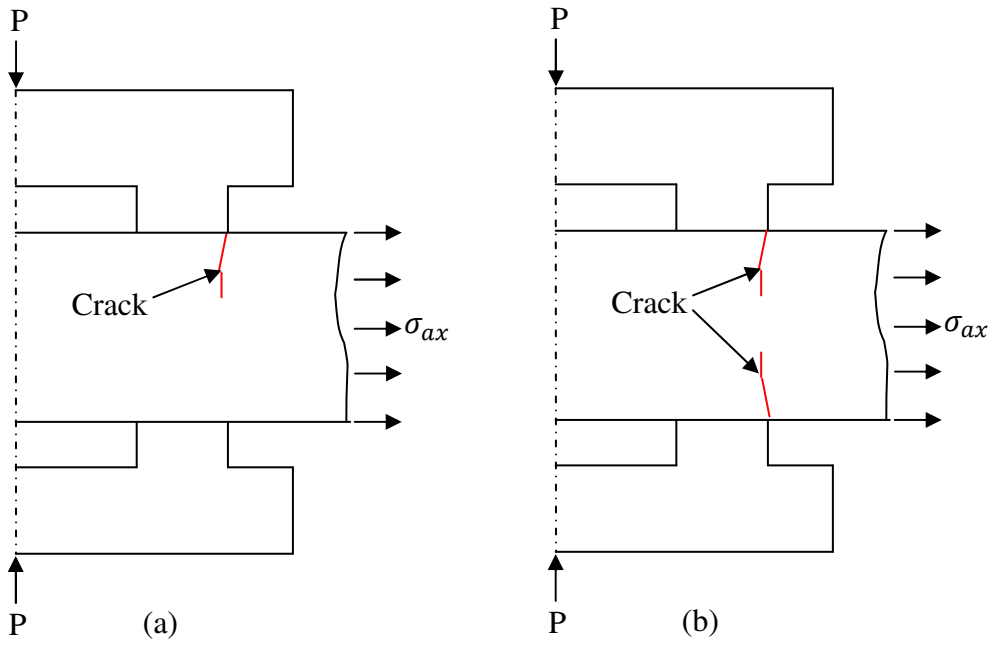

Figure 5.8: (a) Single edge crack and (b) Double edge crack

In experimental work, crack for some specimens propagate from both side, but there also some specimens where crack only propagates from one side of the surface. As the main crack grows even further, stress intensity factor will be different for the cases of single edge crack and double edge crack (Figure 5.8). Hence, the analysis for both cases are required in this stage.

Total lifetime prediction is then produced by summing up the prediction for crack initiation and crack propagation.

CHAPTER 6. CRACK INITIATION IN COMPLETE CONTACT FRETTING FATIGUE

6.1 Introduction

In this chapter, Finite element prediction of crack nucleation behaviour in complete contact fretting fatigue is presented. As discussed earlier, complete contact will create stress singularity at the edge of the contact. Thus, this analysis will discuss crack nucleation behaviour in the presence of stress singularities with the fretting parameters involved.

In order to present a clear picture, this analysis will start with linear elastic analysis, followed by elastic-plastic analysis, and lastly an analysis in the presence of wear. Smith Watson Topper (SWT) damage parameter will be used for fretting fatigue crack initiation and life prediction. In addition, Fatemi Socie (FS) parameter will also be used to analyse damage in shear, again in the presence of stress singularities.

6.2 Model Description

Specimen geometry and schematic test arrangement used in the experimental work [24] has been described in Chapter 4. Due to symmetry, a quarter 2D finite element model has been used to represent the fretting fatigue tests, as shown in

Figure 6.1. Since the specimen is 8 mm thick, plane strain elements are used in the analysis. Mesh is refined towards the edges of contact region with a coarse mesh away from the contact region to reduce processing time. Matched meshes are used on the master and slave contact surfaces.

A Lagrange multiplier contact algorithm is used to strictly enforce the sticking condition when shear stress is less than the critical value according to the Coulomb friction law [104]. The coefficient of friction used in this analysis is based on the values extracted from the experimental analysis described in Section 4.5.1.

The loading history is represented in Figure 6.2. In the first analysis step, a normal load, P is applied to the fretting pads. In the next step, the specimen is loaded by a cyclic fatigue load $\sigma(t)$ with a maximum value σ_{max} and a stress ratio of R = -1.

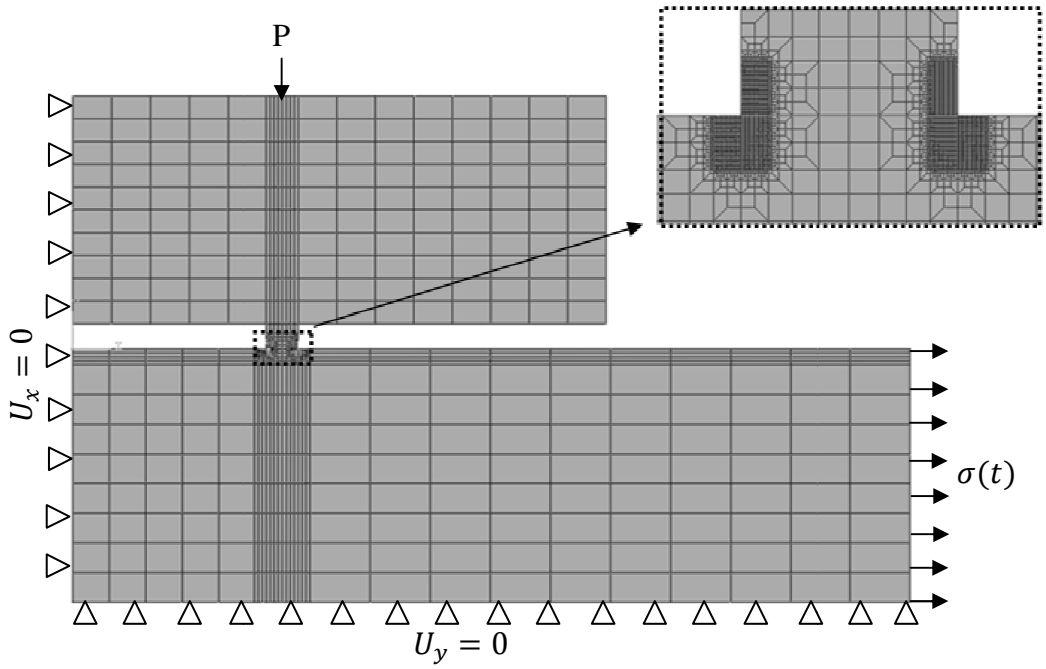

Figure 6.1: Finite element model of a quarter of the fretting specimen-pad arrangement.

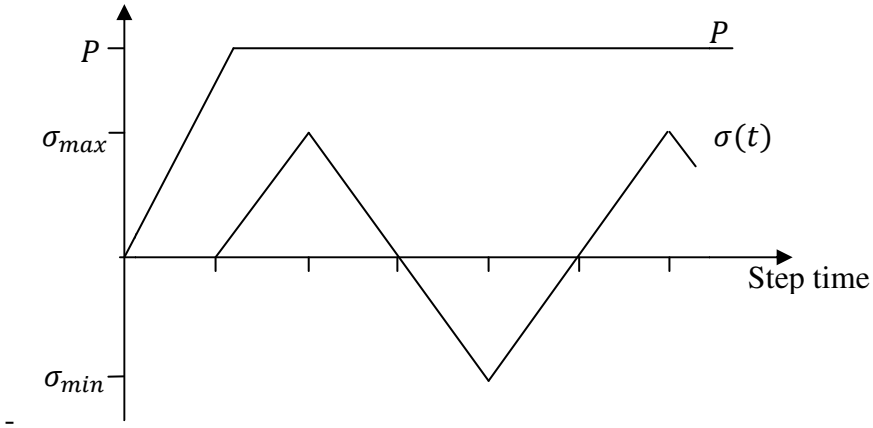

Figure 6.2: Normal load and cyclic axial load history applied to the finite element model.

The analysis is carried out using Computer Shared Facilities (CSF), A cluster of machines which included Intel and AMD processors with various specs, and owned by the school of Mechanical, Aerospace and Civil Engineering, University of Manchester. in total can submit up to 288 cores in the multiple nodes which are connected with Infiniband at any one time. By using Single core, LEFM analysis for one complete cycle of fatigue take 1 minutes 20 to 2 minutes 25 seconds, varying between specimens. Much higher

computational time is taken by both EPFM model and wear model where average of 6 minutes 20 second to 8 minutes is needed for each cycle.

Crack initiation location and the number of cycles for initiation is determined by implementing SWT and FS parameters on the critical plane where the product between the maximum stress and the total strain amplitude is maximum. Element centroidal stresses and strain ranges were calculated using the two-dimensional transformation equations for stress and strain at 5° intervals over a 180° range. The maximum normal stress σ_{max}, and the corresponding range for normal strain $\Delta\varepsilon$ and shear strain $\Delta\gamma$ were obtained to determine the SWT and FS values.

Fatigue parameters in SWT and FS calculations were obtained from the strain life data for Aluminium Alloy 2014 collated by Walker et al [105] and shown in Figure 6.3.

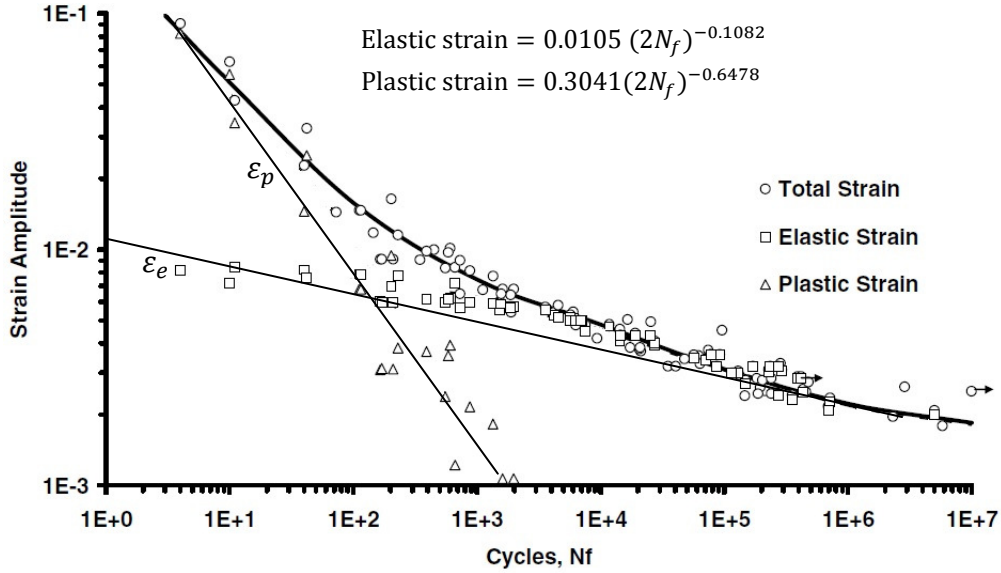

Figure 6.3: Strain-Life Curves for 2014-T6/-T651[105].

Based on Section 2.4.1 and Figure 6.3, fatigue parameters that will be used in SWT and FS fatigue crack initiation criteria are as follows:

$$\varepsilon_f' = 0.3041$$

$$\gamma_f' = \sqrt{3}\varepsilon_f'$$

$$c = -0.6478$$

$$\frac{\sigma_f'}{E} = 0.0105$$

$$\tau_f' = \frac{\sigma_f'}{\sqrt{3}}$$

$$b = -0.1082$$

6.3 Validation of finite element model against theory

In order to validate the finite element model, fundamental stress distribution in contact, as discussed in Chapter 2, is used. Two sets of analyses are performed for validation. First analysis is to establish the best mesh size, and the second analysis is to compare the results with theory.

Several mesh sizes ranging from 100 μm to 10 μm are used in order to ensure accuracy. The pressure distribution at the contact surface for various meshes is shown in Figure 6.4. Based on this analysis, it can be seen that models with mesh sizes of 100 μm and 50 μm fail to adequately represent the singularities at the edges. On the other hand, pressure distribution profiles for models with mesh size of 25 μm and 10 μm are able to show the singularities at the edges and both are in good agreement. Hence, a mesh size 10 μm is chosen for subsequent analysis.

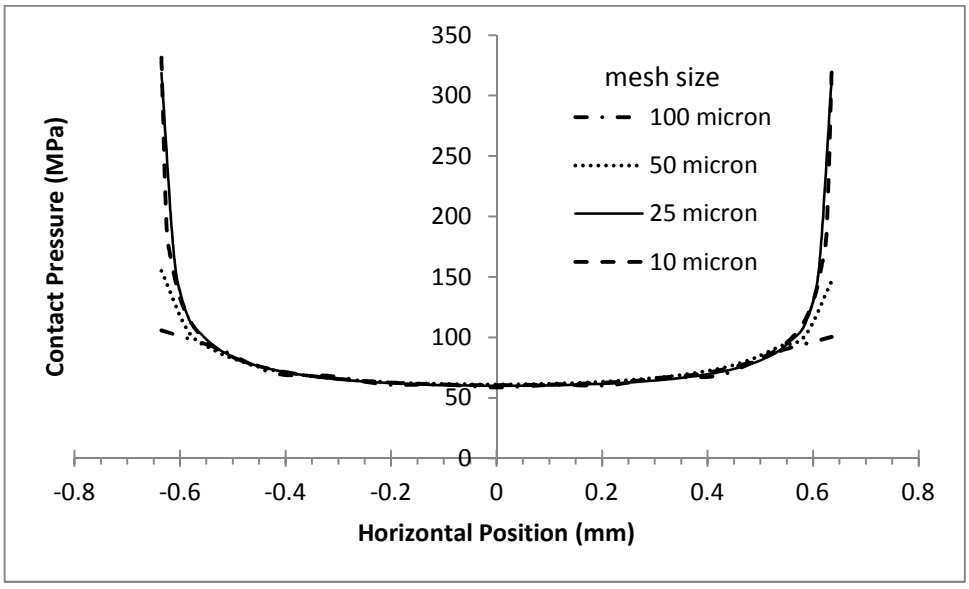

Figure 6.4: Pressure distribution at the contact surface for different mesh sizes.

Two models are employed for validating the analysis against the theoretical solution. First model uses properties for the materials used in the experiments. The second model is designed to closely represent the theoretical solution for a rigid punch against an

elastic surface. In order to get a rigid punch, the Young's modulus of the pad is set to be 1000 times higher than the original Young's modulus.

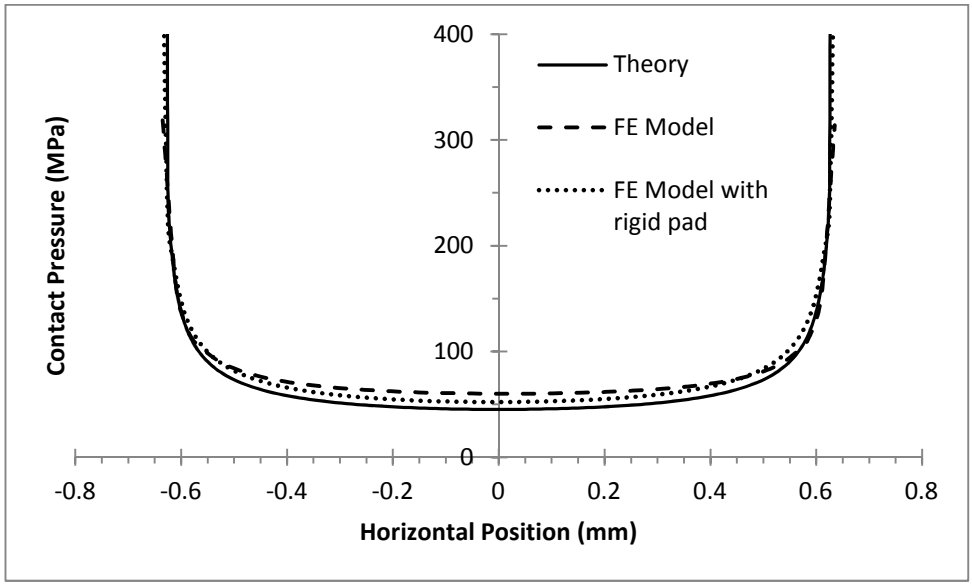

Figure 6.5: Comparison of theoretical contact pressure with simulation results.

The pressure distributions are shown in Figure 6.5. Both models show a good agreement with the theoretical results. As expected, model representing a nearly rigid punch gives better results and closely follows the theory. As a result, this model is adopted for further analysis.

6.4 Results

To achieve a better understanding of the crack nucleation process, this section is divided into three sub-sections; results from linear elastic analysis, results from elastic-plastic analysis, and lastly results with elastic-plastic analysis including the effects of wear.

Crack nucleation predictions are compared with the earliest cracks detected in the experiments which are about 0.1mm in length

6.4.1 Linear elastic analysis

In linear elastic analysis, material is modelled as fully elastic with no plasticity effects. Linear elastic model is only valid for use in SWT and FS predictions if under cyclic loading conditions stress in any element of the model does not exceed the yield stress. In real materials, once the yield strength is exceeded, the strain value will follow the plastic strain curve and will be higher than what is predicted by the linear elastic model. As

SWT and FS parameters are a combination of maximum stress and strain amplitude, their values as predicted by linear elastic model are lower. Consequently, lower values of SWT and FS parameters make the prediction for the number of cycles for crack nucleation to be higher. Nevertheless, this analysis is still useful in producing an approximate prediction for the trend of the number of cycle and location of crack nucleation. Elastic-plastic analysis will also be used here to investigate the effect of plastic deformation and wear on fretting specimens.

By referring to Table 4.1, almost all predicted number of cycles to produce crack nucleation is less than 10% of the number of cycles to produce a 0.1mm long crack in the experiments except for specimen with axial stress 70MPa and normal stress 20MPa and specimen with axial stress 125MPa and normal stress 20MPa. The trend for the number of cycles to produce crack nucleation over the range of normal and axial loads by SWT criterion is similar to the experiments. The predicted number of cycles decrease as either of the axial or normal loads increase. On the other hand, results from FS prediction are found to be inconsistent. As FS is based on shear, any parameters that affects the shear stress will also affect this prediction.

The big difference on this prediction compared to the experimental test occurs as the result of stress singularities at the edge of any complete contact. As SWT and FS parameters depend upon stress and strain, these parameters are also affected by these singularities. The singularity is clearly seen by plotting variation of SWT parameters with depth, as shown in Figure 5.4.

Table 6.1 Crack nucleation prediction by linear elastic models

Axial Load (MPa)	Normal Load (MPa)	Number of cycle to produce 0.1mm crack (experimental)	Crack nucleation prediction (SWT)		Crack nucleation prediction (FS)	
			Number	% of exp.	Number	% of exp.
70	20	270,000	43000	15.93	2400	0.89
	80	380,000	4800	1.26	4950	1.30
	120	830,000	2750	0.30	3700	0.44
100	20	147,000	9000	6.12	960	0.65
	80	50,400	1350	2.68	550	1.09
	120	24,000	1300	5.42	550	2.29
125	20	40,000	8200	20.5	2600	6.50
	80	9,400	520	5.53	220	2.34
	120	4,000	370	9.25	220	5.50

Figure 6.6 shows the variation of the SWT parameter across the contact surface. Highest SWT parameter is found to occur exactly at the leading edge. This prediction is in accordance with the experimental observation.

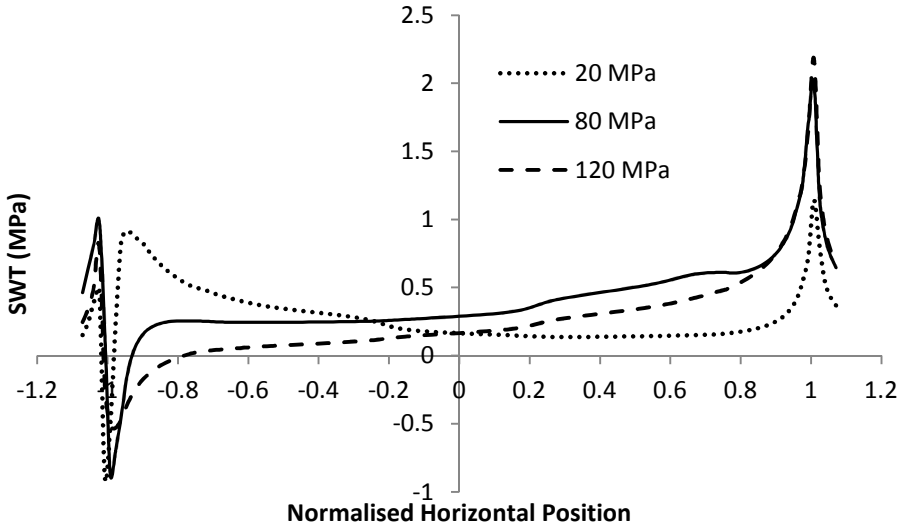

Figure 6.6: Variation of SWT parameter across the contact surface for different applied normal loads and axial stress of 100 MPa.

Non-uniformity in the trend for the SWT parameter is due to different COF values used for each specimen. As shown in Figure 6.7, by fixing the COF value to 1 for all cases, a uniform pattern is obtained with gradually increasing SWT parameter for increasing normal load.

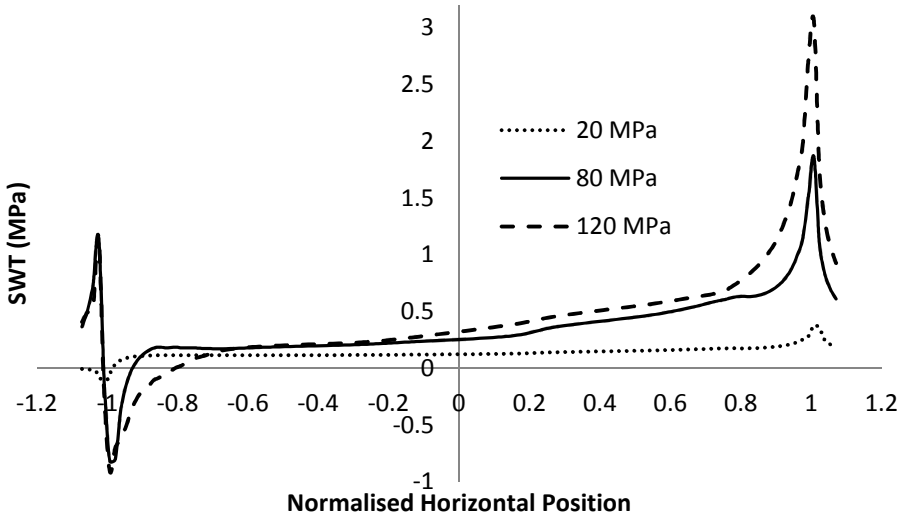

Figure 6.7: Variation of SWT parameter across the contact surface for different applied normal loads for the axial stress of 100 MPa and a fixed COF value.

Fretting pad is found to be rotating during cyclic loading in almost all cases. This behaviour can be seen by looking at the contact stress during compressive and tensile loading, as shown in Figure 6.8. During compressive loading, the trailing edge is lifted with no contact stress whilst at the same time high pressure is created at the leading edge as the edge is forced further into contact. This behaviour is reversed in tensile loading.

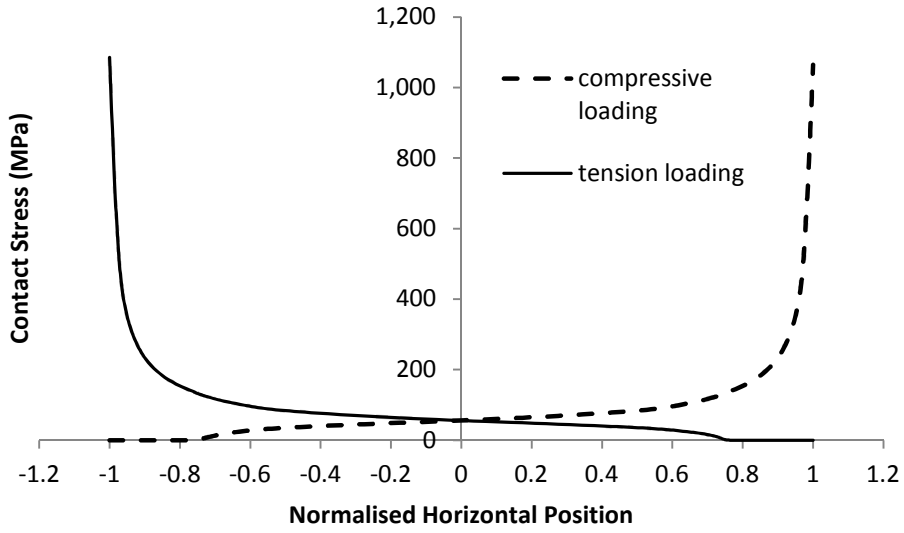

Figure 6.8: Typical Contact Pressure distribution across the contact surface during compressive and tensile loading.

Fretting pad rotation occurs due to a combined effect of the shear stress that arises due to slip and the normal load applied to the pad. Shear stress generates a rotating moment of the pad which is resisted by the moment created by the normal load. For this reason, rotation is pronounced for specimens with low normal loads and axial stress values of 70 and 100 MPa. Except for the specimen with axial stress of 125 MPa which produces higher slip, rotation is found to occur in all specimens as the shear stress created by slip is high enough to counter the effect of the normal load.

6.4.2 Elastic Plastic Analysis

Table 6.2 shows the predicted number of cycles for crack nucleation as predicted by the elastic-plastic model. As expected, the number of cycles predicted by this model is lower than predicted by the linear elastic model for both SWT and FS criteria. The difference can be explained by examining the difference between the two models.

Table 6.2 Crack nucleation prediction by elastic-plastic model.

Axial Load (MPa)	Normal Load (MPa)	Number of cycle to produce 0.1mm crack (experimental)	Crack nucleation prediction (SWT)		Crack nucleation prediction (FS)	
			Number	% of exp.	Number	% of exp.
70	20	270,000	1480	0.77	4950	1.83
	80	380,000	405	0.10	5300	1.40
	120	830,000	420	0.05	4250	0.50
100	20	147,000	1450	1.12	4950	3.37
	80	50,400	360	0.62	610	1.21
	120	24,000	310	1.40	580	2.42
125	20	40,000	720	2.30	3200	8.00
	80	9,400	265	2.81	520	5.53
	120	4,000	170	4.35	380	9.50

In general, the main difference between linear elastic and elastic-plastic models is the hardening process when the stress exceeds the yield strength. Hardening is caused by the slip process which produces plastic deformation and a residual stress. As discussed earlier, high stress occurs in the specimen at the edges of the fretting pads in every compressive and tensile cycle. This high stress creates plastic deformation and residual stress at the edge. Figure 6.9 shows the map of residual stress caused by plastic deformation in one of the samples.

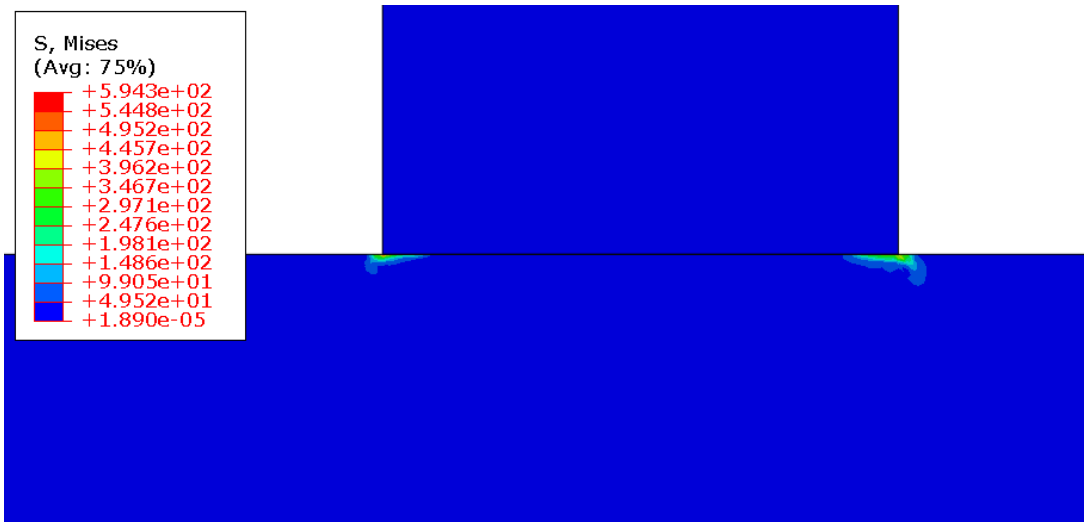

Figure 6.9: Residual stress in the specimen with the axial stress of 100MPa and a normal load of 80MPa.

As SWT and FS parameters are obtained from a multiplication between maximum stress and strain amplitude, the effect of residual stress on SWT can be seen by focusing on

studying the effect of residual stress on maximum stress, normal strain amplitude and shear strain amplitude for the elements near the surface and compared with the linear elastic model, as shown in Figure 6.10.

Plastic deformation and residual stress seem not to have any significant effect on the normal strain amplitude. However, shear strain amplitude and maximum stress on the elements near the edges show a considerable difference. Due to plastic deformation, the effect of sharp edges decreases which lowers the value of shear amplitude. Maximum stress for the edge elements experiencing residual stress also seem to be much higher.

In each cycle, any element reaching the yield stress undergoes permanent deformation which affects the stress in the next cycle. Hence the value of SWT parameter in each element evolves in the elastic-plastic model. Figure 6.11 and 6.12 show the evolution of SWT and FS parameters with loading cycles across the contact surface. In general, significant evolution occurs below the 10^{th} cycle but the values of these parameters saturate after the 10^{th} cycle.

The evolution is also found to be more significant at lower values of normal load. This is due to pad rotation which occurs when the specimen is subjected to lower normal loads, as discussed earlier.

With elastic-plastic model, the SWT prediction gives lower number of cycles as compared to the FS prediction for all cases. According to Fatemi and Socie [15], as the critical element is now more dominant in unidirectional tension rather than shear, the SWT prediction will give more accurate results. Hence, only SWT will be studied further in wear models.

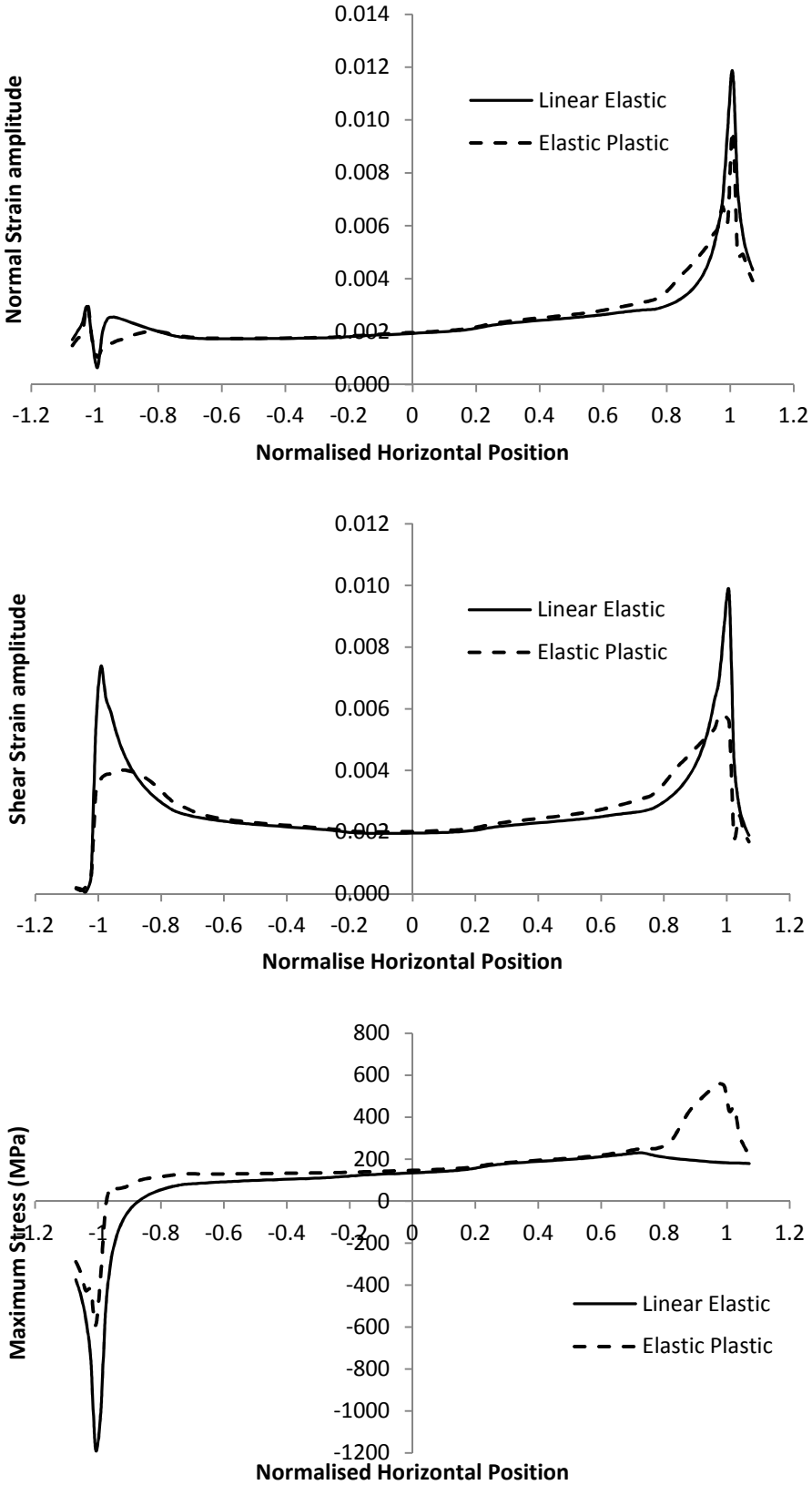

Figure 6.10: Variation of normal and shear strain amplitudes and maximum stress across the contact surface for a specimen with axial stress of 100 MPa and contact stress of 80 MPa.

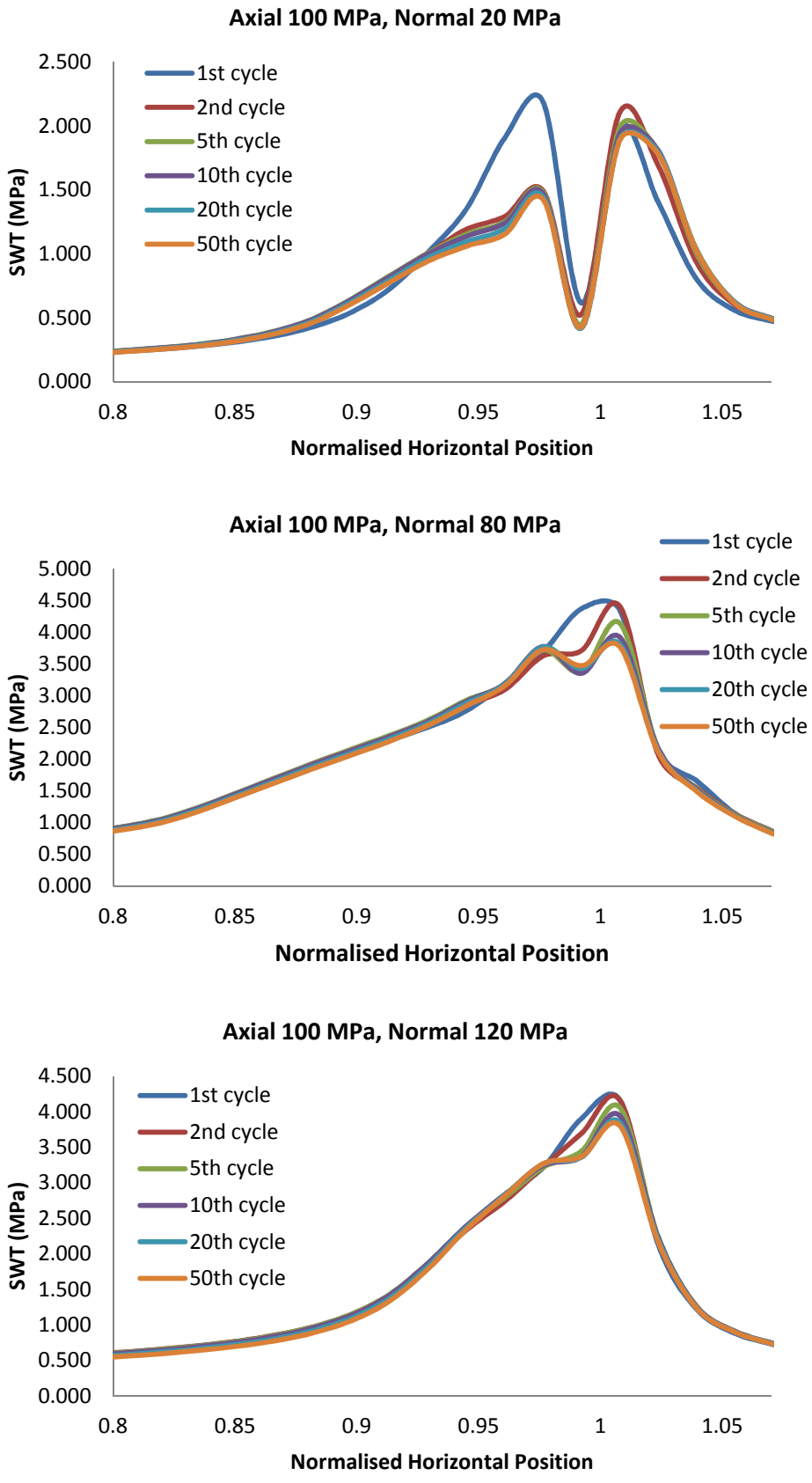

Figure 6.11: Evolution of SWT parameter with loading cycles across the contact surface.

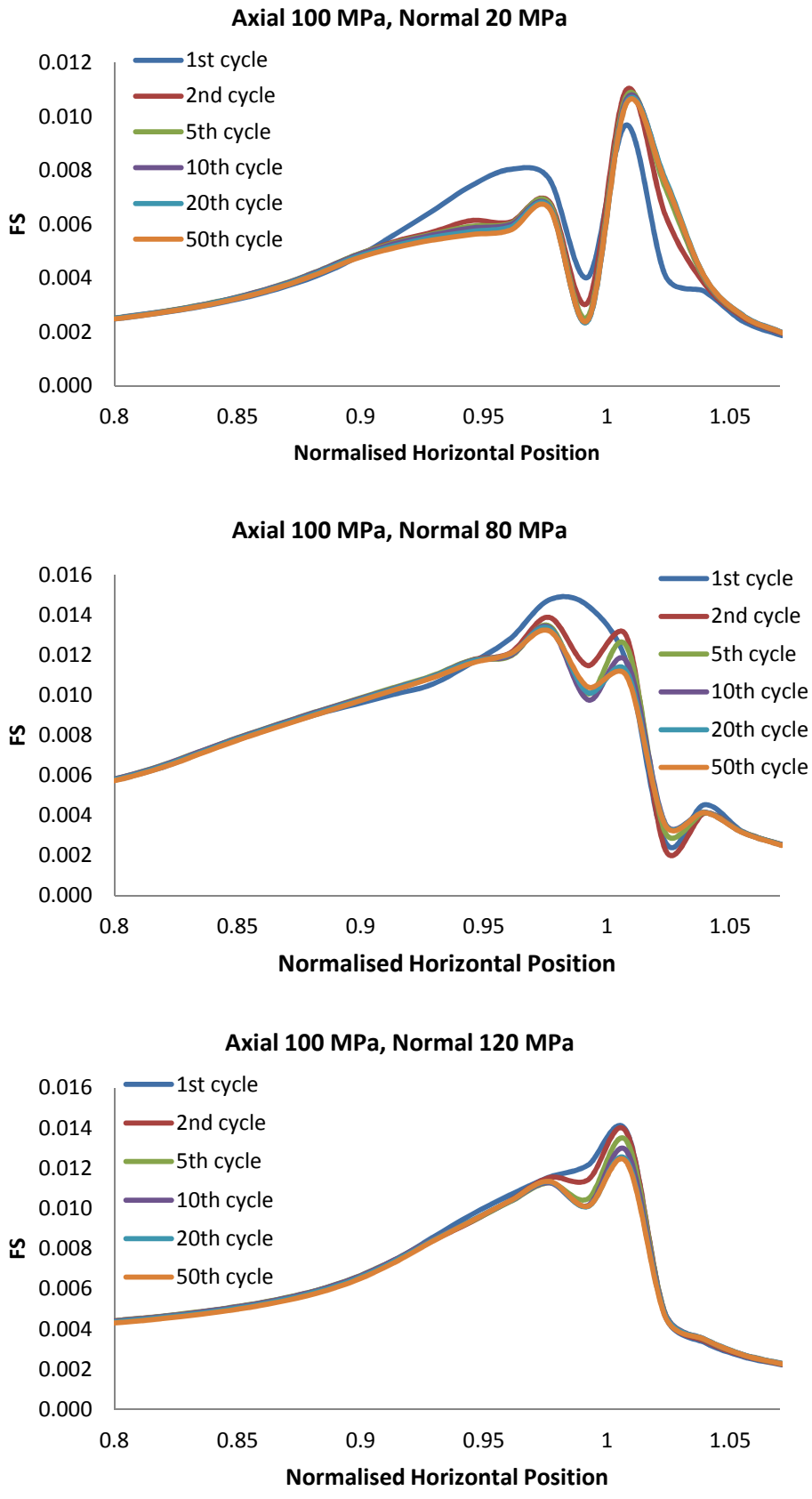

Figure 6.12: Evolution of FS parameter with loading cycles across the contact surface.

6.4.3 Wear Analysis

Table 6.3 gives crack nucleation predictions with elastic-plastic model including wear. Compared to elastic-plastic model (without considering wear), the number of cycles for wear model is slightly higher. This increase seems to be proportional to the number of cycles predicted by the elastic-plastic model (Table 6.2).

Table 6.3 Crack nucleation predictions by the elastic-plastic model including wear.

Axial Load (MPa)	Normal Load (MPa)	Number of cycle to produce 0.1mm crack (experimental)	Crack nucleation prediction (SWT)	
			Number	% of exp.
70	20	270,000	3100	1.15
	80	380,000	430	0.11
	120	830,000	467	0.05
100	20	147,000	2850	1.94
	80	50,400	380	0.75
	120	24,000	314	1.31
125	20	40,000	970	2.43
	80	9,400	280	2.98
	120	4,000	170	4.25

This proportional increment can be understood by referring to SWT evolution focusing on the element near the leading edge, as shown in Figure 6.13. The trend is almost the same as produced by the elastic-plastic model. However, different from the elastic plastic model, the SWT parameter in this case keeps evolving over the cycles without saturation. This is because wear occurs to the surface for every cycle due to normal stress and slip. As the number of cycles increase, wear on the surface also increases thereby reducing the SWT parameter for the element.

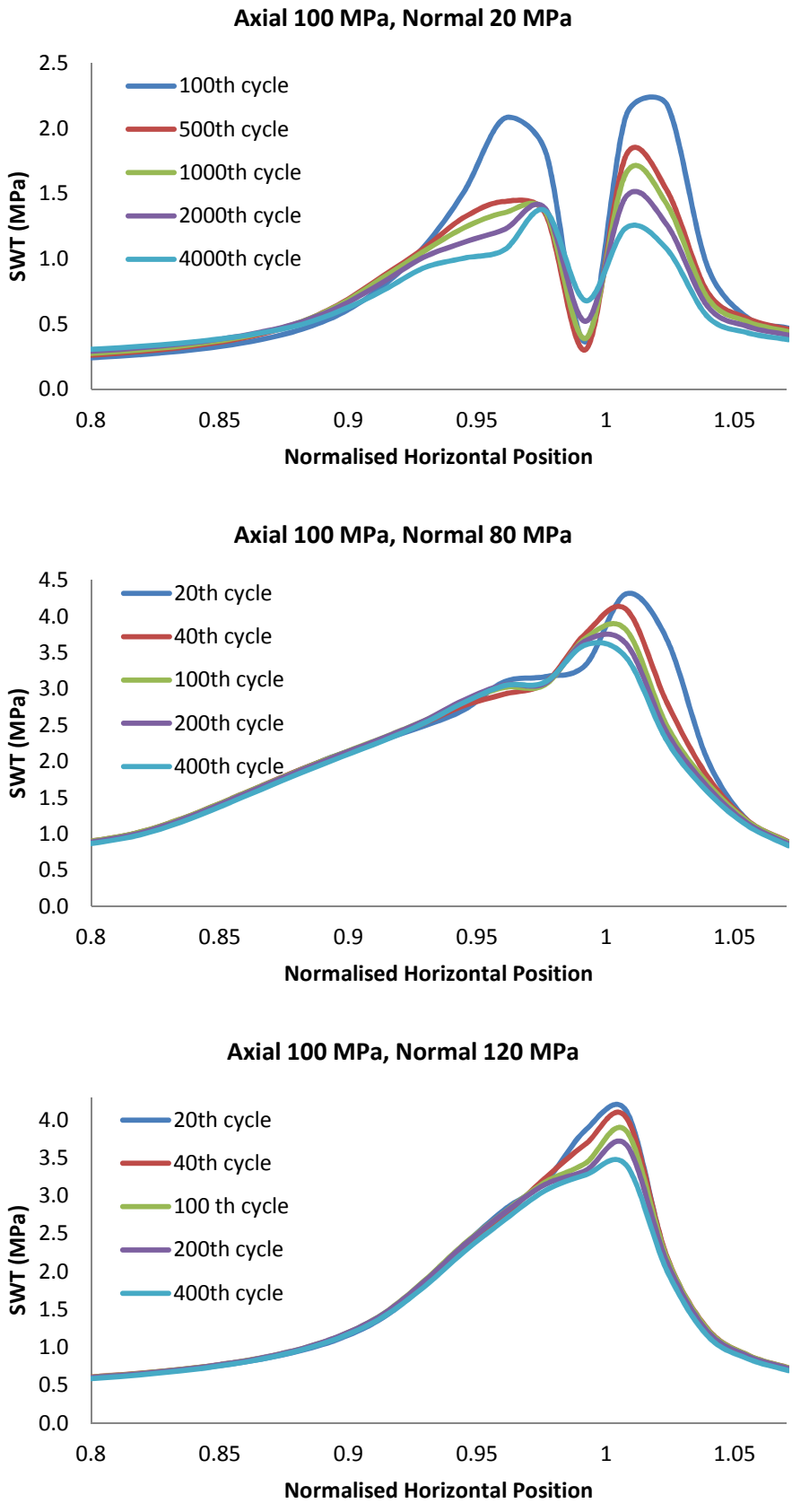

Figure 6.13: Evolution of SWT parameter with applied load cycles across the contact surface.

6.5 Averaging Method

In this analysis, crack nucleation is predicted, as by the previous models, to occur within 10% of the cycles to produce a 0.1mm long crack experimentally. The reason for such phenomena may be associated with the high stress gradient at the critical element due to singularities. In order to take the effect of singularities into account, an averaging technique is used in this analysis. This analysis uses averaging of SWT parameter, as proposed by Aroujo [84] over several elements on a certain area near the critical element to produce an average SWT parameter (SWT_{avg}).

By comparing predictions with different averaging size in Figure 6.14, it can be seen that the difference between wear and elastic model is minimised as the averaging size increases. It is also found that the biggest difference between the two models is less than 15%. For the next analysis, only averaging as applied to the wear model will be discussed.

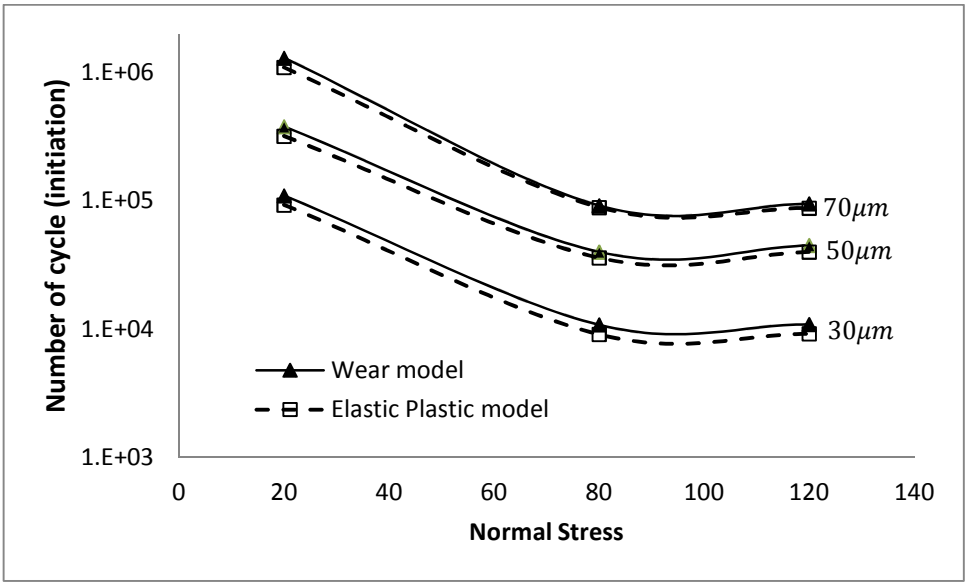

Figure 6.14: Comparison of elastic plastic and wear models with different averaging size for predicting crack initiation.

Figure 6.15 and Table 6.4 shows the results obtained by applying several averaging sizes ranging from 30μm to 70μm and compared with the experimental data. Overall, it is clear that the averaged results give a better prediction when compared with the experimental data than the non-averaged ones. A detailed examination of each plot reveals that the prediction for specimen with normal stress of 20 MPa agrees well with the experimental results with an average size of 30 μm. For specimens with normal stress of

80 and 120 MPa and with applied axial stress of 100 and 120 MPa, the best fits with the experimental data are obtained with an averaging size of 50 μm. Specimens with normal stress of 80 and 120 MPa and the applied axial stress of 70 MPa require a greater averaging size of 70 μm to produce good agreement with the experimental data.

These results agree with Aroujo [84], who suggests that the range of averaging dimension appears to be of a similar order of magnitude as the grain size. The averaging size for all the specimens is almost one or two times the grain size of the Aluminium alloy (L65) used in this study [106].

Aroujo [5] also suggests that this averaging parameter may not be a true material constant but depends upon loading and some other factors. In this study, a similar trend is observed between pads rotation and the averaging size. As discussed at the end of Section 6.4.1, fretting pads rotation is pronounced for specimens with low normal loads. Specimens with normal load of 20 MPa are also found to be significantly affected by plastic deformation and wear as compared to other specimens, as shown in Figures 6.11 and 6.12. The material properties near the critical element may change due the plastic deformation and degradation due to wear. If taken into account in the SWT parameter, these changes in material properties may produce the same averaging size as other specimens.

For specimens with normal stress of 80 and 120 MPa, fretting pad rotation is more significant for high applied axial stress. Consequently, plastic deformation produced by this high stress due to pad rotation also seems to influence the results. However, a limited number of experimental results do not allow a more conclusive evidence.

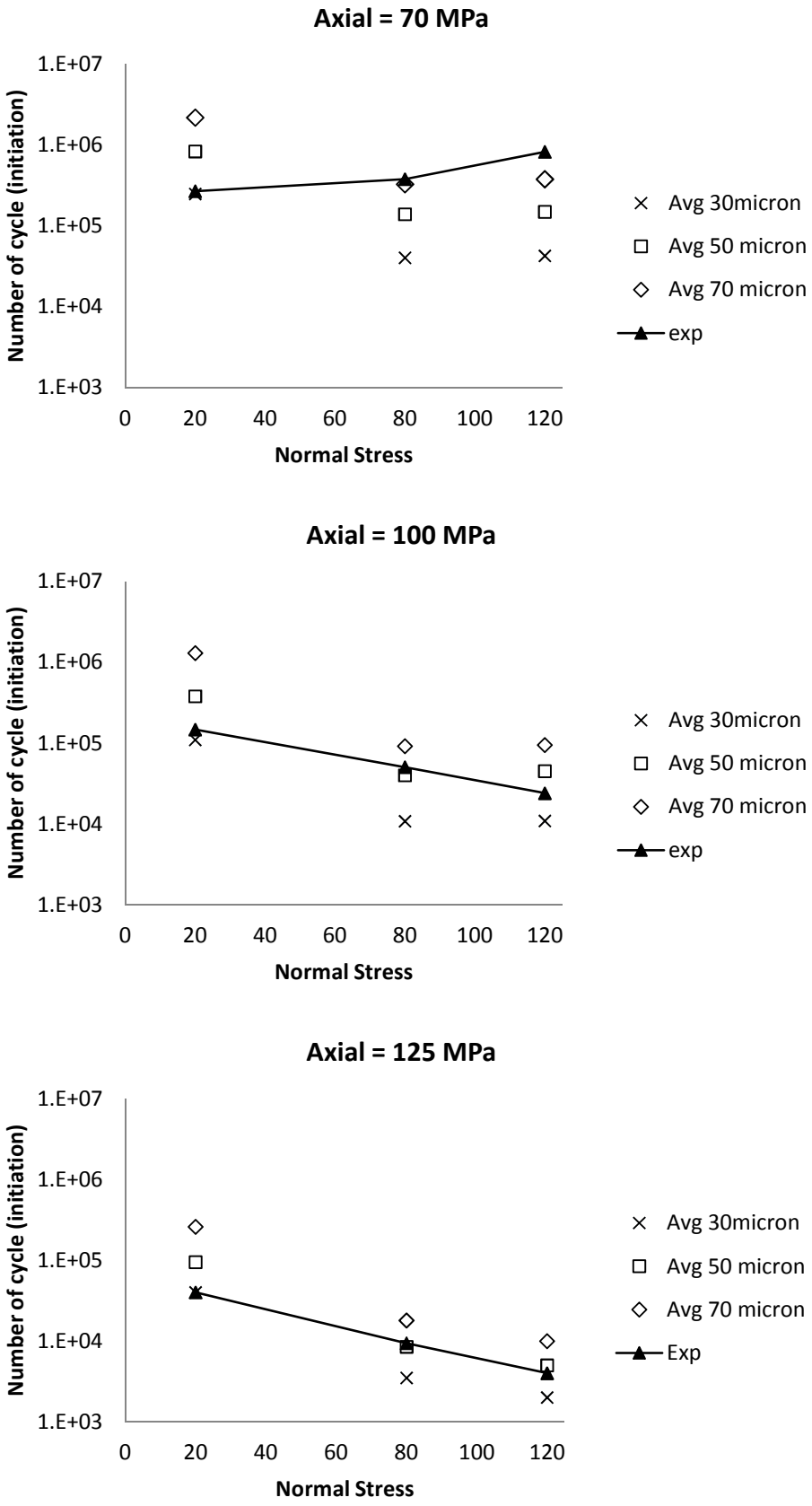

Figure 6.15: Effect of averaging size on crack initiation prediction.

Table 6.4 Crack nucleation predictions by the averaging methods.

Axial Load (MPa)	Normal Load (MPa)	Crack Nucleation Prediction Based on SWT and Averaging method on several averaging area					
		30 μm		50 μm		70 μm	
		Number of cycle	% of exp.	Number of cycle	% of exp.	Number of cycle	% of exp.
70	20	250000	92.6	840000	311.1	2200000	814.8
	80	40500	10.7	140000	36.8	330000	86.8
	120	42800	5.2	150000	18.1	380000	45.8
100	20	110000	74.8	380000	258.5	1300000	884.4
	80	10800	21.4	40000	79.4	92000	182.5
	120	10900	45.4	45000	187.5	95000	395.8
125	20	40000	100.0	95000	237.5	260000	650.0
	80	3500	37.2	8500	90.4	18000	191.5
	120	2000	50.0	5000	125.0	10000	250.0

6.6 Conclusion

In this analysis, crack nucleation is predicted by the models to occur within 10% of the cycles to produce a 0.1mm long crack experimentally. It shows that the crack nucleated much below 0.1mm. A further analysis on averaging analysis found that averaged results with a dimension of one to two times the grain size gives a better prediction which agrees well with the experimental data.

CHAPTER 7. CRACK PROPAGATION IN COMPLETE CONTACT FRETTING FATIGUE

7.1 Introduction

This chapter discusses the behaviour of crack propagation in complete contact fretting fatigue. Crack propagation analysis was carried in two stages. In the first stage, the focus was on crack propagation in order to establish the behaviour of crack growth for a small crack. In the second stage, fretting fatigue total life from the models (from initiation to propagation) was predicted and compared with the available experimental data.

7.2 Model Description

This analysis used the same model as used previously and presented in Section 6.2 but with the addition of a stationary crack. The analysis followed the conventional finite element procedure and the stationary crack was modelled with different crack lengths to determine the required stress intensity factors. An initial crack of 30μm was located at the leading edge based on the earlier prediction in section 6.4. This crack length was chosen based on the crack length at nucleation found in the experimental work described in Section 4.5.4. This initial crack was orientated based on direction of maximum shear stress and found to be identical with experimental results. This initial crack was then extended with small increments (20-50μm) for crack up to 0.5mm, and with larger increments of 0.25mm beyond.

The crack was modelled in ABAQUS using embedded line (referred to as “seam” in ABAQUS). In order to enhance the accuracy of the model, mesh refining was carried out near the crack tip. A partitioning strategy was employed to generate the crack and to facilitate the generation of a uniform focused mesh.

The analysis is done using personal desktop with Intel i7 processor using Abaqus 6.11 licensed to The University of Manchester. The propagation analyses using conventional method, where remeshing is need for every increment, for early stage (crack length below 1mm), remeshing is done for every 0.1mm crack extention, but, as the crack becomes stable, remeshing is only done for every 0.5mm increment.

7.3 Crack path in complete contact fretting fatigue

Defining the correct crack path is important in modelling and analysing crack propagation, especially for small cracks. Crack orientation greatly influences stress intensity [75] and affects crack propagation analysis as crack grows and kinked.

In this study, two criteria, which have been shown to work well to determine crack growth direction, are used. These criteria are based on Maximum Tangential Stress (MTS) by Faanes [92] and Maximum Tangential Stress Range (ΔMTS) by Giner [93]. Faanes [92] used mathematical formulations to determine stress intensity factors for mode I and mode II analyses. These values were then used to determine the stress field in front of the crack tip. Giner [93], on the other hand, analysed the problem with ABAQUS for a single pad complete contact.

Figure 5.1 shows the results from the analysis. Overall, ΔMTS produced better predictions compared to MTS criterion, although both criteria assumed the crack to propagate in the direction of maximum tangential stress. However, MTS considers the stress field in front of the crack tip when the tangential stress is maximum which occurs when the applied axial stress is tensile. ΔMTS, on the other hand, considers the stress field over one complete cycle.

Contact stress at maximum tension and compression during the applied axial stress cycle can be observed in Figure 6.8. It can be seen that there is no contact stress at the surface near the leading edge in tensile loading. But the contact stress is very high at maximum applied compressive stress due to a small rotational movement of the fretting pad. In other words, during maximum tensile loading, the stress at the leading edge is almost like the specimen with only axial stress but without any contact effect. This may be the reason why MTS crack is almost straight. Meanwhile, ΔMTS which considers the stress field for the whole cycle in the calculation is able to incorporate the multi axial effect in the prediction.

The effect of crack profile on K_I is shown in Figure 7.2. K_I profile from ΔMTS agrees well with K_I profile obtained from the experiments. Small difference is observed for MTS until the crack length reaches 2mm.

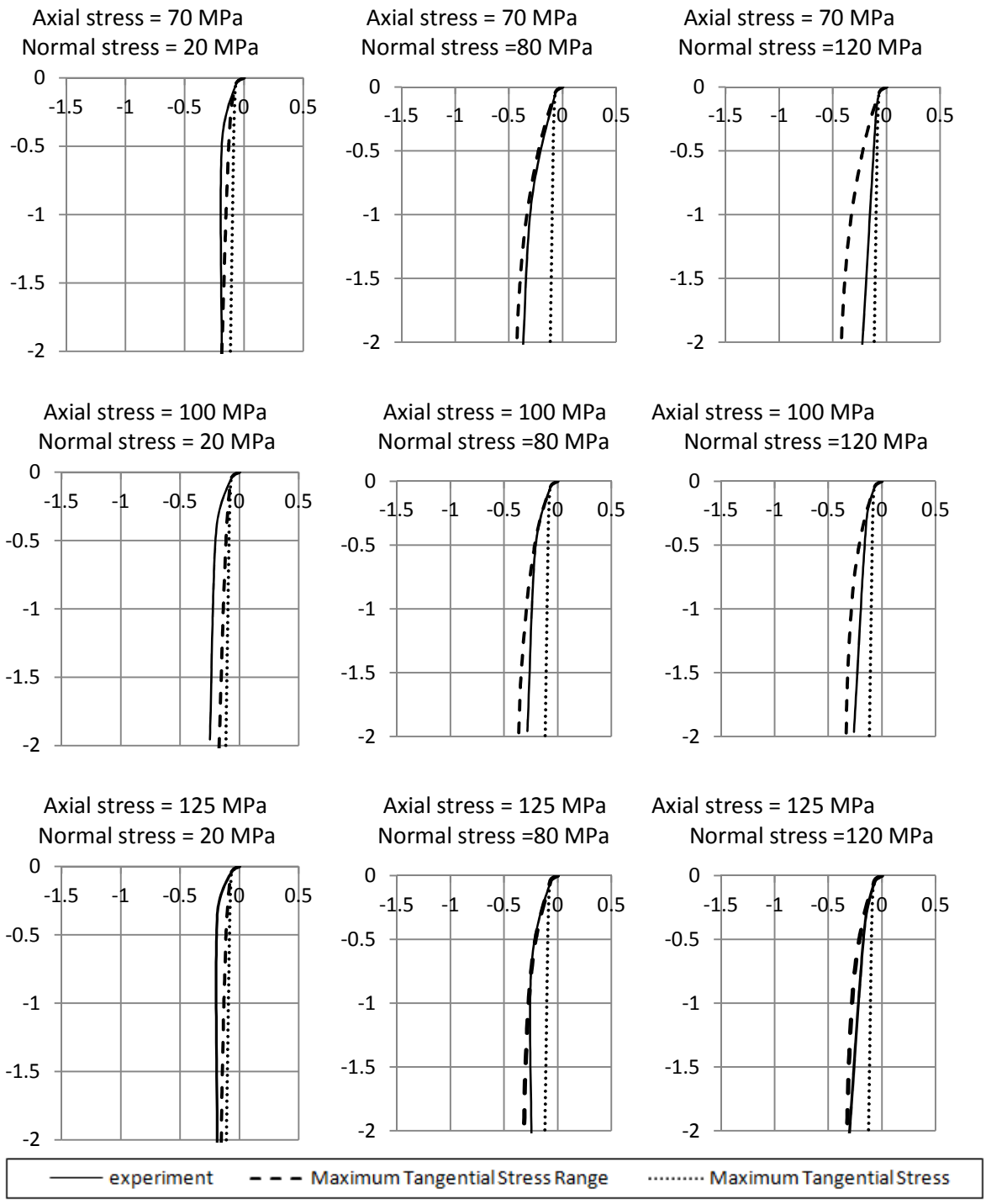

Figure 7.1: Comparison of crack path observed in the experimental work and predicted by FEM using MTS and ΔMTS criteria.

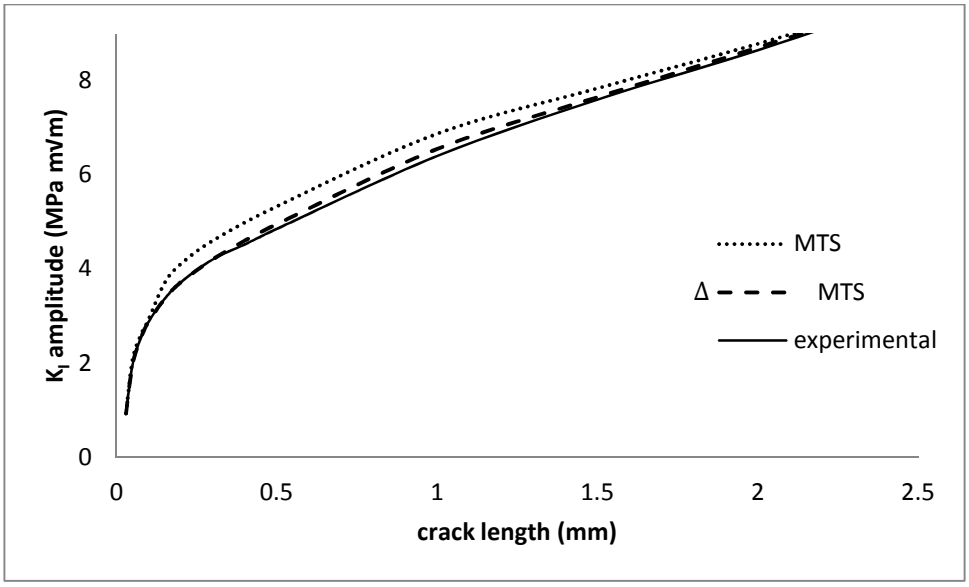

Figure 7.2: Variation of K_I with crack length along crack paths predicted by MTS and ΔMTS criteria and its comparison with experiments.

7.3.1 Crack Propagation Analysis

Paris law was used to analyse crack propagation in which crack growth is related to ΔK. However, before starting this analysis, it was important to establish the extent to which LEFM analysis was applicable and whether or not the analysis using EPFM was required. Based on the accepted practice [107], LEFM is acceptable if plastic zone size at the crack tip (r_p) is less than 1/50 of the crack length (a). Under plane strain conditions, r_p is given by:

$$r_p = \frac{1}{6\pi}\left[\frac{K_I}{\sigma_y}\right]^2 \tag{7.1}$$

Figure 7.3 shows the variation of r_p/a with crack length. r_p/a for the specimens with higher values of normal stress of 80 MPa and 120 MPa have peak values at a small crack length of about 0.1mm. These values then gradually decrease as the crack becomes longer. This does not happen with the specimen with normal stress of 20 MPa. This clearly shows that the sudden increment (or peak) in case of higher normal loads is created as a result of a strong multi-axial stress field at the fretting pad.

The plastic zone size indicates that the analysis with normal stress of 80 MPa and 120 MPa for a crack length below 0.1 mm is not acceptable with LEFM. This threshold length is low and only 0.1mm with an axial stress of 70 MPa. It increases to about 0.4mm for the specimen with the applied axial stress of 100MPa. For specimen with axial stress of 125 MPa, this length is up to 1mm. For the specimen with normal stress of 20 MPa, where a sudden increase in the plastic zone size is not observed, only one load case with axial stress of 125 MPa has a certain length below which LEFM is not applicable.

In order to analyse crack growth with a combination of LEFM and EPFM, an equivalent stress intensity factor K_{eq} was used. For cases where LEFM was acceptable ($r_p/a < 0.02$), K_{eq} was taken to be equal to K_I from LEFM analysis. For cases where LEFM was not applicable ($r_p/a \geq 0.02$), K_{eq} was derived from Eq.(2.20) given as:

$$K_{eq} = \sqrt{\frac{EJ}{(1-\nu^2)}} \tag{7.2}$$

Comparison of ΔK from LEFM analysis and a combination of LEFM and EPFM analysis is presented in Figures 7.4 and 7.5.

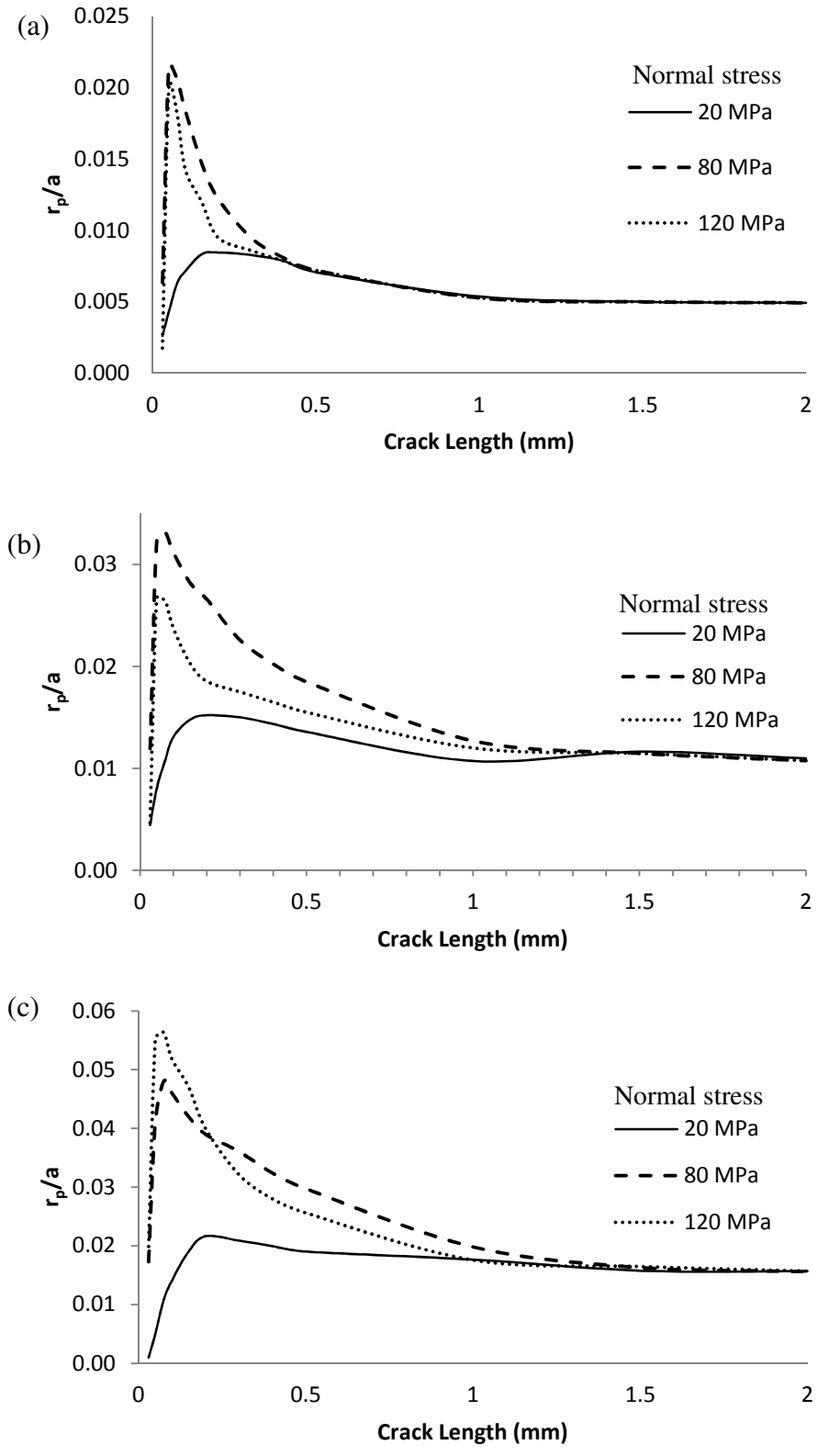

Figure 7.3: Variation of plastic zone size (r_p) at the crack tip with crack length for different normal stress values and the applied axial stress of: (a) 70 MPa, (b) 100 MPa, (c) 125 MPa.

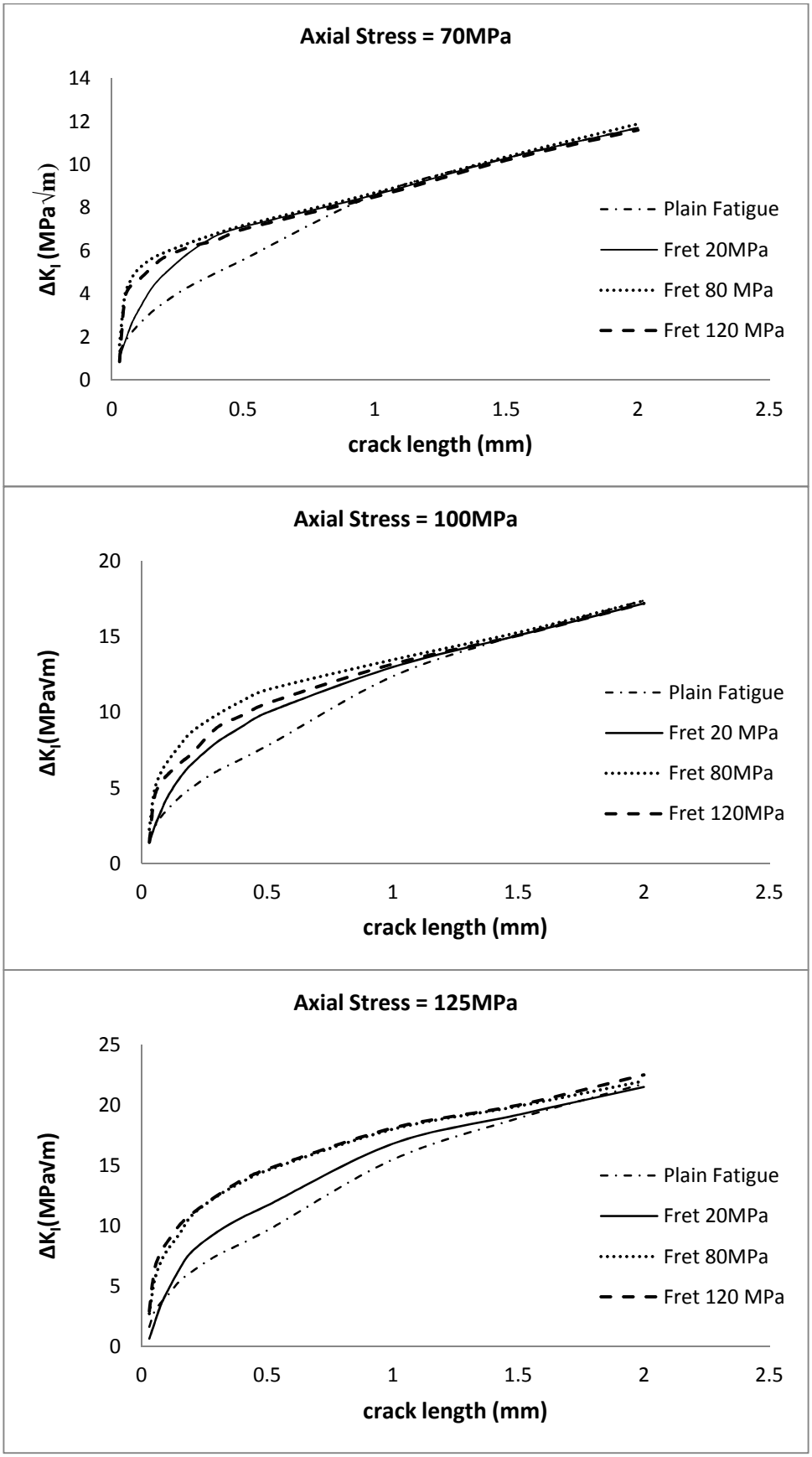

Figure 7.4: ΔK_I predicted for different axial and normal loads using LEFM approach.

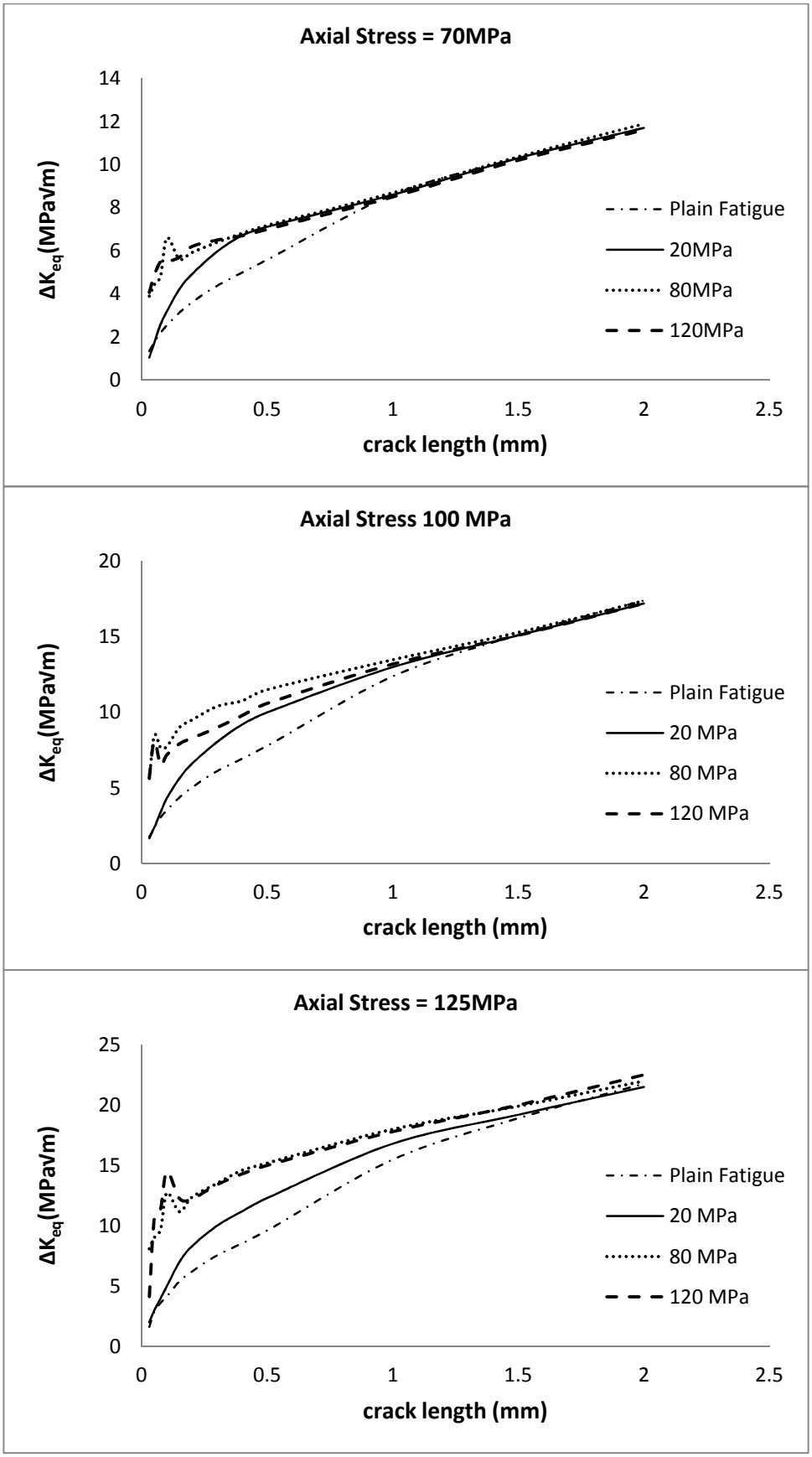

Figure 7.5: ΔK_{eq} predicted for different axial and normal loads using a combined LEFM - EPFM approach

As seen from the trend of the range of stress intensity factors (ΔK), different normal loads give different levels of stress intensity for small cracks. The difference narrows, however, as the crack becomes longer which shows that the effect of normal load is limited to a certain crack length. The length is proportional to the applied axial stress.

By comparing Figures 7.4 and 7.5, another pattern for ΔK is observed. For combined LEFM-EPFM model, ΔK creates a small peak at a crack length of about 0.1mm before following a steady increment. This peak may occur because of the heterogeneous stress field on the specimen surface near the fretting pad. This heterogeneous stress field may cause retardation to crack growth, thereby, slowing it and sometimes stopping the propagation [79-81].

Threshold stress intensity factor (ΔK_{th}) for the material used is $4.12MPa\sqrt{m}$ [108]. For all applied axial stress values, ΔK for specimens with normal stress of 20 MPa is lower than ΔK_{th} until crack length exceeds 0.15mm. However, a previous study on small cracks has found that cracks can still grow when ΔK is below ΔK_{th} [109].

Once ΔK value is obtained, the next step is to calculate crack propagation rate based on Paris equation:

$$\frac{da}{dN} = C(\Delta K_{eq})^n \tag{7.3}$$

Where n = 2.2, C = $3 \times 10^{-10}\, m/cycle$ are material constants for BS-L65 aluminium alloy used in this study [108].

Prediction of crack growth rate is compared with the crack growth rate from experiments in Figures 7.6 – 7.8. Overall, the predictions match the experimental data for almost all cases except for axial stress of 100 MPa and Normal Stress of 120 MPa. However, based on Figure 4.6, this difference might come from an error in the experiments. This particular load case has a spurious pattern of crack growth rate compared to all other load cases.

The peak in the growth rate when the crack is small occurs due to a heterogeneous stress field at the fretting pad which makes the propagation rate to slow down. Almost all load cases show crack propagation rates for small cracks to be lower than predicted.

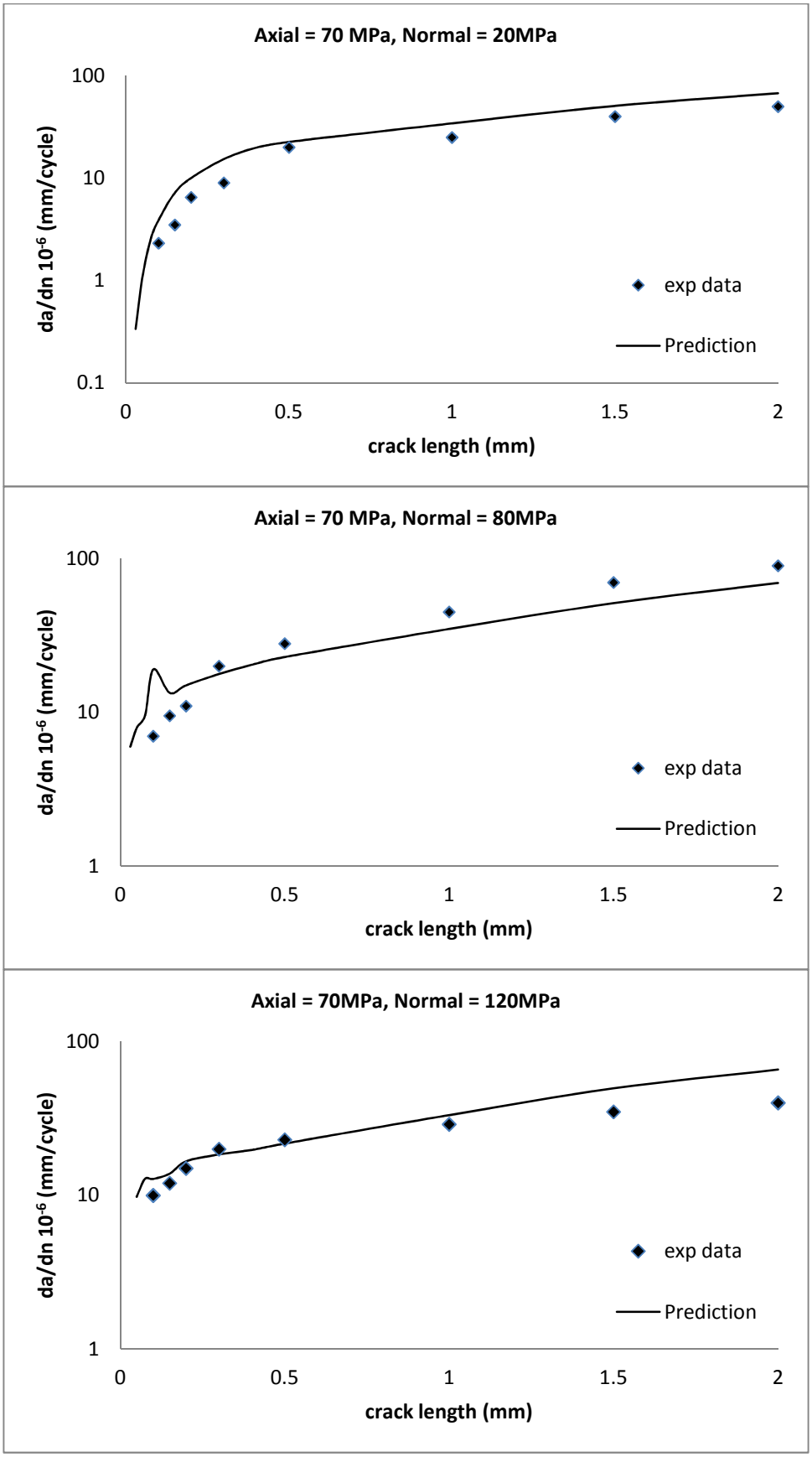

Figure 7.6: Crack propagation rates for a specimen with different normal loads and the applied axial stress of 70 MPa.

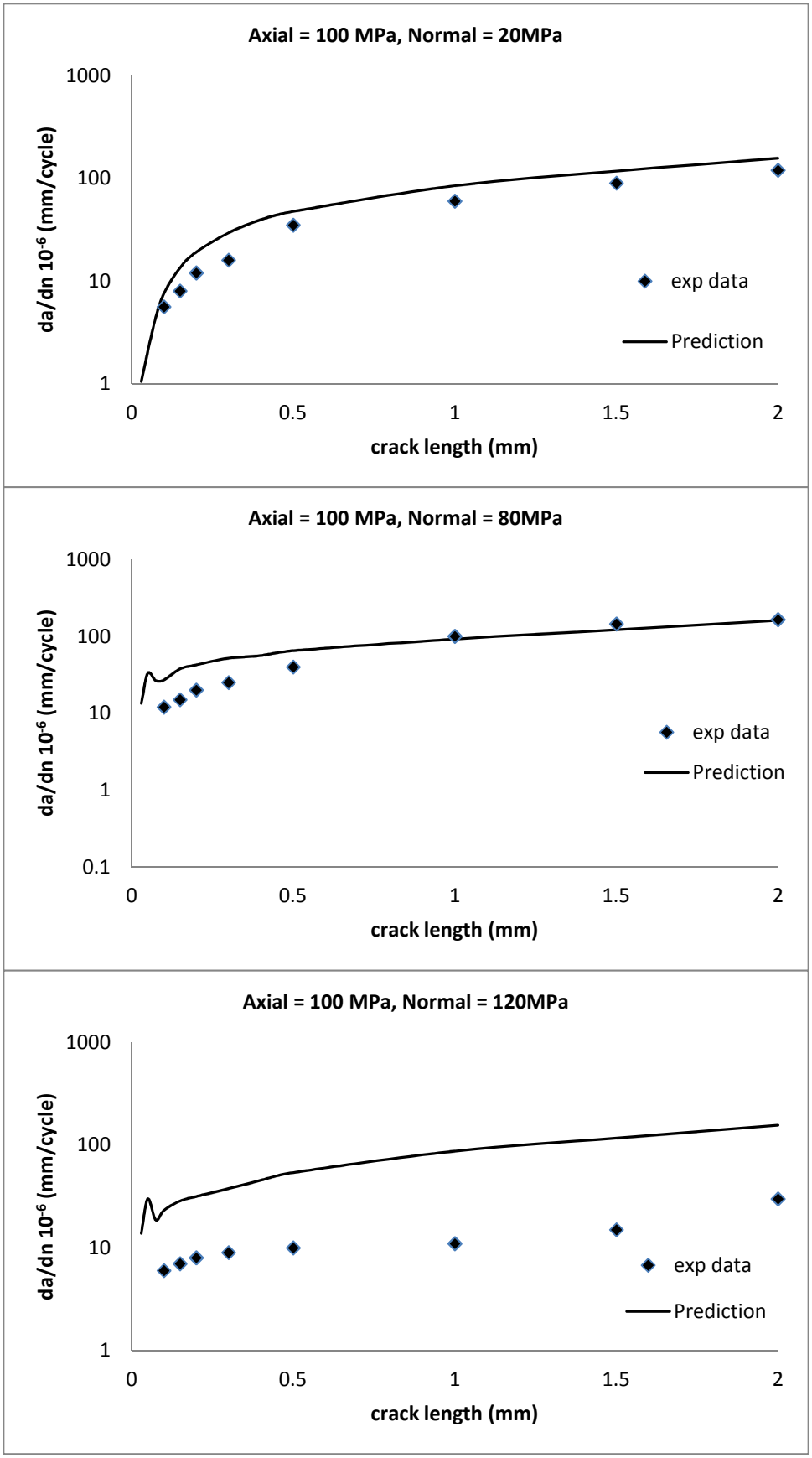

Figure 7.7: Crack propagation rates for a specimen with different normal loads and the applied axial stress of 100 MPa.

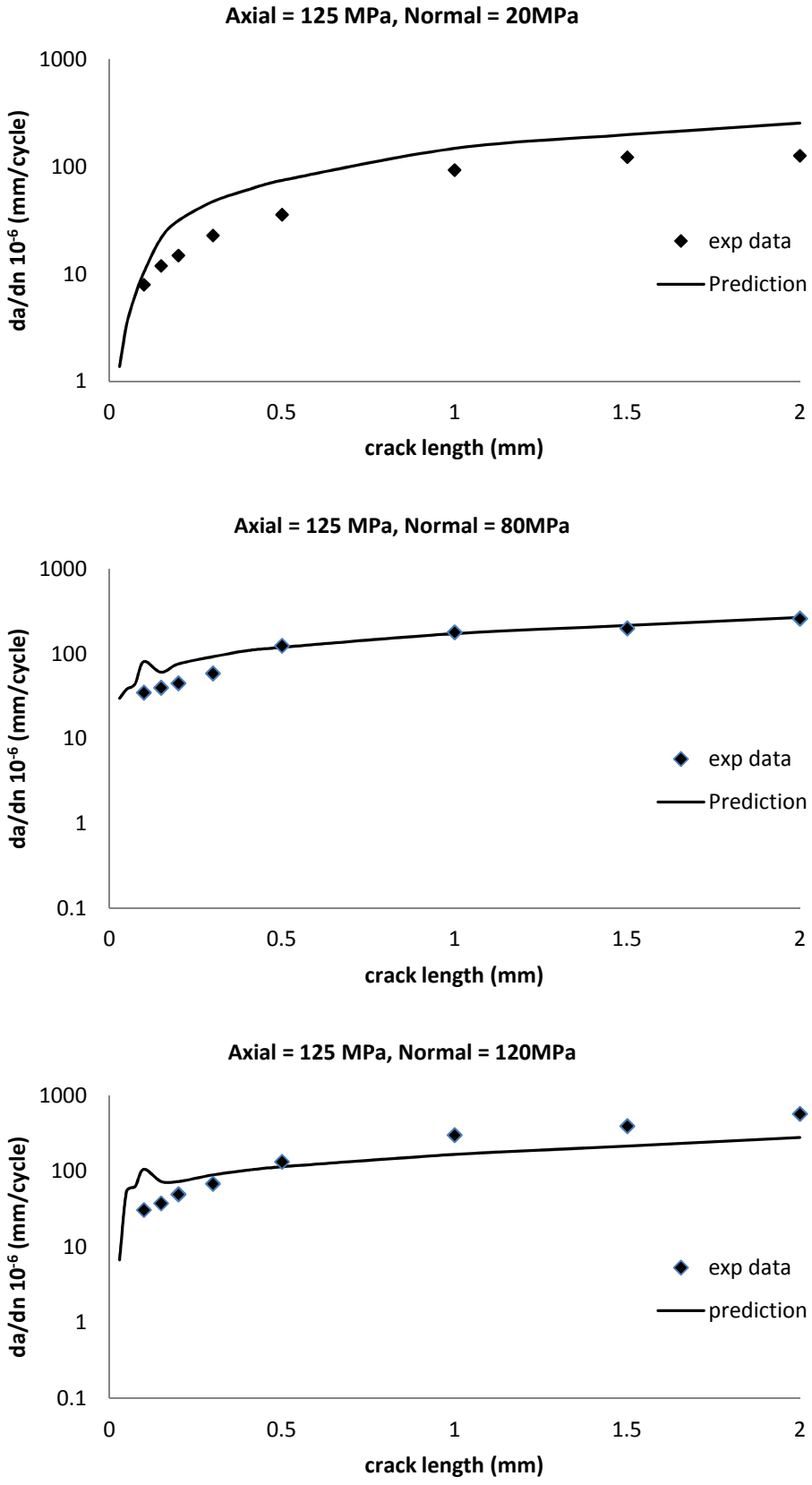

Figure 7.8: Crack propagation rates for a specimen with different normal loads and the applied axial stress of 125 MPa.

Finally, crack propagation rate (*da/dn*) prediction is used to calculate the predicted number of cycles for each crack length increment (Δa). Number of cycles for a certain increment can be obtained from:

$$\Delta N = \frac{\Delta a}{da/_{dn}} \tag{7.4}$$

A number of studies [96, 109, 110] show that crack propagation for small crack normally deviate from Paris law. Hence, this study uses reverse counting for number of cycles to clearly see the difference for a small crack. This is done by setting number of cycles for a 2mm crack predicted by the model to be the same as obtained from the experiments. Starting with this, the number of cycles for smaller crack lengths is calculated using:

$$N_{i-\Delta a} = N_i - \frac{\Delta a}{da/_{dn}} \tag{7.5}$$

The predicted number of cycles from this approach are presented in Figures 7.9 - 7.11. Predicted number of cycles for crack propagation together with the predicted number of cycles for crack initiation, as obtained earlier in Chapter 6, can then be compared with the experimental data.

The predicted number of cycles for all the specimens with cracks longer than 1mm agree well with the experiments except for the load case of axial stress of 100 MPa and normal stress of 120 MPa. As expected, Paris equation works well when the crack is long enough and is not influenced by loading at the fretting pad.

This method of analysis has limitation for cracks below 1 mm. Predicted number of cycles for specimens with axial stress of 70 MPa agree well with the experimental data. However, with axial stress of 100 MPa, a difference is observed for a small crack. This difference becomes larger as the normal load increases. Specimens with applied axial stress of 125 MPa and normal stress of 20 MPa show a significant deviation from the experiments as compared to other load cases.

In all cases, the predicted number of cycles is higher than the experimental results. In other words, it can be seen that the propagation from experimental work is slower than predicted. High plastic zone over crack length ratio as shown in Figure 7.3 and stress intensity create a small peak for crack length of 0.1mm as shown in Figure 7.6, Figure 7.7, and Figure 7.8 can be the main reason for this difference. Plastic zone has been known to

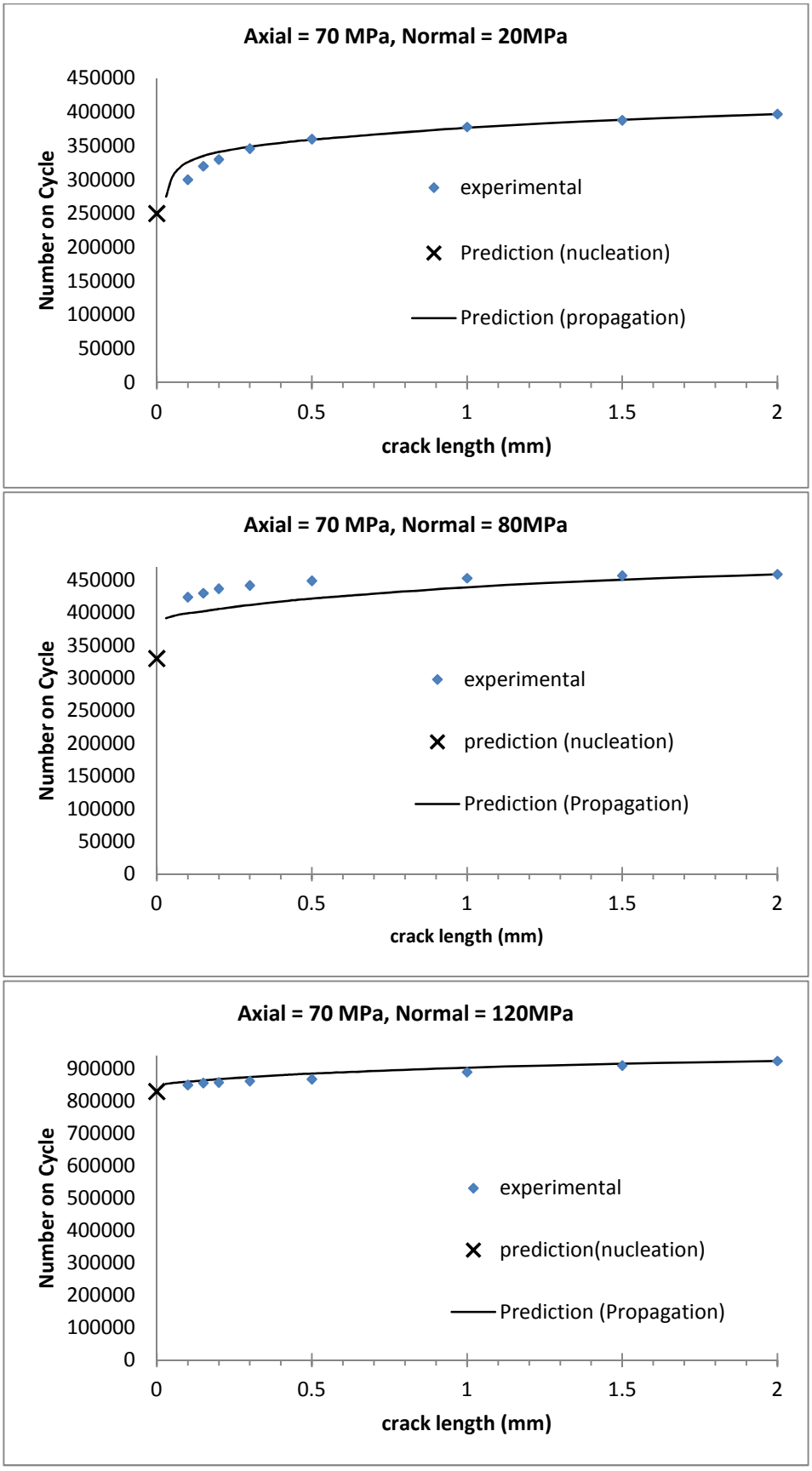

Figure 7.9: Predicted number of cycles of crack propagation for specimen with different normal loads and the applied axial stress of 70 MPa.

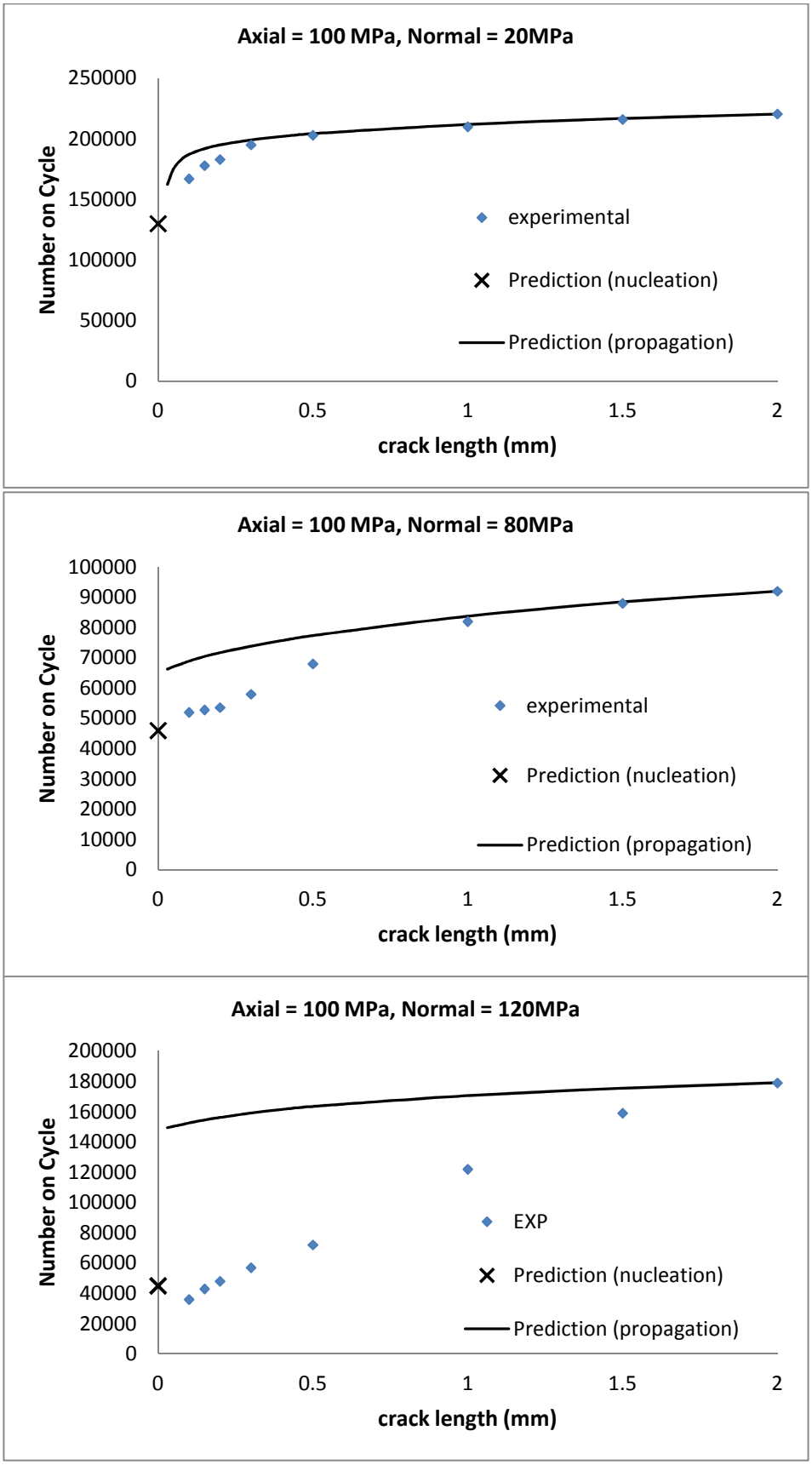

Figure 7.10: Predicted number of cycles of crack propagation for specimen with different normal loads and the applied axial stress 100 MPa.

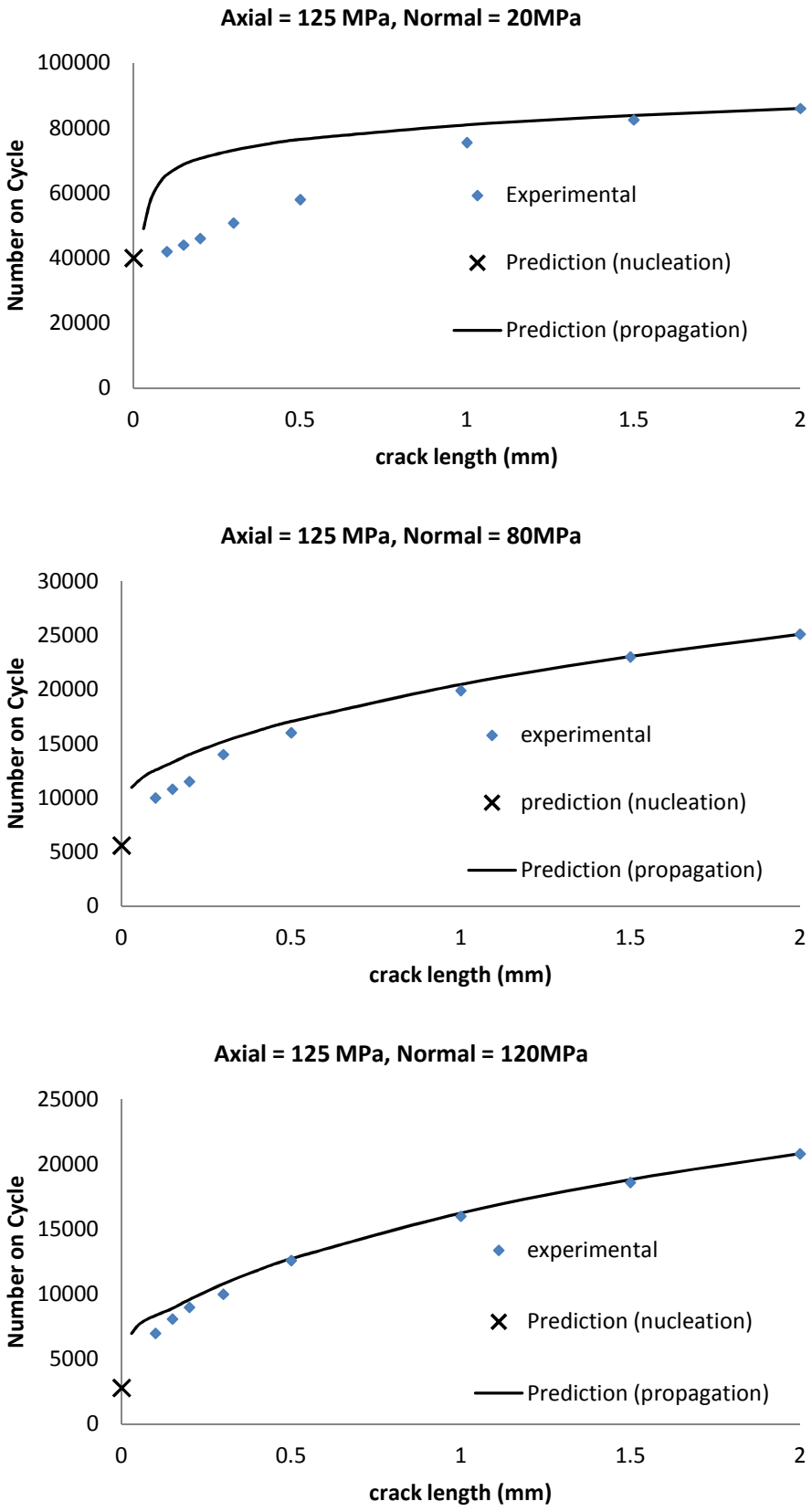

Figure 7.11: Predicted number of cycles of crack propagation for specimen with different normal loads and the applied axial stress 125 MPa.

give the effect to slow down the rate as plastic deformation blunts the crack [111]. The small peak that occurs by the heterogeneous stress field near the surface also can cause retardation to slow down the crack [79-81].

7.3.2 Analysis with single edge and double edge cracks

As the fretting pads clamp the specimen, cracks are expected to propagate from both contact surfaces. However, in most cases, due to misalignment and material defects, a dominant crack propagates only from one of the surfaces. Nevertheless, analysis with a double edge crack is required to be compared with a single edge crack analysis.

Figure 7.12 shows a comparison of maximum stress intensity factor ($K_{I\,max}$) for a single edge crack and with a double edge crack. $K_{I\,max}$ values are similar for crack length below 1 mm. A small difference starts to appear after 1mm and this difference becomes pronounced as the crack length increases. $K_{I\,max}$ for a single edge crack is greater than that for a double edge crack as bending occurs in case of a single edge crack in line with crack opening.

However, the effect of crack types (single edge or double edge) seems not so significant in determining total life of the specimen, as shown in Figure 7.13. Total lifetimes predicted by both models are in close agreement.

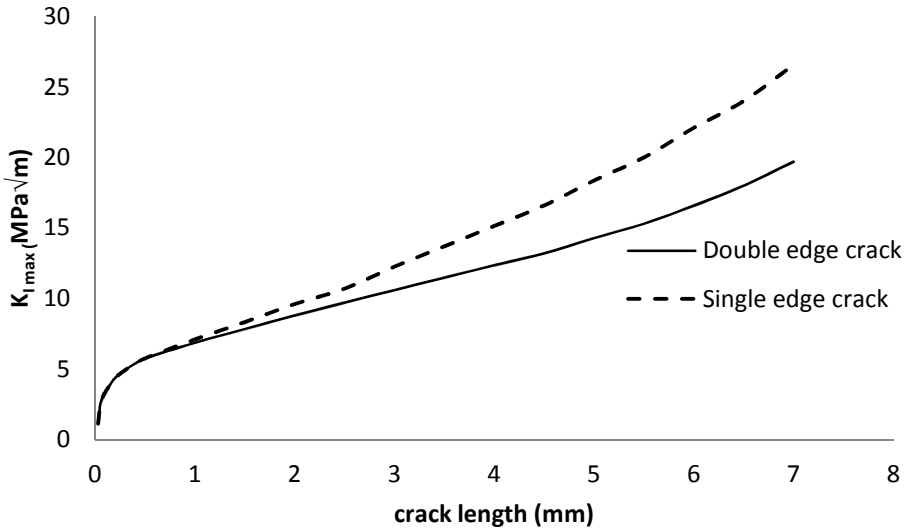

Figure 7.12: Variation of maximum stress intensity factor with crack length for single and double edge cracks.

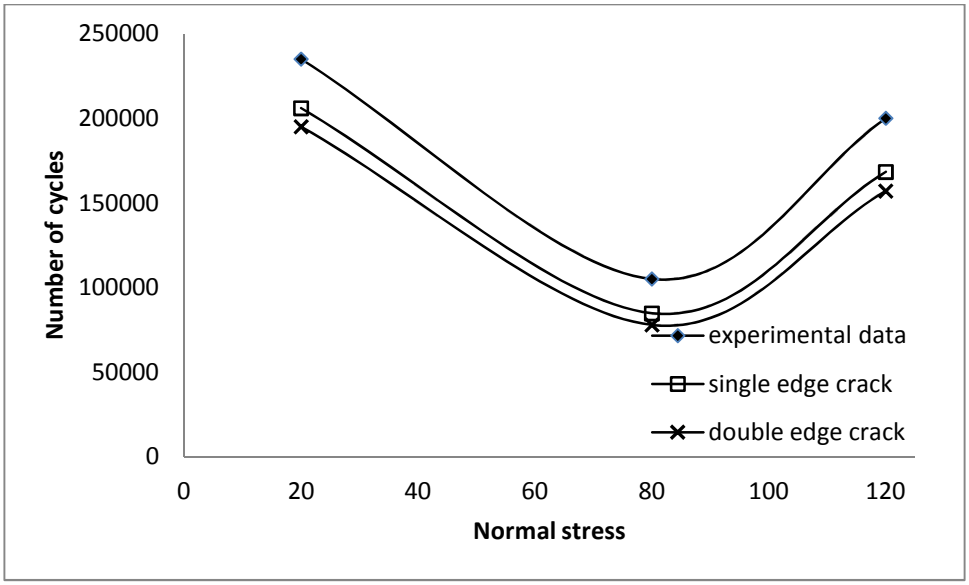

Figure 7.13: Total lifetimes for specimen with axial stress of 100 MPa using single edge and double edge crack models.

7.4 Total Lifetime Prediction

Figure 7.14 shows the predicted total lifetimes and compared with experimental data. The estimated results are scattered within $\pm 50\%$ or with average of 23% of the experimental data. This clearly shows that the models developed here are capable of satisfactorily predicting lifetime in complete contact fretting fatigue.

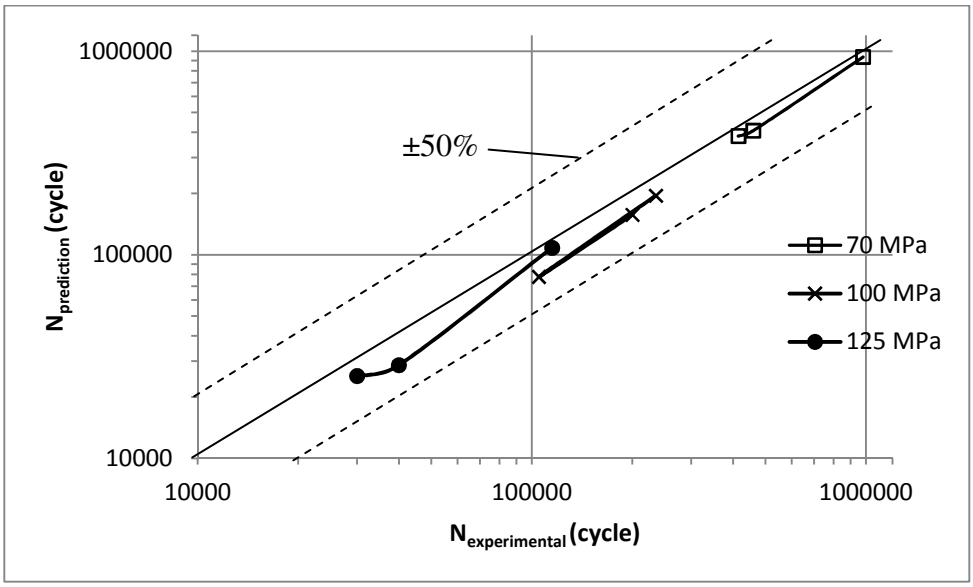

Figure 7.14: Prediction of total fretting fatigue lifetimes and their comparison with the experimental data.

7.5 Conclusions

From the results, it can be concluded that a combination of damage and fracture mechanics approach can provide a good estimation tool for predicting fretting fatigue behaviour.

Fracture mechanics analysis on crack propagation with LEFM seems to be more accurate compared to damage mechanics analysis on crack initiation. Most of the lifetime for each specimen is spent on crack nucleation rather than the propagation. This explains the difference between the total lifetimes given by the models and the experiments.

CHAPTER 8. CONCLUSIONS AND FUTURE WORK

8.1 Conclusions

Fretting fatigue, which is caused by oscillatory micro-slip that occurs between two components subjected to a clamping pressure and vibratory excitation or an oscillatory tangential force, remains as a major source of premature failure in a number of engineering assemblies. In general, fretting fatigue life is often divided into crack nucleation and crack propagation.

The overall aim of this project was to develop a robust finite element model for the prediction of total life in complete contact fretting fatigue. This study uses the earlier extensive experimental investigation to study these fretting fatigue phenomena by Royal Aerospace Establishment (RAE Fanborough). Two different fatigue perspectives have been considered: fatigue crack nucleation and fatigue crack propagation. The two techniques which are studied separately were then combined to produce total life prediction. The method helps to explain a number of key phenomena on the interaction between complete contact.

The conclusions are drawn for each stage as follows:

8.1.1 Crack Initiation Analysis

Crack initiation analysis is determined based on strain-life multiaxial fatigue relationship. Smith-Watson-Topper (SWT) and Fatemi-Socie (FS) criteria are chosen to predict crack initiation in complete contact fretting fatigue. A comparative analysis is carried out with three models based on linear elastic, elastic plastic, and elastic plastic with wear under fretting contact conditions.

Linear elastic model is able to produce contact pressure profile which is in good agreement with theoretical contact pressure for complete contact. However, this contact profile is not realistic as the singularities at both edges exceeded the yield stress of the material.

Fatigue cycles were found to create micro rotation of the fretting pad. This rotation forced the edge singularities to be stronger. As this study considered a stress ratio of R = -1, both edges were affected by these strong singularities.

Elastic plastic model is found to be an improvement on the LEFM model as it takes into account material hardening when yield stress is exceeded. It is found that singularities at the edges result in plastic deformation in the specimen near both edges. Surface deformation changes the contact pressure profile and also affects the SWT and FS parameters. However, with this plastic deformation, the SWT parameter evolves only in the first 10 cycles before becoming saturated.

Wear model improves the elastic model by simulating material wear at the contact surface. Surface deformation due to wear affects the contact pressure profile as well as the SWT parameter. Continuous SWT evolution occurs throughout a loading cycle. Miner's Rule is used here in the cumulative damage model for the prediction of crack initiation.

All these three models used in this study predict the location of fretting crack nucleation which occurs at the leading edge and confirm the experimental results. However, in predicting number of cycle for crack nucleation, with regards to all improvement made in elastic plastic and wear models, crack nucleation is still predicted to occur within 10% of the cycles to produce a 0.1mm long crack experimentally. The reason of this rather unsatisfactory result comes from the fact that SWT parameter is influenced by the steepest stress gradient due to singularities at the edge of the fretting pad.

A further analysis using averaging approach exhibits a better prediction when compared with the experimental data. The observations shows that, in overcoming the singularities, several nodes surround the critical element need to be averaging together. The size for averaging that match the experimental results varies between one to two times the grain sizes. The averaging size was found to depend on loading and some other factors such as wear and plastic deformation.

8.1.2 Crack Propagation analysis

Crack propagation analysis is determined based on fracture mechanics theory. In the early stage, as contact stress influence the crack growth, this particular stage is considered as multiaxial fatigue crack growth. Under the multiaxial stress state created by fretting loads, it is possible for cracks to change direction. Hence, crack orientation and crack propagation are the two most important parameters to be considered in this particular phase.

In determining crack path in fretting fatigue, a criterion which takes into account both the stress and strain for a whole loading cycle is needed as the contact stress varies

during the fatigue cycle. Maximum tangential stress range (ΔMTS) criterion was found to give a good prediction.

In early stage, plastic zone over crack length ratio is over 1/50 which makes LEFM analysis in this stage is invalid. Hence, in predicting crack propagation, a combined LEFM-EPFM model with well-established Paris Equation analysis is used. With the aid of EPFM analysis to study stress intensity factor, heterogeneous stress field on stress intensity could be clearly addressed. This heterogeneous stress field and large plastic zone in front crack tip is found to create retardation on crack propagation. These factors justify a different crack propagation analysis for small crack. After this early stage, crack propagation agrees well with experimental results.

The predictions of crack propagation on single surface as well as both surfaces were included in the analysis. As results shows that the difference on these two types of cracks is small compared to total life, this method of analysis can well be established as a robust technique suitable for any type of crack propagation

The fraction of fretting fatigue lifetime spent in crack initiation and crack propagation for both experimental analysis and finite element prediction varies from one specimen to another. Therefore, combinations of crack initiation with and propagation analysis are important in analysing fretting fatigue.

With this analysis, the estimated results is scattered with average of 23% of the experimental data. It can be concluded, therefore, that a combination of damage and fracture mechanics approach can provide a good estimation tool for predicting total fretting fatigue life.

8.2 Recommendation for Future Work

Some suggestions for future work are:

1. Averaging technique gives a more accurate solution for predicting crack initiation where contact stress varies rapidly in complete contact fretting fatigue. In this study, it is found that the dimension of averaging area is varies depend on plastic deformation on the surface. There is still no guideline to determine the averaging dimensions. Further studies are needed analysing this behaviour in metallurgical

aspect until guidelines on how to choose the best averaging size for given contact conditions could be produce could give a great contribution

2. In this study, material properties were assumed to be constant throughout in all the analyses. However, in reality, material properties can change significantly due to several factors such as degradation caused by wear and plastic deformation which occur in almost all fretting fatigue conditions. A modelling strategy which takes into account this material degradation should considerably improve the analysis.
3. In this study, although EPFM has been include in early stage of crack growth, there still a different between the predicted propagation rate compared to experimental results. It would also be interesting to study small crack growth behaviour under fretting fatigue conditions where the plastic zone in front of crack tip is considerably big and stress near the contact edge is rapidly varying.
4. In this study, wear, surface deformation and residual stress in creating crack initiation are not included in the propagation analysis. It would be worthwhile to include these factors in crack propagation analysis, especially in the analysis with small crack.

APPENDIX 1: USER SUBROUTINE

User Subroutine UMESHMOTION for Wear Modelling

```
C     USER INPUT FOR ADAPTIVE MESH CONSTRAINT
C
      SUBROUTINE UMESHMOTION(UREF,ULOCAL,NODE,NNDOF,
     $     LNODETYPE,ALOCAL,NDIM,TIME,DTIME,PNEWDT,
     $     KSTEP,KINC,KMESHSWEEP,JMATYP,JGVBLOCK,LSMOOTH)
C
C     UREF = wear rate mm3/Nmm
C     ULOCAL = nodal displacement pass into the routine from abaqus
C     NODE = node numbers pass into the routine
C     NNDOF = determines the number of degrees of freedom at each node
C     LNODETYPE = classified node depending on their position,
constraints and their grouping
C     ALOCAL = local coordinate system
C     NDIM = number of coordinate dimensions
C     TIME = current value of the timestep
C     DTIME = the time increment
C     PNEWDT = ratio of suggested new time increment
C     KSTEP = Step number
C     KINC = Increment number
C     KMESHSWEEP = mesh sweep number
C     JMATYP = variable that must be passed into the GETVRN
C     JGVBLOCK = variable that must be passed into the GETVRN,
GETNODETOELEMCONN, and GETVRMAVGATNODE
C     LSMOOTH = surface smoothing after mesh motion, set LSMOOTH=1 to
activate
C
      include 'ABA_PARAM.INC'
C
C     USER DEFINED DIMENSION STATEMENTS
C
      CHARACTER*80 PARTNAME
      DIMENSION ARRAY(1000)
      DIMENSION ULOCAL(*)
      DIMENSION JGVBLOCK(*),JMATYP(*)
      DIMENSION ALOCAL(NDIM,*)
      PARAMETER (NELEMMAX=100)
      DIMENSION JELEMLIST(NELEMMAX),JELEMTYPE(NELEMMAX)
      PARAMETER (CHARLENGTH = 5.0D-3,ELINC = 0.1D0)
C
      common/wear/
     $ isclock,
     $ imclock,
     $ isnodes(2000),
     $ imnodes(2000),
     $ tempslip(2000),
     $ spress(2000),
     $ sslip(2000),
     $ oldslip(2000),
     $ slipdif(2000),
     $ sopen(2000),
     $ sxcrd(2000),
     $ sycrd(2000),
     $ sincslip(2000),
     $ islave(100000),
     $ imasterreg(100000)
```

```
C
C     INITIALISE
      cnt1 = 1
C     assume node is a slave as initial guess
      master = 0
C     initialise some variables used for interpolating
      CPRESS = 0
      COPEN = 0
C
C     Internal Subroutine
C
      LOCNUM = 0
      JRCD = 0
      PARTNAME = ' '
      JTYP = 1
      LTRN = 0
C
      CALL GETPARTINFO(NODE,0,PARTNAME,LOCNUM,JRCD)
      NELEMS = NELEMMAX
C
      CALL GETNODETOELEMCONN(NODE,NELEMS,
     $     JELEMLIST,JELEMTYPE,JRCD,JGVBLOCK)
C     retrieve contact stress and contact shear
      CALL GETVRMAVGATNODE(NODE,JTYP,'CSTRESS',ARRAY,JRCD,
     $     JELEMLIST,NELEMS,JMATYP,JGVBLOCK)
      CPRESS = ARRAY(1)
      CSHEAR = ARRAY(2)
C     retrieve contact slip and contact open
      CALL GETVRMAVGATNODE(NODE,JTYP,'CDISP',ARRAY,JRCD,
     $     JELEMLIST,NELEMS,JMATYP,JGVBLOCK)
      COPEN = ARRAY(1)
      CSLIP = ARRAY(2)
C
      CALL GETVRN(NODE,'COORD',ARRAY,JRCD,JGVBLOCK,LTRN)
      XCOORD = ARRAY(1)
      YCOORD = ARRAY(2)
C
C     loop to identify and numbering all master nodes
C
      IF((CPRESS.EQ.0).AND.(COPEN.EQ.0))THEN
        master=1
        IF(imasterreg(NODE).EQ.0)THEN
          imclock=imclock+1
          imnodes(imclock)=NODE
          imasterreg(NODE)=imclock
        END IF
      ELSE
        islaveg=1
        IF(islave(NODE).EQ.0)THEN
          isclock=isclock+1
          islave(NODE)=isclock
        END IF
        spress(islave(NODE))=CPRESS
        sslip(islave(NODE))=CSLIP
        slipdif(islave(NODE))=oldslip(islave(NODE))-sslip(islave(NODE))
        sxcrd(islave(NODE))=XCOORD
        sycrd(islave(NODE))=YCOORD
      END IF
C     loop to link data from slave nodes to master nodes
      IF(master.EQ.1)THEN
        DO cnt1=1,isclock
```

```
            IF(ABS(XCOORD-sxcrd(cnt1)).LT.0.004D0)THEN
            cpressm=spress(cnt1)
            cslipm=sslip(cnt1)
            slipdifm=slipdif(cnt1)
            oldslip(cnt1)=cslipm
            END IF
          END DO
        END IF
C
C       Calculate wear using Archard Equation for every nodes
C       w=k x cpress x slip where K=9.62 X 10-8mm3/Nmm
C       cycle jump = 100 K become 9.62 X 10-6mm3/Nmm
        IF(KINC.LE.14) THEN
        W_dist=0
        ELSE
        W_dist=0.00000962D0*cpressm*ABS(slipdifm)
        END IF
C       Change nodes location
        ULOCAL(2)=ULOCAL(2)-W_dist
C
C
        WRITE(6,*)KINC,imasterreg(NODE),cpressm,slipdifm,W_dist,ULOCAL(2)
        RETURN
        END
```

APPENDIX 2 ABAQUS CONTACT MODELLING

Contact constraint is designed to allow forces to be transmitted from one part of the model to another. Below is summarised the contact constraint used in Abaqus based on Abaqus Analysis User Manual.

In Abaqus, contact conditions are defined as a discontinuous constraint, where the contact constraint is only applied when the clearance between two surfaces becomes zero. In other words, the surfaces are in contact. The analysis has to be able to detect when two surfaces are in contact and apply the contact constraints accordingly. Similarly, the analysis must be able to detect when two surfaces separate and remove the contact constraints.

The interaction between contacting surfaces consists of two components: normal to the surfaces and tangential to the surfaces. The normal component transmits forces normal to the contacting surface. Forces normal to the surface or contact pressure change dramatically when the contact clearance is zero and the pressure is transmitted between the surfaces, as shown in Figure A2.1. As the surfaces separate, the contact pressure between them will becomes zero or negative, and the constraint is removed.

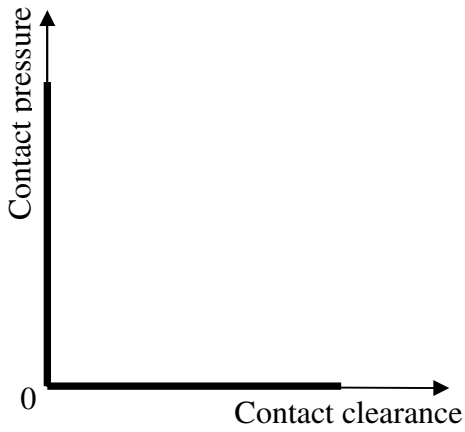

Figure A2.1 Contact pressure-clearance relationship

The tangential component consists of the relative motion (sliding) of the surfaces and frictional shear stresses. Coulomb friction is a common friction model used to describe sliding and shear stress. Coulomb frinction model characterizes the frictional behavior between the surfaces using a coefficient of friction.

According to Coulomb Friction, the tangential motion is zero until the surface traction reaches a critical shear stress value (τ_{crit}), which depends on the normal contact pressure, given by the following equation

$$\tau_{crit} = \mu P$$

Where μ is the coefficient of friction and P is the contact pressure between the two surfaces. This equation gives the limiting frictional shear stress for the contacting surfaces.

Abaqus/Standard uses the Newton-Raphson method to obtain solutions for any nonlinear problems including problems with contact constraints. In a nonlinear analysis, the solution cannot usually be obtained by solving a single system of equations. Instead, the solution is obtained by applying the specified loads gradually and incrementally working toward the final solution. Therefore, using Newton-Raphson Method, Abaqus/Standard breaks the simulation into a number of load increments and finds the approximate equilibrium configuration at the end of each load increment(Figure A2.3). It often takes Abaqus/Standard several iterations to determine an acceptable solution to a given load increment. The sum of all of the incremental responses is the approximate solution for the nonlinear analysis. Thus, Abaqus/Standard combines incremental and iterative procedures for solving nonlinear problems.

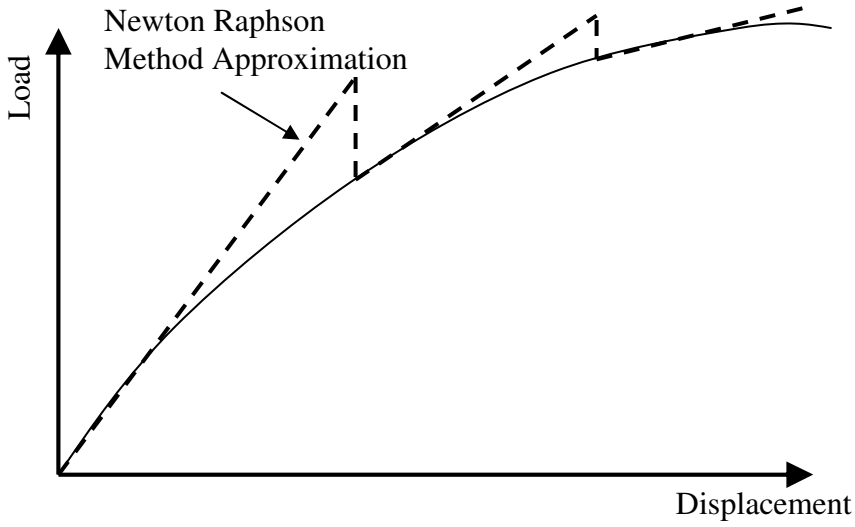

Figure A2.2 Newton Raphson approximation on a nonlinear Problem

In Contact problem, Abaqus cannot converge in the problem where there is discontinuity between the two states, sticking or slipping. To solve this problem, ABAQUS provides two schemes in defining friction in order to solve convergence problem if occurs.

In Abaqus, modelling that follows exactly the basic coulomb friction is referred to as Lagrange. Lagrange multipliers increase the computational cost of the analysis by adding more degrees of freedom to the model and often by increasing the number of iterations required to obtain a converged solution. The Lagrange multiplier formulation may even prevent convergence of the solution, especially if many points are iterating between sticking and slipping conditions. This effect can occur particularly if locally there is a strong interaction between slipping/sticking conditions and contact stresses.

The other model is based on penalty method that permits some relative motion of the surfaces (an "elastic slip") when they should be sticking.

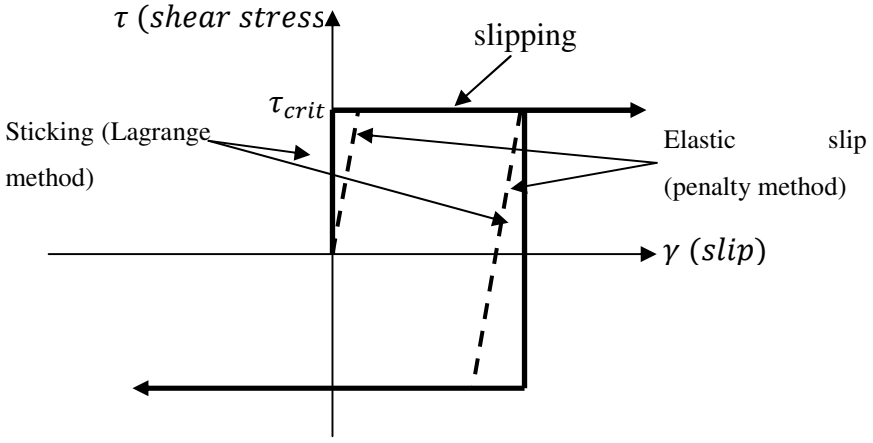

Figure A2.3 Frictional behaviour

Fgure A2.4 shows standard loop for contact constrain analysis. By applying Contact Constraint, Abaqus/Standard examines the state of all contact interactions at the start of each increment to establish whether slave nodes are open or closed. If a node is closed, Abaqus/Standard determines whether it is sliding or sticking. Abaqus/Standard applies a constraint for each closed node and removes constraints from any node where the contact state changes from closed to open. Abaqus/Standard then carries out an iteration and updates the configuration of the model using the calculated corrections.

In the updated configuration, Abaqus/Standard checks for changes in the contact conditions at the slave nodes. Any node where the clearance after the iteration becomes negative or zero, the status is changed from open to closed. Any node where the contact pressure becomes negative and the status changed from closed to open. Abaqus/Standard continues to iterate until the discontinuities are sufficiently small (or no severe discontinuities occur).

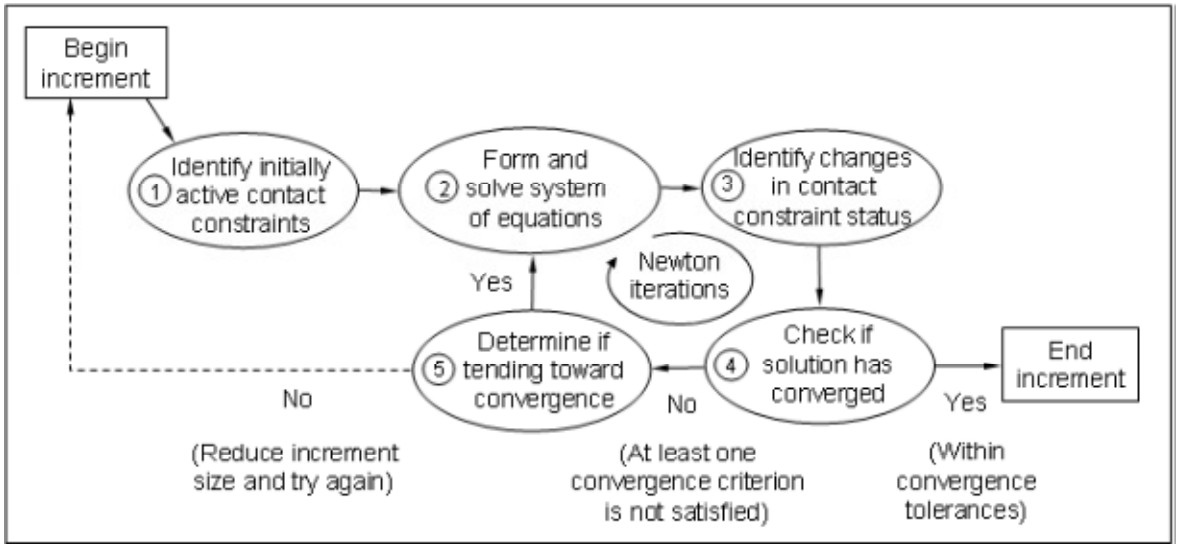

Figure A2.4 Standard loop for Contact Constrains

APPENDIX 3: EFFECT OF PLASTIC DEFORMATION AND WEAR ON CONTACT PRESSURE PROFILE

Stress profile in complete contact has been discussed in adequate detail in Section 6.4.1. In complete contact, stress singularities occur at both edges of the specimen surface. In tension loading, the singularities occur at the trailing edge while in compressive loading, the singularities occur at the leading edge, as described in Figure 6.8.

In elastic-plastic analysis, these stress singularities that approach the yield limit produce ploughing effect, as shown in Figure A3.1. High normal stress at the edge pushes the surface down and high shear stress pushes the surface to ploughing out.

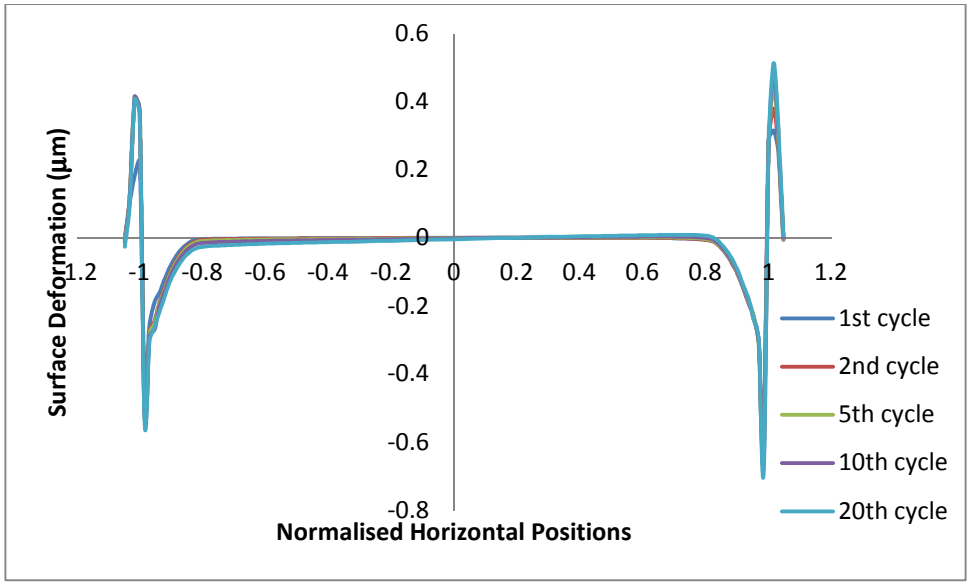

Figure A3.1: Predicted Surface Deformation for specimen with axial stress 100MPa and Normal stress 80 MPa.

The effect of loading cycles at the leading edge is shown in Figure A3.2. The deformation is high for early cycles. However, the deformation becomes saturated after a few cycles. This can be seen as the deformation for 10^{th} cycle and 20^{th} cycle are almost identical.

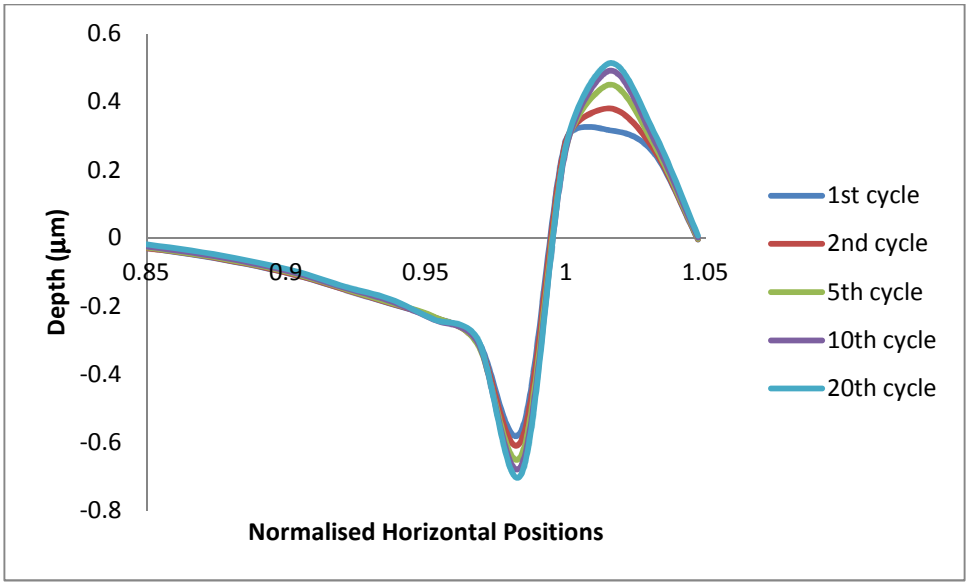

Figure A3.2 Predicted surface deformation focusing at the leading edge for specimen with axial stress 100MPa and normal stress 80 MPa.

This deformation affects the loading profile as shown in Figure A3.3. Initially, before the surface deformation, the loading profile due to the complete contact with only normal load produce a U-shape profile where the maximum pressure occurs at the edge. However, the loading profile is changed at both edges as a result of the deformation where the stress near the edge becomes lower and the singularities at the edge are weakened.

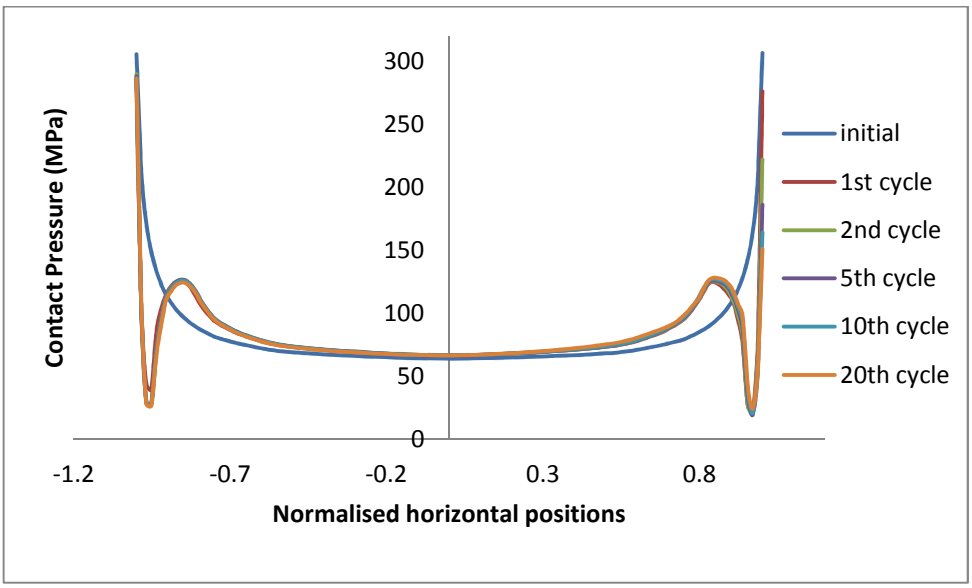

Figure A3.3: Stress evolution for specimen with axial stress 100 MPa and normal stress 80MPa affect by plastic surface deformation

Appendix 3: Effect of Plastic Deformation and Wear on Contact Pressure Profile

By focusing on the stress profile at the leading edge in Figure A3.4, the stress singularities are decreasing by the cycle. By 20th cycle, the stress is almost half of the initial stress.

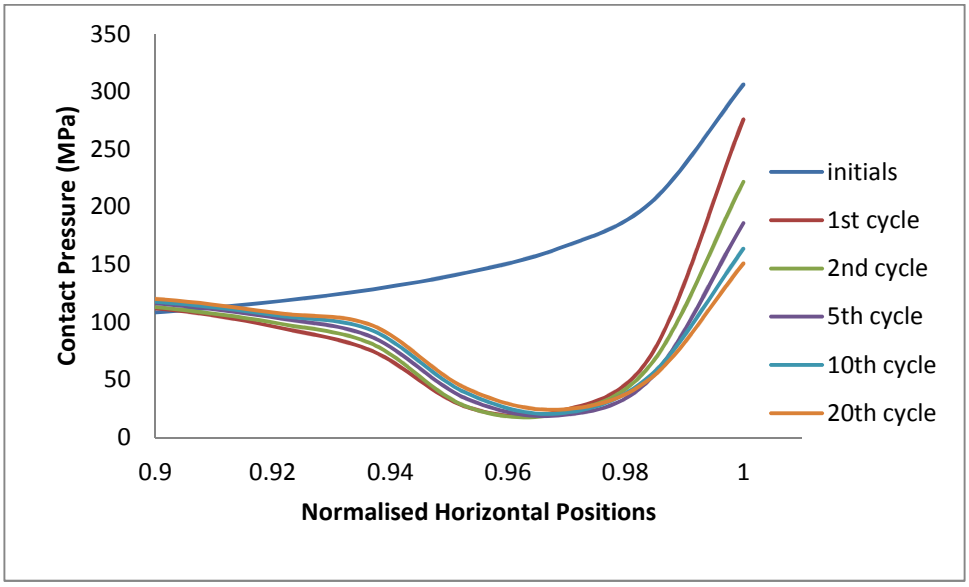

Figure A3.4: Shear evolution for specimen with axial stress 100 MPa and normal stress 80MPa affect by plastic surface deformation focusing at the leading edge.

Figure A3.5 shows the surface deformation due to wear. It can be seen that unlike plastic deformation, it is not just the edge but the entire contacting surface, which deforms due to wear. It appears that the surface near to the leading edge is worn more than the surface near the trailing edge. Based on Archard Equation discussed is Section 5.2.2, parameters which produce wear are contact pressure and slip. Contact pressure can be seen in Figure A3.3 while slip is shown in Figure A3.6. Based on these figures, contact pressure is almost symmetric. However, slip range is higher towards the leading edge. This is the cause of why the surface near the leading edge is worn more than the other side.

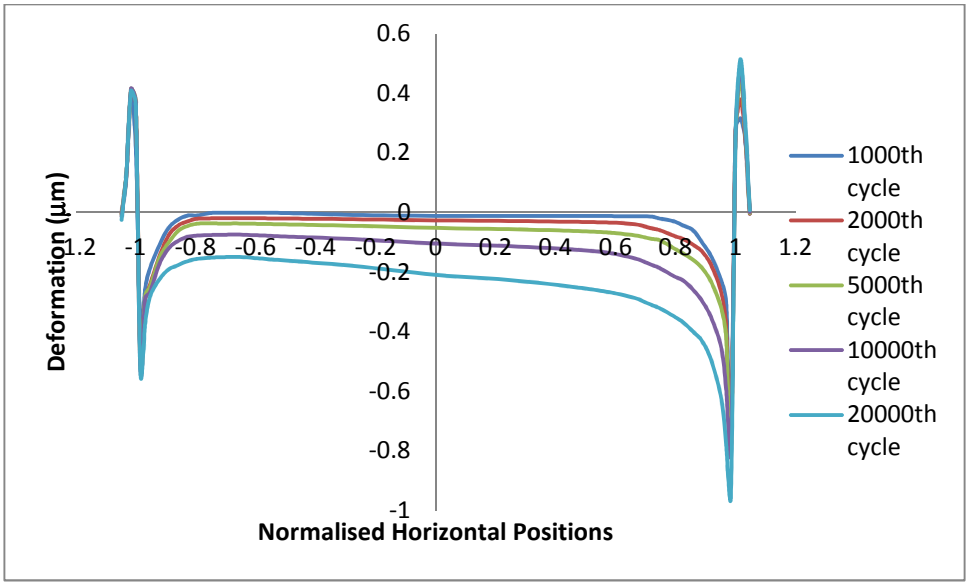

Figure A3.5 Predicted surface deformation due to wear for specimen with axial stress 100 MPa and normal stress 80 MPa.

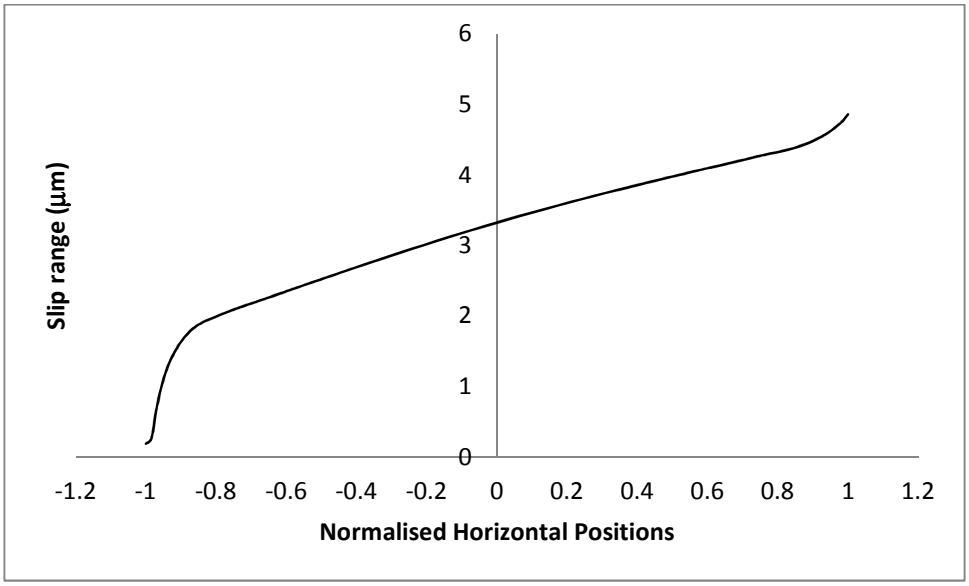

Figure A3.6 Slip Range for one cycle for specimen with axial stress 100 MPa and normal stress 80 MPa

Observing the contact pressure, shown in Figure A3.7, it can be seen that as the surface near the leading edge is worn more than the surface near the leading edge, pressure on the surface near the trailing edge increases with the number of cycles, while the pressure on the trailing edge decreases with the number of cycles.

Appendix 3: Effect of Plastic Deformation and Wear on Contact Pressure Profile

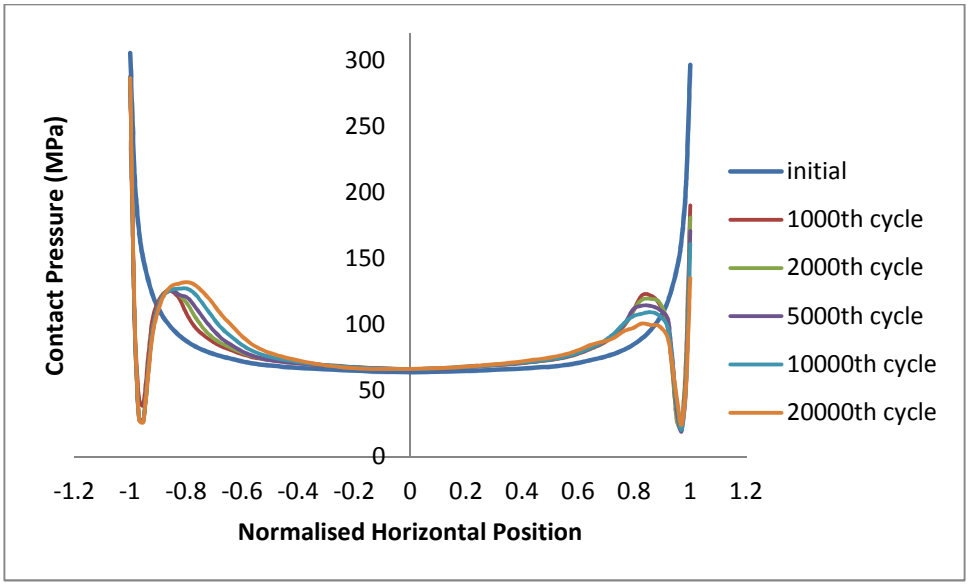

Figure A3.7: Stress evolution for specimen with axial stress 100 MPa and normal stress 80MPa due to plastic surface by wear.

APPENDIX 4: PUBLICATIONS

Conference

1. M.H. Maslan, M.A. Sheikh, S. Arun, Prediction of Fatigue Crack Initiation in Complete Contact Fretting Fatigue, 2013 International Conference on Material Science and Mechanical Engineering, October 27-28, 2013 Kuala Lumpur

2. M.H. Maslan, M.A. Sheikh, Prediction of Crack Propagation Direction in Fretting Fatigue, MACE conference, April 9, 2014 Manchester, United Kingdom

Journal

1. M.H. Maslan, M.A. Sheikh, S. Arun, Prediction of Fatigue Crack Initiation in Complete Contact Fretting Fatigue, Applied Mechanics and Materials, 467(2014) pp 431-437

Prediction of Fatigue Crack Initiation in Complete Contact Fretting Fatigue

M. H. Maslan[1, a], M. A. Sheikh[2,b] and S. Arun[3,c]

[1,2,3]School of Mechanical, Aerospace and Civil Engineering, PO Box 88, Manchester, M60 1QD, United Kingdom

[a]mohamadhaidir.maslan@manchester.ac.uk, [b]mohammad.a.sheikh@manchester.ac.uk, [c]sutham.arun@manchester.ac.uk

Keywords: Fretting Wear; Fatigue; Complete Contact

Abstract. Fretting induced cracking is commonly observed in industrial components that are in contact and are subjected to small oscillatory movements between them. Fretting causes a considerable reduction in fatigue strength. In this paper, finite element modeling is used in conjunction with Smith Watson Topper (SWT) criterion to estimate crack initiation in fretting. The predictions from the analysis are compared with the experimental results. It is concluded that the analysis must include the effect of residual stress and wear profile with debris effect for better predictions.

Introduction

Fretting fatigue involves two or more solids in contact that experience relative displacements of small amplitude. Fretting occurs when two pieces of material, pressed together by an external static load, are subjected to transverse cyclic loading, as in bolted flanges, riveted lap-joints, and press-fits such as a gear or bearing on a shaft.

A number of factors have been reported which might influence the magnitude and rate of fretting process. Dorbomirski et al. [1] has classified these as primary and secondary factors. Primary factors have a direct effect on the fretting process, whereas the secondary factors are only indirectly linked to the primary factors. The primary factors are normal load, coefficient of friction and slip magnitude.

Generally, normal contact in fretting can be divided into two categories, complete, and incomplete contact. In complete contact, the size of the contact is independent of the contact load whereas in incomplete contact, the contact size is dependent on the contact load. Complete and incomplete contacts generate different load profiles and hence lead to significantly different effect on fretting fatigue.

One of the highly cited works in discussing the effect of slip important is by Blanchard et al. [2] and Zhou et al. [3] on constructing the Material Response Fretting Map. The material response fretting map, as shown in Fig. 1, shows the failure mode of a component subjected to fretting as a function of the normal force and displacement amplitude. Although slip magnitude has been stated as a primary factor, research shows that it is interdependent on other factors.

As in plain fatigue, fretting fatigue life of structural components is usually considered in terms of crack initiation and crack propagation. In recent years, many studies have used multiaxial fatigue criterion to establish correlations with fretting fatigue experimental data. One of the widely used criterion is Smith–Watson–Topper (SWT). This criterion is based on the calculations of the maximal normal stress and the maximal strain amplitude on the critical plane:

$$SWT = \sigma_{max}\frac{\Delta\varepsilon}{2} = \frac{\sigma'^2_f}{E}(2N_f)^{2b} + \sigma'_f\varepsilon'_f(2N_f)^{b+c} \quad (1)$$

where σ_{max} is the peak normal stress on a plane, $\Delta\varepsilon$ the maximum normal strain range on the same plane within one fatigue cycle, σ'_f is the fatigue strength coefficient, E is Young's modulus, N_f is the number of cycles for crack initiation, b is the fatigue strength exponent, ε'_f is the fatigue ductility coefficient and c is the fatigue ductility exponent.

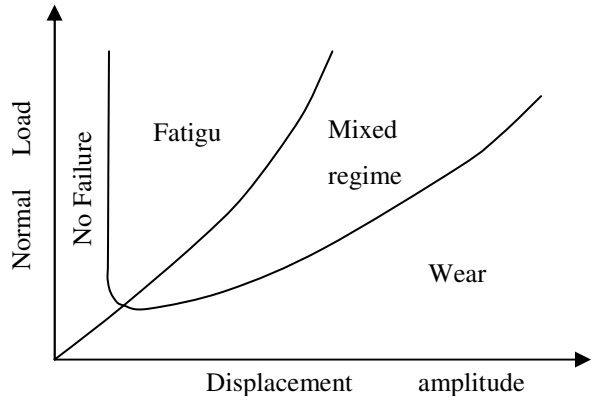

Fig 1. Material response fretting map [4].

SWT has been extensively used in fretting fatigue predictions. Buciumeanu et al [5] in their work on incomplete contact, in a special shape specimen which produces two zones of flat contact, found that more accurate results are obtained if a new parameter, the stress concentration factor due to the fretting scar effect, K_t is used. Madge et.al [6] have included the effect of material removal due to wear using Archard method [7] in incomplete contact. Their analysis show that wear over lifetime produces a major evolution of SWT and hence affect the predicted fatigue life and failure position. This work shows a good correlation on fretting maps as shown in Fig. 1. However this method still has a weakness as it neglects the effects of near-surface features and wear debris, which is significant in severe wear[8]. Araujo and Nowell [9] have uses SWT approach to estimate fretting fatigue initiation life in nearly complete contact, and found that these methods are not adequate for rapidly varying contact stress fields. They suggested that one method alone would not be adequate for evaluating fretting fatigue initiation life in tests with different geometries and further modification is needed for each configuration.

In this study, finite element method is used together with SWT to predict number of cycles for crack initiation for specimens made from an aerospace aluminium alloy, BS L65 (Aluminum 2014), in complete contact with BS S98 (2.5 % Nickel-Chrome-Moly) *steel* pads. Various combinations of axial cyclic loading and normal stress are used to identify the factors that influence the results and which will be used to modify SWT approaches in the future work.

Experimental Details

The finite element analysis is based on the experimental works of Fernando et al [10]. A general fretting fatigue test apparatus was used which consisted of flat fretting bridge pads over a specimen of rectangular cross section. The geometry of pads and specimen are shown in Fig. 2. The material investigated was a fully artificially-aged 4 percent copper

aluminium alloy. The fretting pads were made of BS S98 steel. Table 1 gives the elastic properties of these materials.

Table 1 Materials Properties.

Materials	Young Modulus, E	Poisson Ratio, v	Yield Stress
BS L65	74.0 GPa	0.33	420 MPa
BS S98	210 GPa	0.29	1002 MPa

Three axial load amplitudes, 70 MPa, 100 MPa and 125 MPa with stress ratio, R= -1 were investigated, together with various values of normal load covering the range of 20 MPa – 120 MPa. The results of the experiments used in this analysis are summarised in Table 2. Potential Drop technique was used to get an estimation of the crack length during the fatigue test. The measurements were reported to be reliable for cracks longer than 0.1 mm [10].

Table 2 Experimental Results.

Test No	Axial Stress (MPa)	Normal Stress (MPa)	Crack Initiation (number of cycles)	Fatigue Life (number of cycles)
126	70	20	270,000	415,000
127	70	80	216,200	460,000
134	70	120	150,000	980,000
123	100	20	147,000	Not fail
122	100	60	85,000	116,000
124	100	80	50,400	105,000
145	100	100	36,000	210,000
125	100	120	24,000	200,000
128	125	80	9,400	35,000
130	125	120	4,000	30,000

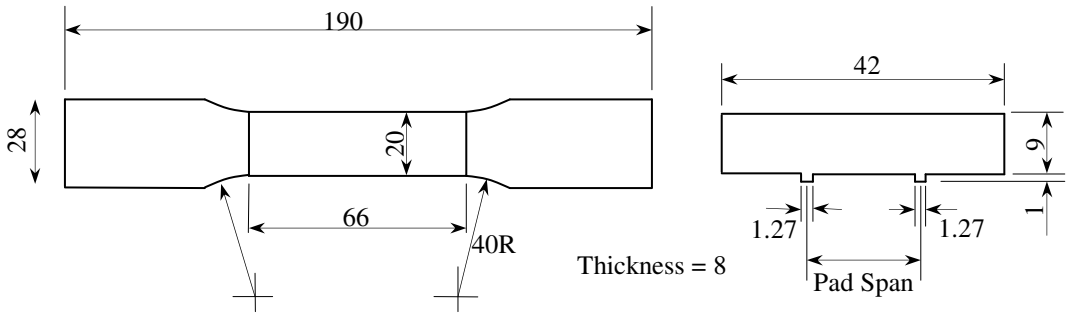

Fig 2. Specimen and fretting pad (all dimensions in mm).

Numerical Modelling

Due to symmetry conditions, a quarter 2D finite element model has been used to represent the fretting fatigue tests, as shown in Fig. 3. Since the specimen is 8 mm thick, plane strain elements are used in the analysis. Mesh is refined towards the contact region with a coarse mesh elsewhere, to reduce processing time. Matched meshes are used on the master and slave contact surfaces.

A Lagrange multiplier contact algorithm was used to strictly enforce the stick condition when the shear stress is less than the critical value according to the Coulomb friction law. Fernando et al [10] have suggested that a constant COF value of 1 is representative for the tests studied here. The loading history is represented in Fig. 4. In the first analysis step, a normal load, P is applied to the fretting pads. In the next step, the specimen is loaded by a cyclic fatigue load $\sigma(t)$ with a maximum value σ_{max} and a stress ratio, R of -1.

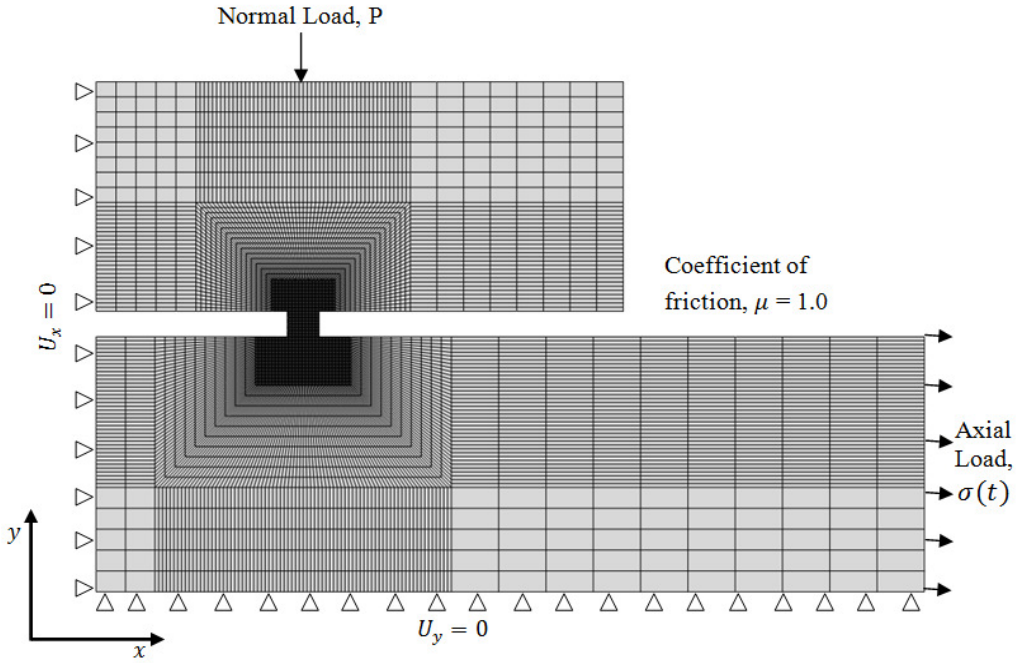

Fig. 3. Quarter finite element model.

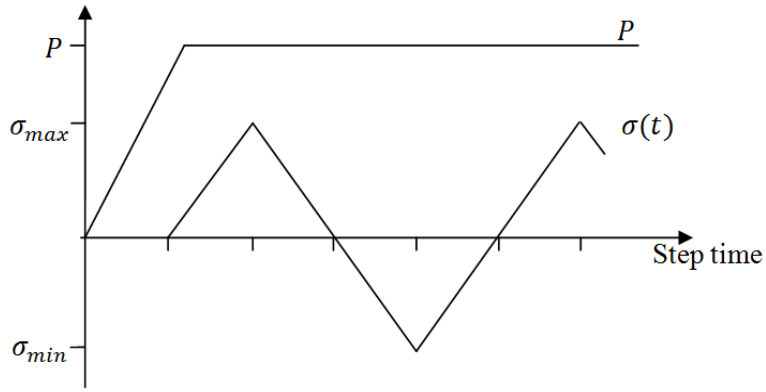

Fig. 4. Normal load and cyclic axial load history applied to the finite element model.

Crack initiation location and the number of cycles for initiation is determined by implementing SWT parameters on the critical plane where the product between the maximum stress and the total strain amplitude is maximum. Element centroidal stresses and strain ranges were calculated using the two-dimensional transformation (Mohr's circle) equations for stress and strain on every 5° intervals over a 180° range. The maximum normal stress σ_{max}, and the corresponding strain range $\Delta\varepsilon$ are determined. These values together with fatigue properties (Table 3) are then employed in Eq. 1 to establish the SWT values and calculate the number of cycles for crack initiation.

Table 3 Fatigue properties for 2014-T6/651 Aluminum alloy [11].

σ_f' (MPa)	b	ε_f'	C
777	-0.1082	0.3041	-0.6478

Results and Discussion

In Fig. 5, predicted number of cycles for crack initiation from SWT analysis together with experiment values are plotted against normal load for all the three axial loads. In general, for each axial load, both experimental and SWT predicted cycles decrease with increasing applied normal load. As normal load produces a compressive stress normal to the surface, localised stress and strain also increase as a result of multiaxial loading. This leads to a reduction in fatigue strength.

At low normal stress, SWT prediction is much higher than experimental. However, the decreasing pattern predicted from SWT is more pronounced compared to the experimental. This condition produces two dominant regions; a region where SWT prediction is much higher than experimental, and the other region where SWT prediction become lower than the experimental.

In order to predict the failure process that leads to crack initiation, normal stress is plotted against the relative slip amplitude and mapped on Material Response Fretting Map in Fig. 6. By comparing Fig. 5 and Fig. 6, it can be seen that SWT prediction is higher than experimental in the wear region. Whereas SWT prediction is lower than experimental in the cracking region. SWT prediction matches with experimental in location where cracking and wear compete with each other.

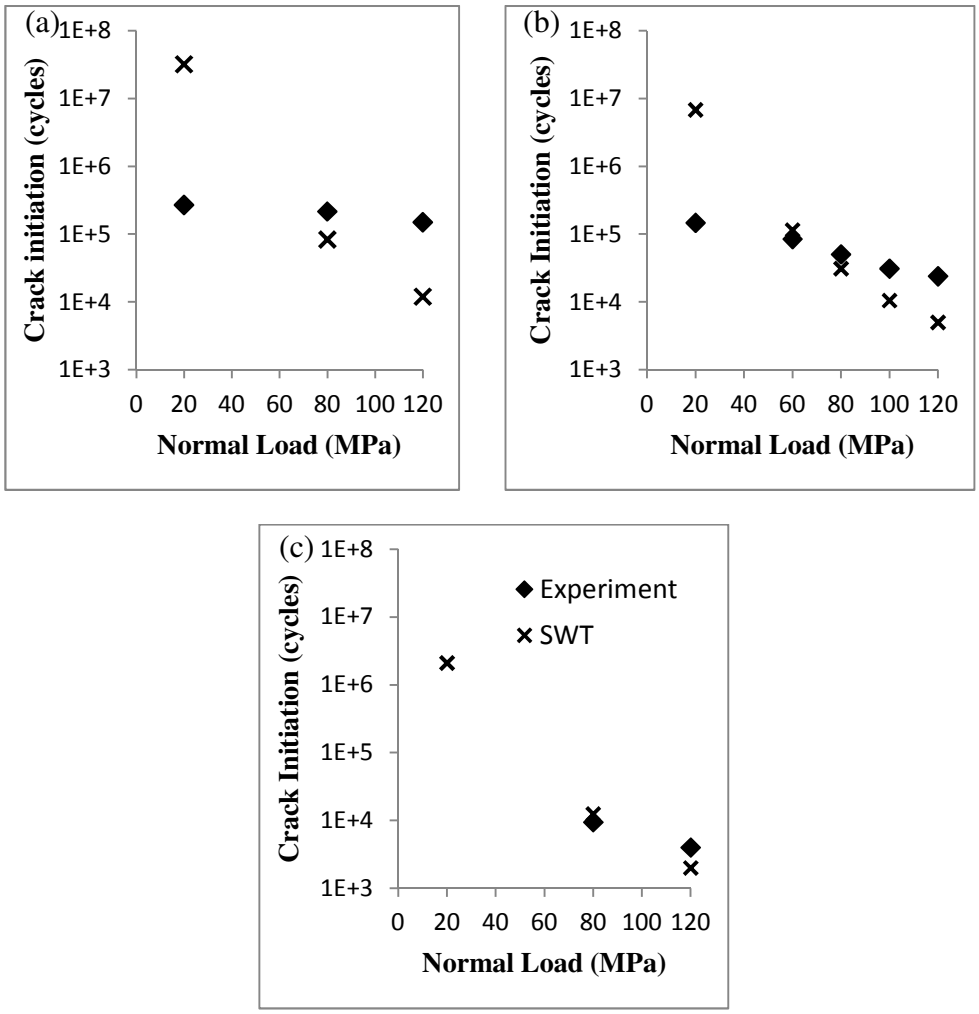

Fig. 5. Crack initiation cycles vs normal load for (a) maximum axial stress = 70 MPa, (b) maximum axial stress = 100 MPa, (c) maximum axial stress = 125 MPa.

In wear region, the profile of surface as well as contact stress changes due to material removal or wear. Madge et al. [6] in their work show that pressure redistribution due to wear reduces the risk of crack initiation. However, it is noted that although Archard approach [7] is able to simulate the shape of the wear scars, this approach neglects some important factors of the fretting process such as change of microstructure, wear debris, the appearance of local plastic deformation and oxidation. Everitt et al.[8], in their research on debris, found that wear produces compacted and oxidised debris layer with a high hardness and low in stiffness. The thickness is proportional with the loading, wear and number of cycles. Furthermore, Mohd Tobi et al. [12] in their research on fretting wear and cyclic plasticity found wear to be responsible for delamination and debris generation at the wear scar edge that lead to crack nucleation.

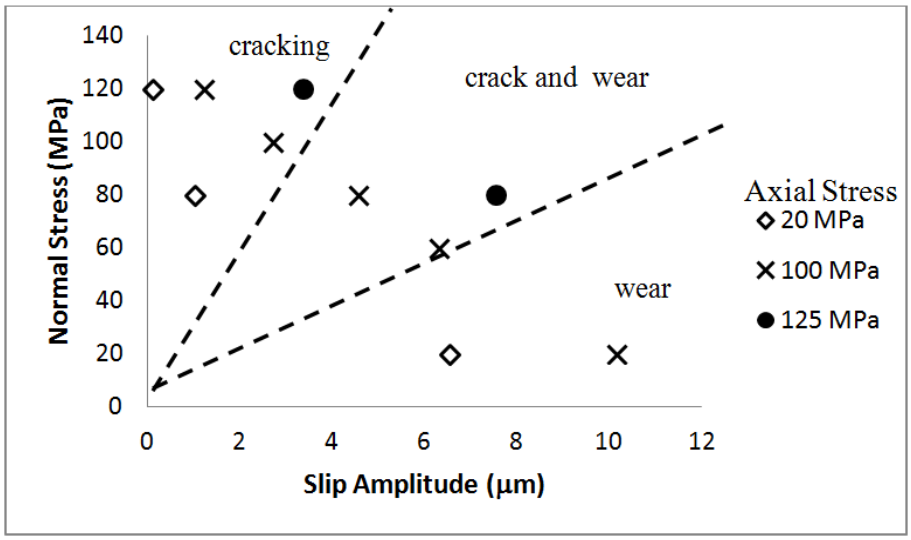

Fig 6. Normal Stress vs slip amplitude, mapping on fretting map.

In the cracking region, it is expected that cracking would be purely dependant on fatigue. Predicted number of cycles from SWT should agree with experimental. However, SWT predictions here are lower than experimental. To explain this disagreement, contact stress is plotted along the contact region in Fig 7. Yield stress for the specimen is 420 MPa (Table 1) which is lower than the contact stress at both edges during loading and unloading for normal stress above 80 MPa. Compressive residual stress is potentially induced in this region. This situation can be compared to a specimen with induced residual stress either by shot peening [13], deep rolling [14], laser shock peening[15], which can decrease the stress intensity range, increase the fretting crack growth life, and lower the probability of fretting fatigue failure. In some cases, residual stress can even completely suppress fretting fatigue [16].

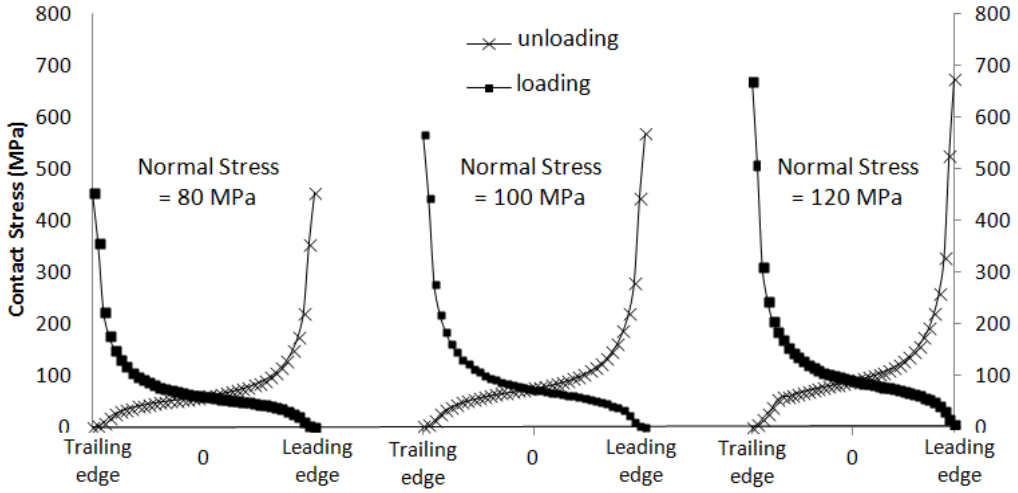

Fig 7. Contact stress distribution at the contact surface during loading and unloading.

Conclusion

This work on predicting number of cycles for crack initiation shows that SWT based analysis is inappropriate. This research has found two factors to be responsible. An adequate simulation would include transformation of wear profile due to cyclic plasticity, and surface degradation. It is also proposed an extension of SWT criterion that includes the effect of the compressive residual stresses induced at the contact on crack nucleation in fretting wear.

References

[1] J.M. Dobromirski in: *Standardization of Fretting Fatigue Test Methods and Equipment STP 1159*, edited by R.B.Waterhouse, M. H. Attia Publications/ASTM, Philadelphia (1992), p. 60

[2] P. Blanchard, C. Colombier, V. Pellerin, S. Fayeulle and L. Vincent: Metallurgica Transaction Vol. 22A (1991), p. 1535

[3] Z.R. Zhou, S. Fouvry and L. Vincent: Wear Vol. 155 (1992), p. 317

[4] S. Fouvry, P.Kapsa and L. Vincent: Wear Vol. 200 (1996), p. 186

[5] M. Buciumeanua, I. Crudu, L. Palaghianb, A.S. Mirandaa and F.S. Silvaa: International Journal of Fatigue Vol. 31 (2009), p. 1278

[6] J.J. Madge, S.B.Leen and P.H. Shipway: Wear Vol. 263 (2007), p. 542

[7] J.F. Archard: Journal of Applied Physics Vol. 24 (1953), p. 981

[8] N.M. Everitt, J. Ding, G. Bandak, P.H. Shipway, S.B. Leen and E.J. Williams: Wear Vol. 267 (2009), p. 283

[9] J.A. Arau´jo and D. Novell: International Journal of Fatigue Vol. 24 (2002), p. 763

[10] U.S. Fernando, G.H. Farrahi, M.A. Sheikh in: *Fretting fatigue behaviour of BS L65 aluminium alloy, Progress report, SIRIUS*, University of Sheffield: Sheffield (1992)

[11] S. K. Walker and A.C. Quilter in: *ICAF 2011 Structural Integrity: Influence of Efficiency and Green Imperatives*, edited by J. Komorowski Publications/Springer, Dordrecht. (2011) p.375

[12] A.L. Mohd Tobi, J. Ding., G. Bandak, S.B. Leen and P.H. Shipway: Wear Vol. 267 (2009), p. 270

[13] G.H. Majzoobia and A.R. Ahmadkhani: Surface and Coatings Technology Vol. 205 (2010), p. 102-109.

[14] G.H. Majzoobia, K. Azadikhah and J. Nemati: Materials Science and Engineering Vol. 516 (2009), p. 235-247.

[15] K.K. Liu and M.R.Hill: Tribology International Vol. 42 (2009), p. 1250

[16] K.S. Chan, M.P.Entight, J.P. Moody, P.J. Golden, R. Chandra and A.C. Pentz: International Journal of Fatigue Vol. 32 (2010), p. 815

REFERENCES

1. R.J. Atkinson, W.J. Winkworth, G.M. Norris *Behaviour of Skin Fatigue Cracks at the Corners of Windows in a Comet I Fuselage*, in *Reports and Memoranda No. 3248*. 1962, Aeronautical Research Council Report and Memoranda: London.
2. A. Sóbester, *Stratospheric Flight: Aeronautics at the Limit*. 2011, New York, US: Springer.
3. J.L. Kolstad, J. Burnett, J.K. Lauber, J.T. Nall, L.V. Dickinson, *Aircraft Accident Report--Aloha Airlines, Flight 243, Boeing 737-200, N73711, near Maui, Hawaii, April 28, 1988, NTSB/AAR-89/03*. 1989, National Transportation Safety Board: Washington.
4. A.P Hersman, R.L. Sumwalt, C.S. Hart, M.R. Rosekind, E.F.Weener, *Rapid Decompression Due to Fuselage Rupture, Southwest Airlines Flight 812, NTSB/AAB-13/02*. 2013, National Transportation Safety Board: Washington.
5. H. Hertz, *Über die berührung fester elastischer Körper.* Journal für die reine und angewandte. Mathematik, 1881. **92**: p. 156-171.
6. D.A. Hills, D. Nowell, *Mechanics of Fretting Fatigue*. 1994: Kluwer Academic Publisher.
7. K.L. Johnson, *Contact Mechanics*. 2001: Cambridge University Press.
8. B. Bhushan, B. K. Gupta, *Handbook of Tribology*. 1991: Mc Graw Hill.
9. J.F. Archard, *Contact and Rubbing of Flat Surfaces.* Journal of Applied Physics, 1953. **24**(8): p. 981-988.
10. ASTM, *ASTM Dictionary of Engineering Science & Technology*. 2005, ASTM International.
11. J. Schijve, *Fatigue of Structures and Materials*. 2003: Springer.
12. G. Venkataraman, Y. Chung, Y. Nakasone, T. Mura, *Free energy formulation of fatigue crack initiation along persistent slip bands: calculation of S-N curves and crack depths.* Acta Metallurgica Et Materialia, 1990. **38**: p. 31-41.
13. N.E. Dowling, *Mechanical Behaviour of Materials*. 2012, Virginia: Prentice Hall.
14. K.N. Smith, P. Watson, T.H. Topper, *A stress-strain function for the fatigue of metals.* Journal of Materials, 1970. **4**: p. 767-778.
15. A. Fatemi, D. F. Socie, *A critical plane approach to multiaxial fatigue damage including out of phase loading.* Fatigue & Fracture of Engineering Materials & Structures, 1988. **11**(3): p. 149-165.
16. A.A. Griffith, *The Phenomena of Rupture and Flow in Solids.* Philosophical Transactions of the Royal Society of London. Series A, 1921. **221**: p. 163-198.
17. C.E. Inglis, *Stresses in a Plate due to the Presence of Cracks and Sharp Corners.* Transactions of the Institute of Naval Architects, 1913. **55**: p. 219-241.
18. G.R. Irwin, *Onset of Fast Crack Propagation in High Strength Steel and Aluminum Alloys.* Sagamore Research Conference Proceedings, 1956. **2**: p. 289-305.
19. J.R. Rice, *A path independent integral and the approximate analysis of strain concentration by notches and cracks.* Journal of Applied Mechanics, 1968. **35**: p. 379-386.
20. R.O. Ritchie, *Near-Threshold Fatigue Crack Propagation in Ultra-High Strength Steel: Influence of Load Ratio and Cyclic Strength.* Journal of Engineering Materials and Technology, 1977. **99**(3).

21. E.M. Eden, W.N. Rose, F.L. Cunningham, *The endurance of metals: experiments on rotating beams at University College, London.* Proceedings of the Institution of Mechanical Engineers, 1911. **4**: p. 836-974.
22. J.M. Dobromirski, ed. *Variables of Fretting Process: Are there 50 of them?* Standardization of Fretting Fatigue Test Methods and Equipment STP 1159, ed. M. H. Attia, R. B. Waterhouse. 1992, ASTM Philadelphia.
23. http://www.astmnewsroom.org/default.aspx?pageid=2409. *Fretting Fatigue Testing Is Subject of New ASTM International Standard.* ASTM International News Releases 2011.
24. U.S. Fernando, G.H. Farrahi, M.A. Sheikh, *Fretting fatigue behaviour of BS L65 aluminium alloy, Progress report, SIRIUS*. 1992, University of Sheffield: Sheffield.
25. G.H. Farrahi, G.H. Majzoobi, H. Chinekesh, *Effect of contact geometry on fretting fatigue life of aluminium alloy 2024-t3.* Indian JOurnal of Engineering & Materials Sciences, 2005. **12**: p. 331-336.
26. R.H. Talemi, *Numerical Modelling Techniques for Fretting Fatigue Crack Initiation and Propagation*, in *Department of Mechanical Construction and Production*. 2014, Ghent University: Gent, Belgium.
27. J.J. Madge, *Numerical Modelling of the Effect of Fretting Wear on Fretting Fatigue*. 2008, University of Nottingham.
28. T. Christiner, J. Reiser, I. Godor, W. Eichlseder, F. Trieb, R. Stuhlinger, *The fatigue endurance limit of a high strength CrNi steel in a fretting dominated regime.* Tribology International, 2013. **59**: p. 97-103.
29. R. Hojjati-Talemi, M. AbdelWahab, *Fretting fatigue crack initiation life time predictor tool: Using damage mechanics approach.* Tribology International, 2013. **60**: p. 176-186.
30. M. Sabsabi, E. Giner, F.J. Fuenmayor, *Experimental fatigue testing of a fretting complete contact and numerical life correlation using X-FEM.* International Journal of Fatigue, 2011. **33**(6): p. 811-822.
31. U.S. Fernando, G.H. Farrahi, M.W. Brown, ed. *Fretting fatigue crack growth behaviour of BS L65 4 percent copper aluminium alloy under constant normal load*. Fretting Fatigue, ESIS Publication 18 ed. R.B Waterhouse, T.C. Lindley. 1994, Mechanical Engineering publications Limited: London.
32. J.A. Pape, R.W. Neu, *Influence of contact configuration in fretting fatigue testing.* Wear, 1999. **225-229**: p. 1205-1214.
33. K.K. Liu, M.R. Hill, *The effects of laser peening and shot peening on fretting fatigue in Ti–6Al–4V coupons.* Tribology International, 2009. **42**(9): p. 1250-1262.
34. C. Ruiz, P. H. B. Boddington, K. C. Chen, *An Investigation of Fatigue and Fretting in a Dovetail Joint.* Experimental Mechanics, 1984. **24**(3): p. 208-217.
35. P.M. Wavish, *Representative Specimen for Multiaxial Fretting Fatigue in a Splined Coupling*. 2006, University of Nottingham, UK.
36. L. Chambon, B. Journet, *Modelling of fretting fatigue in a fracture-mechanics framework.* Tribology International, 2006. **39**(10): p. 1220-1226.
37. B. Alfredsson, A. Cadario, *A study on fretting friction evolution and fretting fatigue crack initiation for a spherical contact.* International Journal of Fatigue, 2004. **26**(10): p. 1037-1052.
38. D.A. Hills, D. Nowell, J.J. O'Connor, *On the mechanics of fretting fatigue.* Wear, 1988. **125**(1-2): p. 129-146.
39. I.R. McColl, J. Ding, S.B. Leen, *Finite Element Simulation and Experimental Validation of Fretting Wear.* Wear, 2004. **256**: p. 1114-1127.

40. J. Hintikkaa, A. Lehtovaaraa, A. Mäntylä, *Normal displacements in non-Coulomb friction conditions during fretting.* Tribology International, 2016. **94**: p. 633-639.
41. C.B. Elliott, D.W. Hoeppner, *The importance of wear and corrosion on the fretting fatigue behavior of two aluminum alloys.* Wear, 1999. **236**(1-2): p. 128-133.
42. H. Lee, S. Mall, *Some observations on frictional force during fretting fatigue.* Tribology Letters, 2004. **17**(3).
43. P.L. Hurricks, *The mechanism of fretting - a review.* Wear, 1970. **15**: p. 389-409.
44. M. Varenberg, G. Halperin, I. Etsion, *Different aspects of the role of wear debris in fretting wear.* Wear, 2002. **252**: p. 902-910.
45. Y. Berthier, Ch. Colombié, M. Godet, L. Vincent, *Fretting Wear Mechanisms and Their Effects on Fretting Fatigue.* Journal of Tribology, 1988. **110**(3): p. 517-524.
46. U. Bryggman, S. Söderberg, *Contact conditions and surface degradation mechanisms in low amplitude fretting.* Wear, 1988. **125**(1-2): p. 39-52.
47. G.H. Majzoubi, G.H. Farahi, *Crack Behavior of The Aluminum Alloy 2024 Under Fretting Conditions.* International Journal Of Engineering, 2002. **15**(3): p. 287-292.
48. R.B. Waterhouse, D.E. Taylor, *Fretting debris and the delamination theory of wear.* Wear, 1974. **29**(3): p. 337-344.
49. N.M. Everitt, J.D., G. Bandak, P.H. Shipway, S.B. Leen, E.J. Williams, *Characterisation of fretting-induced wear debris for Ti-6Al-4 V.* Wear, 2009. **267**(1-4): p. 283-291.
50. R.H. Talemi, M.A. Wahab, *Fretting fatigue crack initiation lifetime predictor tool: Using damage mechanics approach.* Tribology International, 2013. **60**: p. 176-186.
51. L. Johansson, *Numerical simulation of contact pressure evolution in fretting.* Journal of Tribology, 1994. **116**(2): p. 247-254.
52. I.G. Goryacheva, P.T. Tajeev, T.N. Farris, *Wear in partial slip contact.* Journal of Tribology, 2001. **123**(4): p. 848-856.
53. J. Ding, S.B. Leen, I.R. McColl, *The effect of slip regime on fretting wear-induced stress evolution.* International Journal of Fatigue, 2004. **26**(5): p. 521-531.
54. J. Ding, S.B. Leen, I.R. McColl, *The effect of slip regime on fretting wear induced stress evolution.* International Journal of Fatigue, 2004. **26**(5): p. 521-531.
55. J.J. Madge, S. B. Leen, P. H. Shipway, *A combined wear and crack nucleation-propagation methodology for fretting fatigue prediction.* International Journal of Fatigue, 2008. **30**(9): p. 1509-1528.
56. D. Nowell, D.A. Hills, D.N. Dai, *Energy dissipation and crack initiation in fretting fatigue.* Tribology Series, 1994. **27**: p. 389-396.
57. A. Kapoor, *Wear by plastic ratchetting.* Wear, 1997. **212**: p. 119-130.
58. S. Fouvry, Ph. Kapsa, L. Vincent, *An elastic–plastic shakedown analysis of fretting wear.* Wear, 2001. **247**(41-54).
59. J.F. Peng, J.H. Liu, Z.B. Cai, M.X. Shen, C. Song, M.H. Zhu, *Study on bending fretting fatigue damages of 7075 aluminum alloy.* Tribology International, 2013. **59**: p. 38-46.
60. J.M. Ambrico, M.R. Begley, *Plasticity in fretting contact.* Journal of the Mechanics and Physics of Solids, 2000. **48**: p. 2391–2417.
61. M. Zhang, *Crystal plasticity modeling of Ti-6Al-4V and its application in cyclic and fretting fatigue analysis*. 2008, Georgia Institute of Technology.
62. C.H. Goh, J.M. Wallace, R.W. Neu, D.L. McDowell, *Polycrystal plasticity simulations of fretting fatigue.* International Journal of Fatigue, 2001. **23**(1): p. 423-435.
63. T. Dick, G. Cailletaud, *Fretting modelling with a crystal plasticity model of Ti-6Al-4V.* Computational Materials Science, 2006. **38**(1): p. 113-125.

64. J.R. Mayeur, D.L. McDowell, R.W. Neu, *Crystal plasticity simulations of fretting of Ti-6Al-4V in partial slip regime considering effects of texture.* Computational Materials Science, 2008. **41**(3): p. 356-365.
65. A.L. Mohd Tobi, J.D., G. Bandak, S.B. Leen, P.H. Shipway, *A study on the interaction between fretting wear and cyclic plasticity for Ti–6Al–4V.* Wear, 2009. **267**(1-4): p. 270-282.
66. C. D. Lykins, S. Mall, V. Jain, *An evaluation of parameters for predicting fretting fatigue crack initiation.* International Journal of Fatigue, 2000. **22**(8): p. 703-716.
67. C. D. Lykins, S. Mall, V. Jain, *Combined experimental-numerical investigation of fretting fatigue crack initiation.* International Journal of Fatigue, 2001. **23**(8): p. 703-711.
68. D.W. Hoeppner, ed. *Mechanisms of Fretting Fatigur and Their Impact on Test Methods Development*. Standardation of Fretting Fatigue Test Methods and Equipment, ASTM STP 1159, ed. M.H. Attia, R.B. Waterhouse. 1992, ASTM: Philadelpia.
69. J.A. Arau´jo, D. Nowell, *The effect of rapidly varying contact stress fields on fretting fatigue.* International Journal of Fatigue, 2002. **24**: p. 763-775.
70. J.J. Madge, S.B. Leen, P.H. Shipway, *The critical role of fretting wear in the analysis of fretting fatigue.* Wear, 2007. **263**: p. 542-551.
71. Archard, J.F., *Contact and Rubbing of Flat Surfaces.* Journal of Applied Physics, 1953. **24**(8): p. 981-988.
72. D. P. Rooke, D.A.J., *Stress intensity factors in fretting fatigue.* Journal of Strain Analysis for Engineering Design, 1979. **14**(1): p. 1-6.
73. D.P. Rooke, D.B. Rayaprolu and M. H. Aliabadi *Crack-Line and Edge Green's Functions for Stress Intensity Factors of Inclined Edge Cracks.* Fatigue & Fracture of Engineering Materials & Structures, 1992. **15**(5): p. 441-461.
74. T. Kimura, K. Sato, *Simplified method to determine contact stress distribution and stress intensity factors in fretting fatigue.* International Journal of Fatigue, 2003. **25**: p. 633-640.
75. M.A. Sheikh, U.S. Fernando, M.W. Brown, K.J. Miller, ed. *Elastic Stress Intensity Factors for Fretting Cracks Using The Finite Element Method*. Fretting Fatigue, ESIS 18, ed. R.B. Waterhouse, T. C. Lindley. 1994, Mechanical Engineering Publications: London.
76. Y.Mutoh, J.Q. Xu, K. Kondoh, , ed. *Observations and analysis of fretting fatigue crack initiation and propagation*. Fretting Fatigue: Advances in Basic Understanding and Applications, ASTM STP 1425, ed. S.E. Kinyon, D.W. Hoeppner, Y. Mutoh 2003, ASTM: West Conshohocken.
77. M.C. Baietto, E. Pierres, A. Gravouil, B. Berthel, S. Fouvry, B. Trolle, *Fretting fatigue crack growth simulation based on a combined experimental and XFEM strategy.* International Journal of Fatigue, 2013. **47**: p. 31-43.
78. J.J. O'Connor, ed. *The role of elastic stress analysis in the interpretation of fretting fatigue failures*. Fretting Fatigue, ed. R.B. Waterhouse. 1981, Applied Science: London.
79. C. Vallellano, J. Domínguez, A. Navarro, *Influence of R ratio and stick zone eccentricity on the prediction of the fretting fatigue limit with spherical contact.* International Journal of Fatigue, 2007. **29**(7): p. 1208-1219.
80. M. Iranpour, F. Taheri, *On the effect of stress intensity factor in evaluating the fatigue crack growth rate of aluminum alloy under the influence of compressive stress cycles.* International Journal of Fatigue, 2012. **43**: p. 1-11.

81. B. Yang, S. Mall, *Mechanics of two-stage crack growth in fretting fatigue.* Engineering Fracture Mechanics, 2008. **75**(6): p. 1507–1515.
82. H. Kitagawa, S.T. *Applicability of fracture mechanics to very small cracks or in the early stage*. in *Second international conference on mechanical behavior of materials*. 1976. Boston: American Society of Metals.
83. M.P. Szolwinski, T.N. Farris, *Observation, analysis and prediction of fretting fatigue in 2024-T351 aluminum alloy.* Wear, 1998. **221**: p. 24-36.
84. J.A. Araújo, D. Nowell, *The effect of rapidly varying contact stress fields on fretting fatigue.* International Journal of Fatigue, 2002. **24**: p. 763–775.
85. C. Navarro, M. García, J. Domínguez, *A procedure for estimating the total life in fretting fatigue.* Fatigue and Fracture of Engineering Materials and Structures, 2003. **26**: p. 459–468.
86. D.F. Socie, J. Morrow, W.C. Chen, *A procedure for estimating the total fatigue life of notched and cracked members.* Engineering Fracture Mechanics, 1979. **11**: p. 851–859.
87. W. Switek, *Early stage crack propagation in fretting fatigue.* Mechanics of Materials, 1984. **3**: p. 257-267.
88. J.A. Alic, A.L. Hawley, *On the early growth of fretting fatigue cracks.* Wear, 1979. **56**: p. 377-389.
89. F. Erdogan, G.C. Sih, *On the Crack Extension in Plates Under Plane Loading and Transverse Shear.* J. Basic Engineering, 1963. **85**(4): p. 519-525.
90. B. Cotterell, J.R. Rice, *Slightly curved or kinked cracks.* International Journal of Fracture, 1980. **16**(2): p. 155-169.
91. R.J. Nuismer, *An energy release rate criterion for mixed mode fracture.* International Journal of Fracture, 1973. **11**(2): p. 245-250.
92. S. Faanes, G. Härkegård, *Inclined cracks in fretting fatigue.* Engineering Fracture Mechanics, 1995. **52**(1): p. 71–82.
93. E. Giner, M. Sabsabi, J.J. Ródenas, F.J. Fuenmayor, *Direction of crack propagation in a complete contact fretting-fatigue problem.* International Journal of Fatigue, 2013. **In Press**.
94. S. Faanes, U.S. Fernando, ed. *Life Prediction in Fretting Fatigue using Fracture Mechanics*. Fretting Fatigue, ESIS 18, ed. R.B. Waterhouse, T.C. Lindley. 1994, Mechanical Engineering Publications: London.
95. U.S. Fernando, M.W. Brown, K.J. Miller, R. Cook, D. Rayaprolu, ed. *Fretting Fatigue Behaviour of BS L65 4 percent copper aluminium alloy under variable normal load*. Fretting Fatigue, ESIS 18, ed. R.B Waterhouse, T.C. Lindley. 1994, Mechanical Engineering Publications: London.
96. S. Faanes, U.S. Fernando, ed. *An Application of a Short Crack Growth Model in Prediction of Fretting Fatigue Life*. Advances in Fracture Resistance and Structural Integrity, ed. V.V. Panasyuk, M.C. Pandey, O.Ye. Andreykiv, J.F. Knott, P. Rama Rao, R.O. Ritchie. 1994, Pergamon. 271–276.
97. Faanes, S., *Inclined cracks in fretting fatigue.* Engineering Fracture Mechanics, 1995. **52**(1): p. 71–82.
98. S. Faanes, *Distribution of contact stresses along a worn fretting surface.* International Journal of Solids and Structures, 1996. **33**(23): p. 3477–3489.
99. R.H.Talemi, M.A. Wahab, E.Giner, M. Sabsabi, *Numerical Estimation of Fretting Fatigue Lifetime Using Damage and Fracture Mechanics.* Tribology Letters, 2013. **52**(1): p. 11-25.

100. J. Ding, D. Houghton, E.J. Williams, S.B. Leen, *Simple parameters to predict effect of surface damage on fretting fatigue.* International Journal of Fatigue, 2011. **33**(3): p. 332–342.
101. J.J. Madge, S.B. Leen, I.R. McColl, P.H. Shipway, *Contact-evolution based prediction of fretting fatigue life: Effect of slip amplitude.* Wear, 2007. **262**: p. 1159-1170.
102. M.A. Miner, *Cumulative damage in fatigue.* Journal of Applied Mechanics, 1945. **67**.
103. J.M. Melenk, I. Babuska, *The partition of unity finite element method: basic theory and applications.* Computer methods in applied mechanics and engineering, 1996. **139**(1): p. 289-314.
104. ABAQUS, *ABAQUS 6.11 Analysis User's Manual.* Dassault Systèmes, Providence, RI, USA, 2011.
105. S. K. Walker, A. C. Quilter, *Cyclic Stress-Strain and Strain-Life Properties of Aerospace Metallic Materials*, in *ICAF 2011 Structural Integrity: Influence of Efficiency and Green Imperatives*, J. Komorowski, Editor. 2011, Springer: Dordrecht.
106. S. Babu, G.D. Janaki Ram, P.V. Venkitakrishnan, G.M. Reddy, K.P. Rao, *Microstructure and Mechanical Properties of Friction Stir Lap Welded Aluminum Alloy AA2014.* J. Materials Science Technology, 2012. **28**(5): p. 414-426.
107. J.E.Srawley, W.F. Brown, ed. *Fracture toughness testing methods*. STP381 Fracture toughness testing and its applications. 1965, American Society for Testing and Materials: Philadelphia.
108. N.V. Londe, T. Jayaraju, P.R. Sadananda, *Estimation of Crack Growth Properties of High Strength Metallic Materials by a Novel Technique.* International Journal of Engineering and Technology, 2010. **2**(6).
109. J.A Araújo, D.N., *Analysis of pad size effects in fretting fatigue using short crack arrest methodologies.* International Journal of Fatigue, 1999. **21**(9): p. 947-956.
110. S. Fouvry, D. Nowell, K. Kubiak, D.A. Hills, *Prediction of fretting crack propagation based on a short crack methodology.* Engineering Fracture Mechanics, 2008. **75**: p. 1605-1622.
111. T.L. Anderson, *Fracture Mechanics Fundamentals and Applications*. 2005, Boca Raton: Taylor & Francis Group.